AD

USAAVLABS TECHNICAL REPORT 69-81

A SURVEY OF ADVANCED ENERGY CONVERSION SYSTEMS AND THEIR APPLICABILITY TO ARMY AIRCRAFT PROPULSION REQUIREMENTS

By

Calvin C. Silverstein

October 1969

U. S. ARMY AVIATION MATERIEL LABORATORIES
FORT EUSTIS, VIRGINIA

CONTRACT DAAJ02-69-C-0001
CALVIN C. SILVERSTEIN
ENGINEERING CONSULTANT
BALTIMORE, MARYLAND

177

DISCLAIMERS

The findings in this report are not to be construed as an official Department of the Army position unless so designated by other authorized documents.

When Government drawings, specifications, or other data are used for any purpose other than in connection with a definitely related Government procurement operation, the United States Government thereby incurs no responsibility nor any obligation whatsoever; and the fact that the Government may have formulated, furnished, or in any way supplied the said drawings, specifications, or other data is not to be regarded by implication or otherwise as in any manner licensing the holder or any other person or corporation, or conveying any rights or permission, to manufacture, use, or sell any patented invention that may in any way be related thereto.

DISPOSITION INSTRUCTIONS

Destroy this report when no longer needed. Do not return it to the originator.

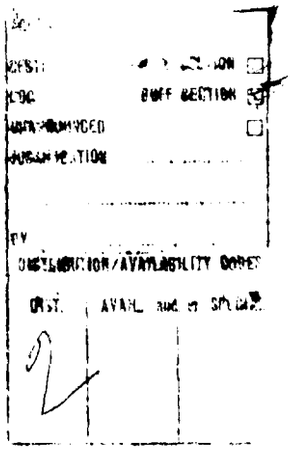

DEPARTMENT OF THE ARMY
U. S. ARMY AVIATION MATERIEL LABORATORIES
FORT EUSTIS, VIRGINIA 23604

The study described herein, which was conducted by Calvin C. Silverstein, was performed under U. S. Army Contract DAAJ02-69-C-0001. The work was performed under the technical management of D. B. Cale, Propulsion Division, U. S. Army Aviation Materiel Laboratories.

Appropriate technical personnel of this command have reviewed this report and concur with the conclusions contained herein.

Task 1G-162204A01409
Contract DAAJ02-69-C-0001
USAAVLABS Technical Report 69-81
October 1969

A SURVEY OF ADVANCED ENERGY CONVERSION SYSTEMS AND THEIR APPLICABILITY TO ARMY AIRCRAFT PROPULSION REQUIREMENTS

Final Report

SIL - 103

By

Calvin C. Silverstein
Engineering Consultant
Baltimore, Maryland

for

U.S. ARMY AVIATION MATERIEL LABORATORIES
FORT EUSTIS, VIRGINIA

SUMMARY

Advanced energy conversion systems have been surveyed, and the applicability of such systems to Army aircraft propulsion requirements has been evaluated. The following systems were included in the survey: closed Brayton cycle, Rankine cycle, intercool-reheat cycle, fuel cells, MHD converters, thermionic converters, thermoelectric converters, radioisotope heat sources, and nuclear reactor heat sources. Conventional or superconducting motors were used to convert the output of the systems which generate electricity directly to shaft output power.

The purpose of the effort was to identify new propulsion systems which are or may potentially be competitive with advanced gas turbine propulsion systems that are currently under consideration. The systems were to be capable of powering helicopters at rated power levels of 500 hp, 3000 hp, and 20,000 hp. The principal evaluatory factor was the specific weight (lb/hp) of a system consisting of the engine, transmission and shafting, and fuel needed for a specified mission. Other considerations such as volume, cost, and reliability were also taken into account.

At the 500-hp and 3000-hp levels, none of the systems considered was competitive with the advanced gas turbines, both currently and in the foreseeable future. At the 20,000-hp level (for which two 10,000-hp engines would be used), the open-cycle MHD converter and the intercool-reheat cycle appear to be competitive with advanced gas turbines on the basis of future technology.

The MHD converter is believed to be best suited for use in a dual-purpose plant, which can provide electricity as well as helicopter propulsive power. Because of the low peak temperature of the intercool-reheat cycle, blade cooling and special high-temperature materials are not required for efficient operation.

It was recommended that MHD converter and intercool-reheat cycle propulsion systems be studied in greater detail.

TABLE OF CONTENTS

TABLE OF CONTENTS (Continued)

LIST OF ILLUSTRATIONS

LIST OF ILLUSTRATIONS (Continued)

LIST OF ILLUSTRATIONS (Continued)

LIST OF ILLUSTRATIONS (Continued)

LIST OF TABLES

LIST OF TABLES (Continued)

LIST OF TABLES (Continued)

INTRODUCTION

At the present time, the open-cycle gas turbine meets Army requirements for a lightweight, compact, and reasonably efficient aircraft propulsion system. However, peak cycle temperatures are limited by stoichiometric combustion considerations, which in turn impose ultimate limits on the minimum specific fuel consumption (lb fuel/hp-hr) and on the maximum specific shaft power (hp/lb/sec airflow) that are attainable with the open-cycle gas turbine. If these limits are to be exceeded, new aircraft propulsion system concepts will be required. While the open-cycle gas turbine is expected to meet Army aircraft propulsion needs in the foreseeable future, the identification of propulsion systems with the potential to compete with the open-cycle gas turbine will be of assistance in the planning of future research and development programs.

In support of Army interest in the identification of new propulsion systems that may be competitive with the open-cycle gas turbine, advanced energy conversion systems were surveyed. The overall objectives of the survey were:

1. To identify systems which are potential candidates for Army aircraft propulsion.

2. To present the current and estimated future status of technology for these systems.

3. To identify critical problem areas relating to system feasibility.

The energy conversion systems that were considered are listed in Table I. They are divided into three broad categories. In the shaft power systems, shaft power is produced directly by the expansion of a working fluid through a turbine. In the direct-conversion electrical generators, the initial energy conversion product is electrical power, which is then transformed to the desired shaft output via an electric motor. In the nuclear systems, thermal energy produced as the result of nuclear reactions is converted to shaft or electrical power by any conversion process that can utilize energy in thermal form.

SCOPE OF SURVEY

The survey was accomplished in three tasks. In Task I, advanced energy conversion systems currently under development were reviewed through contacts with organizations active in such development and via a literature search. In Task II, the data obtained in Task I were analyzed and related to Army aircraft propulsion requirements. In Task III, the various energy conversion systems were evaluated by comparison of their characteristics with the characteristics of advanced gas turbine propulsion systems.

Although most of the energy conversion system data utilized was based upon existing information, calculations were performed to obtain the needed data in two instances. Efficiency calculations were carried out for the intercool-reheat

TABLE I. ENERGY CONVERSION SYSTEMS INCLUDED IN SURVEY
Shaft Power Systems
Closed Brayton Cycle Rankine Cycle Intercool-Reheat Cycle
Direct-Conversion Electrical Generators
Fuel Cell Magnetohydrodynamic (MHD) Converter Thermionic Converter Thermoelectric Converter
Nuclear Systems
Reactor Heat Source Radioisotope Heat Source

cycle, since this is a new concept which is not currently under development. Calculations of heat input and heat rejection system weights were also made for several of the energy conversion systems under development for which little or no relevant information on combustion-fired heat input systems and air-heat-sink heat rejection systems was available.

During Task I, information was obtained for the various energy conversion systems on: power output, efficiency, fuel consumption, weight, volume, reliability, cost, sensitivity to environmental conditions, part-load characteristics, transient response, and structural considerations. For the direct-conversion electrical generators, information was also obtained on motors and transmissions needed to match system electrical output with the shaft power requirement of a helicopter rotor.

As might be expected in a review of developmental systems, wide variations were found in the availability and preciseness of needed data. Nevertheless, the information obtained, along with the judicious use of engineering judgement, was believed to be sufficient to the overall program objectives.

The most important single evaluatory criterion was total system weight. Total system weight consists of the sum of conversion system (engine) weight, power transmission system weight, and fuel weight. (For direct-conversion electrical generators, the motor and mechanical transmission were considered as an integral unit.) Fuel weight was determined for a standardized mission with a specified elapsed time and a specified power-time schedule. The standardized mission was the same as that used in the specification of referenced advanced gas turbine characteristics (see Table II). All weight and volume data are presented in terms of specific weight (lb/hp) and specific volume (ft^3/hp).

TABLE II. ADVANCED GAS TURBINE CHARACTERISTICS

Component	Engine Shaft Power (hp)		
	500	1500*	10,000*
	Specific Weight (lb/shp)		
Engine (W_e)	0.200	0.143	0.125
Transmission & Shafting (W_t)	0.700	0.650	0.500
Fuel (W_f)**	1.108	0.997	0.854
Total ($W_e + W_t + W_f$)	2.008	1.790	1.479
Transmission Input Speed (rpm)	23-35,000	16-25,000	10-20,000
Transmission Output Speed (rpm)	470	250	80-100
Specific Engine Volume (ft^3/hp)	3.24×10^{-3}	$3.01-3.24 \times 10^{-3}$	$1.57-3.15 \times 10^{-3}$
Specific Engine Cost ($/hp)	57.8-76.2	54.8-65.4	22.4-29.4
	Auxiliary Power (hp)		
	25	50	100
Component	Specific Auxiliary Power (lb/hp)		
Auxiliary Power Unit (W_a)	0.333	0.333	0.333
Fuel (W_{fa})***	0.600	0.600	0.600
Total ($W_a + W_{fa}$)	0.933	0.933	0.933

*Two engines per aircraft.

**Based on following mission:

Rated Power	85%	70%	60%	40%
Time	35 min	15 min	2 hr	15 min
Total Mission Time	3 hr 5 min			

***Based on operating time of 1 hr at specific fuel consumption of 0.600 lb/hp-hr.

The original data on energy conversion systems that were collected during Task I represented raw data that could not be applied directly to an assessment of system applicability to Army aircraft propulsion requirements. Since most of the contemplated applications for these systems require electrical power, power is generally given in terms of kw or watts, and power output per unit area is given as kw/ft^2 or w/cm^2. These units have been retained in the presentation of the original system data, not only because the data are raw but because similar units will be found in the technical literature.

During Task II, the original systems were modified in order to conform to the requirements of an aircraft propulsion system. These modifications

included: removal of the electrical generator from shaft power systems, with consequent reductions in weight and increases in system efficiency; addition of motor-transmissions to direct conversion generators, with consequent weight additions and reductions in system efficiency; the addition of heat input components appropriate to a combustion heat source and heat rejection components appropriate to an atmospheric heat sink, in place of components appropriate to a nuclear heat source (except for nuclear systems) and a space heat sink; corrections to account for the effect of system power level on efficiency and weight; corrections to account for the effect of system lifetime, time between overhaul, and reliability on weight; and corrections to system weight and efficiency based on estimated future advances in materials technology, increases in component efficiencies, and reductions in design conservatism. All of the modified data are presented in terms of conventional engineering units (i.e., shaft power is in hp, lengths are in ft or in., etc.)

In Task III, the modified weight and volume data that were developed in Task II for both current and future technology were compared with weight and volume data for advanced gas turbines at power levels of 500 hp, 1500 hp, and 10,000 hp. The characteristics of these gas turbines are given in Table II and Figure 1. Other relevant system characteristics such as cost, reliability, sensitivity to environmental conditions, and transient performance were compared on a more qualitative basis. Critical problem areas limiting the application of the various energy conversion systems to Army aircraft propulsion were identified, along with programs that are planned or under way to alleviate these problems. Recommendations were also made in areas where investigations would be fruitful but are not currently being pursued.

CONTENT OF REPORT

Results of the survey of advanced energy conversion systems and study of their applicability to Army aircraft propulsion requirements are presented in this report. Shaft power systems, direct-conversion electrical generators, and nuclear systems are discussed successively in the next three sections.

The same format is used in each section. First, a given system is described and its principle of operation is briefly stated, and the current status of the system (as of October 1968) is given. Then, current and estimated future specific weights and volumes for the system are presented and compared with comparable data for advanced gas turbines. A discussion of other system characteristics such as cost, reliability, etc., follows. Finally, critical problem areas relating to system development are discussed, and conclusions are drawn concerning system applicability to Army aircraft propulsion requirements.

Following the discussion and evaluation of each energy conversion system, general conclusions are drawn and recommendations are presented.

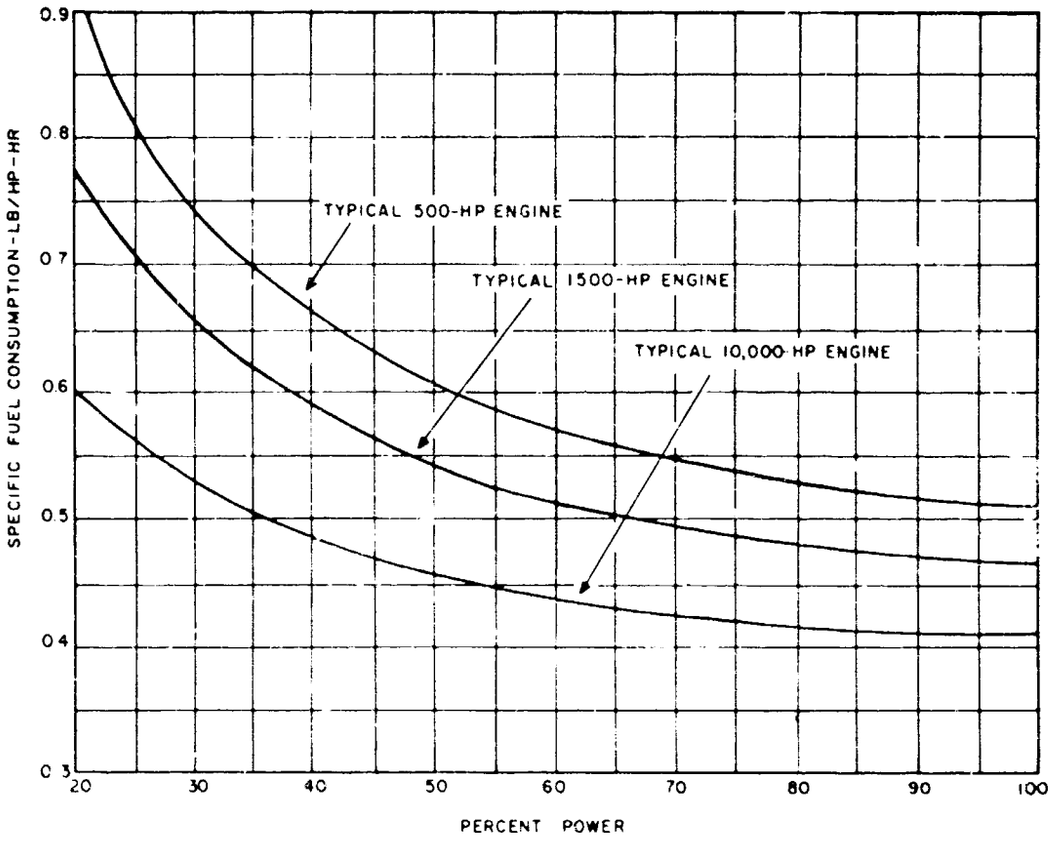

Figure 1. Specific Fuel Consumption Versus Percent Power for Advanced Gas Turbine Engines.

Three appendixes are included in the report. Calculational methods used to determine the performance of the intercool-reheat cycle are given in Appendix I. Calculations used to determine the characteristics of heat input and heat rejection systems are presented in Appendix II. Data and information on conventional and superconducting motors are contained in Appendix III.

SHAFT POWER SYSTEMS

Three shaft power systems were considered in the survey: the closed Brayton cycle, the Rankine cycle, and the intercool-reheat cycle. The closed Brayton cycle and Rankine cycle evaluations are based on advanced systems that are under development for space application. An organic Rankine cycle power plant design for terrestrial application was also used. The intercool-reheat cycle is a new concept, and its evaluation is based on system performance calculations which were carried out expressly for the survey.

CLOSED BRAYTON CYCLE

In the closed Brayton cycle, a gaseous working fluid of arbitrary composition and arbitrary pressure is confined within a closed loop containing at least the following elements: a heater, a turbine, a precooler, and a compressor. A regenerator is also usually included. Figure 2 shows these cycle elements (and in addition an alternator to which the turbine is coupled). Heat generated externally to the loop is added to the gas through the heat transfer surface of the heater. The hot gas then expands through the turbine, generating shaft power. The turbine exhaust flows through the regenerator, where some of its heat is transferred to the compressor discharge stream. Upon leaving the regenerator, the turbine exhaust flows through the precooler, where sufficient heat is removed through heat transfer surfaces to an external heat sink to lower the gas temperature to the required value at the compressor inlet. The gas is then compressed in the compressor and is heated to the turbine inlet temperature by flowing successively through the regenerator and the heater.

The capability of operating at a minimum cycle pressure that is greater than atmospheric results in two significant features. First, the power output of a given turbomachine varies directly as the pressure. Second, for a given power requirement, the size of both rotating machinery and heat exchanger surfaces will vary inversely as a power of the pressure. For example, at 10 atmospheres, turbomachinery diameter would be less than one-third that of a comparable open-cycle machine, and less than one-sixth of the heat transfer surface would be required in the regenerator.[1] While the walls of the containment loop would have to be thicker to withstand the increased pressure, the effect of increased wall thickness on weight is largely offset by the smaller overall dimensions. Thus, as long as the reduced dimensions do not adversely affect component efficiencies, the rotating equipment and regenerator of a pressurized closed Brayton cycle power system should be appreciably smaller and lighter than those of its open-cycle counterpart.

Offsetting these weight reducing factors are the additional ducting required in the closed cycle, the thicker blades to withstand the added bending loads of the higher density gas, and the need for heat exchangers to (1) add heat to the working fluid from the external heat source and (2) remove heat from the working fluid to the external heat sink.

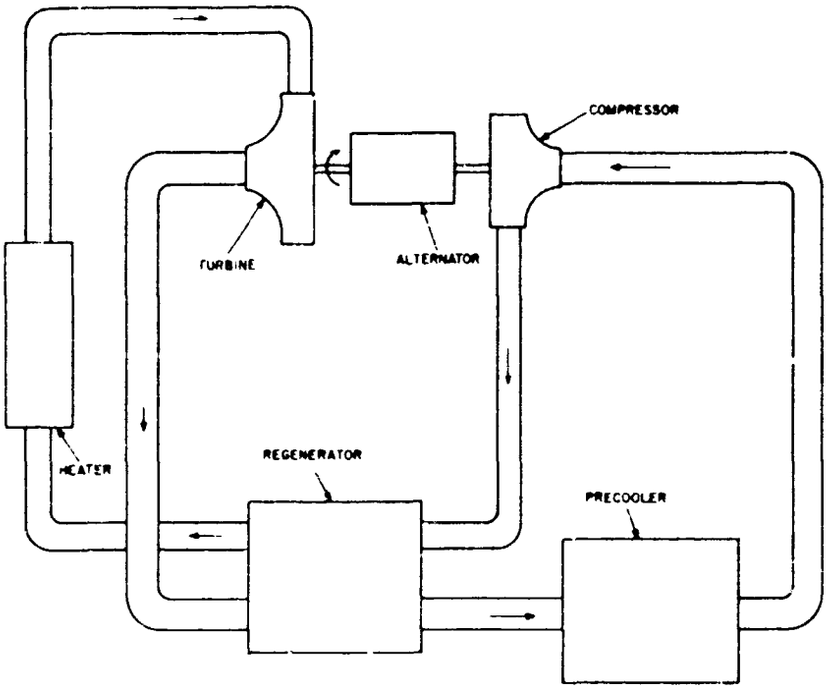

Figure 2. Closed Brayton Cycle Components.[4]

Since the working fluid is completely isolated from the heat source, combustion gases of an externally-fired burner cannot enter the loop interior. The loop interior is thus protected from corrosion or contamination by combustion products. If a chemically inert working fluid is selected in preference to air, oxidation will also not be a problem. These considerations make feasible regeneration at turbine exhaust temperatures well above those at which combustion-gas corrosion of regenerator surfaces would be a problem in an open-cycle system.

The size of a closed Brayton power system is significantly affected by the choice of a working fluid, aside from pressure level considerations. Low molecular weight gases have good heat transfer properties, permitting a reduction in the size of heat exchangers. High molecular weight gases permit the use of fewer turbomachinery stages, thus reducing the size of the compressor and turbine. The effect of gas molecular weight on the heat transfer area and the number of turbomachinery stages is shown in Figures 3 and 4. Helium is seen to require the smallest heat transfer surface and the largest number of stages. A mixture of a light and a heavy gas with an average molecular weight M requires the same number of machinery stages as a pure gas with molecular weight M. However, the heat transfer properties of the mixture are appreciably better than those of the pure gas. Hence, a helium-xenon mixture can be devised which has both favorable turbomachinery and favorable heat transfer characteristics, as shown in Figure 5.

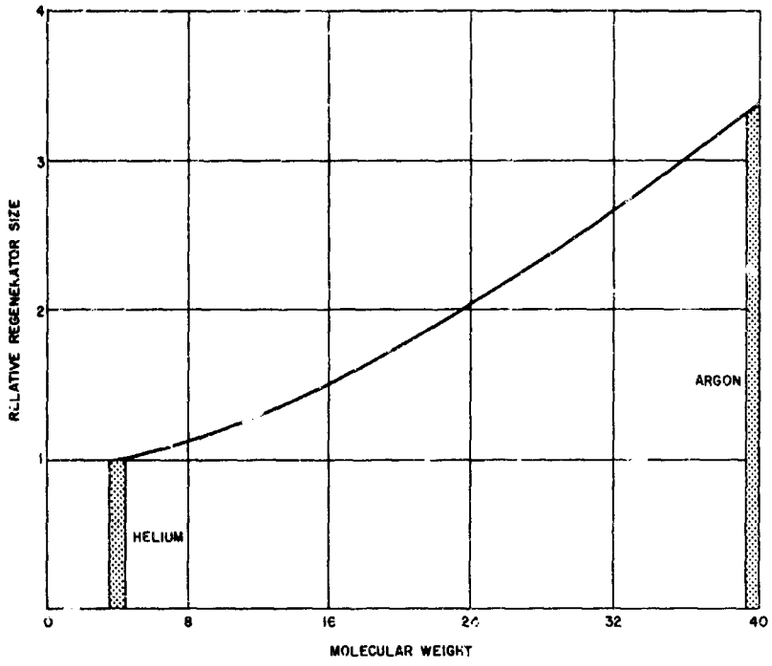

Figure 3. Effect of Gas Molecular Weight on Heat Transfer Area.[8]

Current Status

A number of closed-cycle gas turbines for electrical power generation have been in operation since 1956, although none are operating in the United States. These plants are rated at 2000 to 17,000 kw, with overall efficiencies of 25 to 30 percent.[2] A 20,000-hp closed Brayton cycle system with a helium working fluid at 1000 psi was studied in connection with the Maritime Gas-Cooled Reactor Program.[3] A 500-kw prototype of a ground-transportable nuclear power plant (ML-1) has operated on the Brayton cycle with nitrogen as the working fluid. NASA currently has a 10-kw closed-cycle gas turbine under development which utilizes a mixture of helium (He) and xenon (Xe) as the working fluid.[4,5] A 3-kw Brayton Cycle Demonstrator (BCD) operating on argon has been fabricated and tested.[6,7]

Since the NASA 10-kw generator is representative of the latest closed Brayton cycle technology, its principal features will be described. The He-Xe working fluid used has the same atomic weight as krypton.

The cycle diagram is shown in Figure 6. Gas enters a single-stage radial-inflow turbine at 1600°F and 44 psi. The impeller tip diameter is 5 in., and the turbine efficiency is 0.87. The turbine drives an alternator and a radial compressor with an impeller tip diameter of 4.25 in. and an efficiency of 0.80. (These turbine and

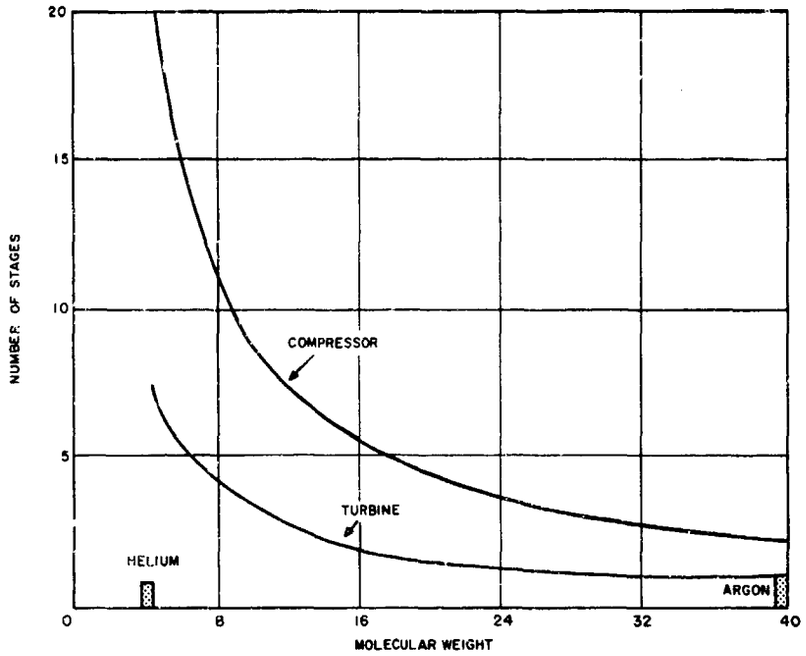

Figure 4. Effect of Gas Molecular Weight on Number of Turbomachinery Stages.[8]

compressor efficiencies have been exceeded in actual tests.) The turbine-compressor-alternator unit has an overall diameter of 13 in. and an overall length of 23 in. About one-half of the length is taken up by the alternator. The shaft speed is 36,000 rpm. The turbine exhaust gas at 25 psi and 1230 °F enters a regenerator of 95 percent effectiveness, where heat is transferred to the compressor discharge gas. Regenerator dimensions are 8.5 x 20 x 20 inches. The turbine exhaust then flows through the waste heat exchanger, where heat is rejected to an external heat sink, lowering the gas temperature to 80 °F. The gas enters the compressor at 23 psi and is discharged at 44 psi. The compressor discharge stream flows successively through the regenerator and heat source heat exchanger, thereby increasing its temperature to the turbine inlet value of 1600°F.

The cycle thermal efficiency (ratio of gross shaft power to heat added to the working fluid) is 36 to 37 percent. The overall system efficiency, which takes into account friction, leakage, alternator efficiency, and system electrical power needs, is 24 to 27 percent. (These are predicted figures; the complete system has not yet been tested.) Estimated component weights are given in Table III. Other cycle parameters are given in Table IV. The power level can be varied with little change in system efficiency by an increase or decrease of gas pressure. This would be accomplished by venting the system to high- or low-pressure auxiliary tanks. However, response of such a system will probably be sluggish.

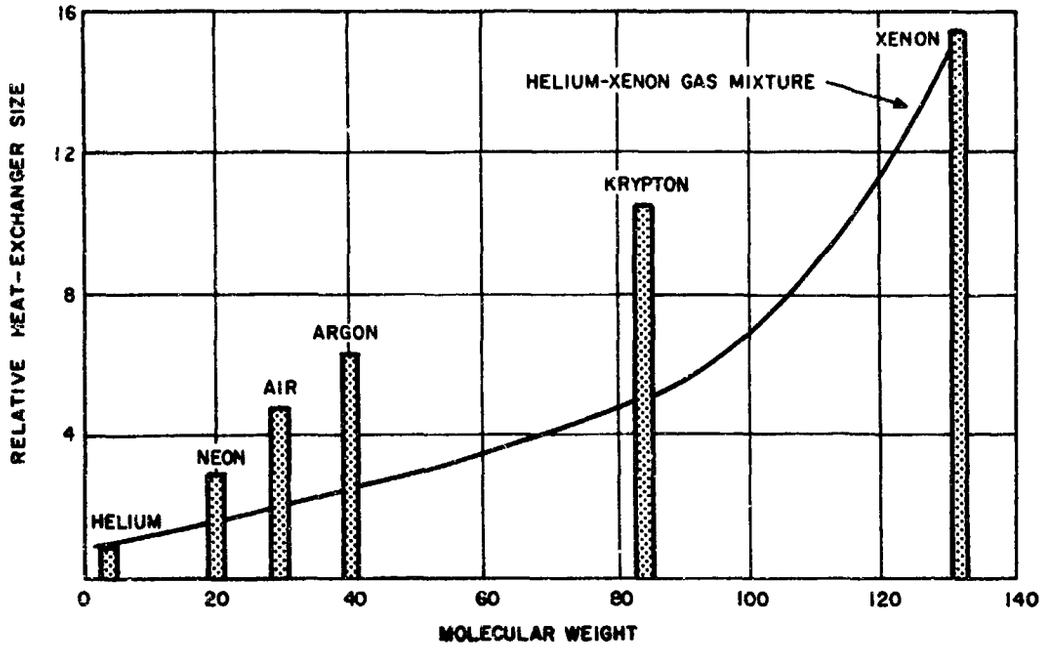

Figure 5. Heat Transfer Area Requirement for Helium-Xenon Mixtures.[9]

TABLE III. ESTIMATED COMPONENT WEIGHTS FOR 10-KW NASA CLOSED BRAYTON CYCLE GENERATOR [5]

Component	Weight (lb)	Specific Weight (lb/kw)
Turbine & Compressor	65	6.5
Alternator	60	6.0
Regenerator	240	24.0
Ducting	85	8.5
Structure & Insulation	180	18.0
Controls	270	27.0
Source Heat Exchanger	107	10.7
Sink Heat Exchanger	60	6.0
Total	1067	106.7

The rotating machinery is supported by hybrid gas bearings. During starts and stops, hydrostatic (externally pressurized) bearings are used. During normal operation, the bearings are supported hydrodynamically. Oil-lubricated ball bearings could also be used.

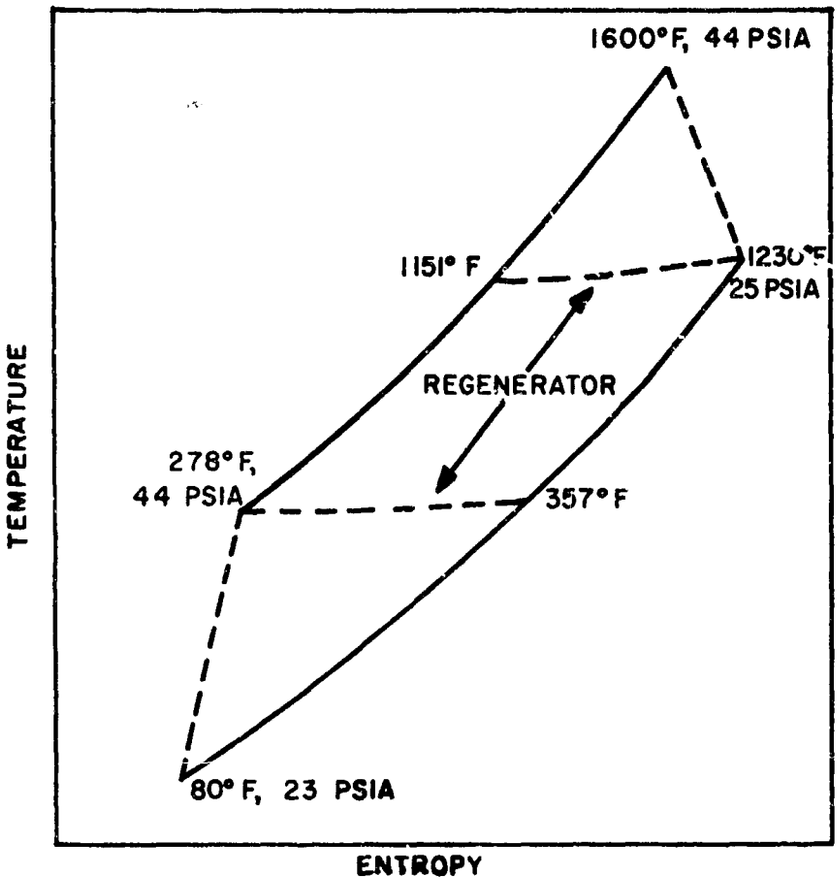

Figure 6. Temperature-Entropy Diagram for NASA Closed Brayton Cycle.

The NASA 10-kw unit is hermetically sealed. If shaft power rather than electrical power were desired, leakage of working fluid through the shaft seal would be a matter of concern. However, seal technology is in a state of rapid advancement, and it should be possible to limit leakage rates to tolerable values.

Application to Aircraft Propulsion

The NASA closed Brayton cycle generator will be used as the basis for determining the characteristics of a closed Brayton cycle aircraft propulsion system. A shaft power rather than a generator output, a system that derives its energy from an externally fired combustion system and utilizes an atmospheric heat sink, and a shaft output of 500, 1500, or 10,000 hp are desired.

TABLE IV. NASA CLOSED BRAYTON CYCLE PARAMETERS[5]

Net Alternator Power		10.00 kw
Radiator Coolant Pump Power		0.22 kw
Control Power		0.42 kw
Gross Alternator Power		10.64 kw
Alternator Efficiency		92 %
Net Shaft Power		11.58 kw
Parasitic Losses:		1.76 kw
Alternator Windage	0.88 kw	
Bearing Friction	0.54 kw	
Seal Leakage	0.34 kw	
Gross Shaft Power		13.34 kw
Cycle Efficiency		37 %
Cycle Input Power		36.1 kw
System Efficiency		27 %
Working Fluid		Helium-xenon mixture
Molecular Weight of Working Fluid		83.8
Shaft Speed		36,000 rpm
Compressor Compression Ratio		1.90
Turbine Expansion Ratio		1.75
Regenerator Effectiveness		0.95

The various factors involved in the evaluation of the system are discussed below.

Specific Weight

The first step in the evaluation is to determine the system efficiency for a shaft power system. From Table IV, the cycle input power is 36.1 kw. The net shaft power is equal to the gross shaft power minus the bearing and seal losses, or, from Table IV, 13.34 kw-0.88 kw = 12.46 kw = 16.7 hp. The system efficiency for a shaft power system (without alternator, controls, and radiator coolant pump) is then 12.46 kw/36.1 kw = 0.345.

The next step is to consider design changes necessary for operation at desired shaft power levels. The power level of the existing NASA system can be increased from 16.7 to 114 hp by increasing the peak gas pressure from 44 psia to 300 psia. This can be accomplished with no change in the size or weight of components, with the exception of the regenerator, since the turbomachinery scroll (and presumably other gas-containing components) has already been designed for a pressure of 300 psia.

The regenerator's size and weight will increase, however, because while the heat to be transferred increases in proportion to the mass flow rate and hence the gas pressure p, the heat transfer coefficient increases as p^x. The exponent x usually has a value between 0.6 and 0.8, depending on the geometry of the heat transfer surface. If the value 0.6 is used for x (which is characteristic of interrupted-flow heat transfer surfaces), the regenerator

surface area and hence the weight will vary as $p^{0.4}$. Then the regenerator weight will increase by a factor of 2.16 in order for the NASA system to produce 114 hp when the pressure is raised to 300 psi.

With further increases in the gas pressure, the power output will undergo a proportional increase without changes in the size of components other than the regenerator. However, the system weight will now increase, in order that gas pressures above 300 psi may be safely contained. A peak cycle pressure of 1300 psia was assumed, which corresponds to a net shaft output of 500 hp. It was assumed that in the power range of 114 to 500 hp, the turbine, compressor, and ducting weights would increase in proportion to the power, the regenerator weight would increase as the $(\text{power})^{0.6}$, and the weight of structure and insulation would remain constant.

In order to develop shaft power in excess of 500 hp, the required increase in mass flow rate must be accommodated by an increase in the flow area rather than pressure, and so the size as well as the weight of system components will increase. Consequently, the system efficiency, which was assumed to be constant up to 500 hp, can be expected to increase somewhat. It was assumed that at power levels above 500 hp, the weight of all components would increase directly as the power and inversely as the system efficiency.

In Table V, the specific weight of major closed Brayton cycle components is given as a function of shaft power. Peak cycle pressure and system efficiencies are also indicated. These data were derived on the basis of the above assumptions and the characteristics of the NASA closed Brayton cycle 16.7-hp shaft power plant.

TABLE V. SPECIFIC WEIGHT OF CLOSED BRAYTON CYCLE COMPONENTS

Shaft Power - hp	16.7	114	500	1500	10,000
Maximum Cycle Pressure - psia	44	300	1300	1300	1300
System Efficiency - %	34.5	34.5	34.5	36.0	38.0
Component	Specific Weight (lb/hp)				
Compressor & Turbine	3.89	0.57	0.40	0.38	0.36
Regenerator	14.35	4.54	2.51	2.41	2.28
Ducting	5.09	0.75	0.75	0.72	0.68
Structure & Insulation	10.78	1.58	0.36	0.35	0.33
Total	34.1	7.44	4.02	3.85	3.66

It is evident from Table V that the regenerator is the heaviest system component. This is a consequence of the high regenerator effectiveness of 0.95. Appreciable weight savings can be realized by using a smaller regenerator

effectiveness, but at the expense of system efficiency. Figure 7 shows the variation of regenerator specific weight and system efficiency with regenerator effectiveness.* Figure 7 indicates that the regenerator weight can be reduced by a factor of 5, at the expense of a 15-percent loss of system efficiency, by a reduction in the regenerator effectiveness from 0.95 to 0.80.

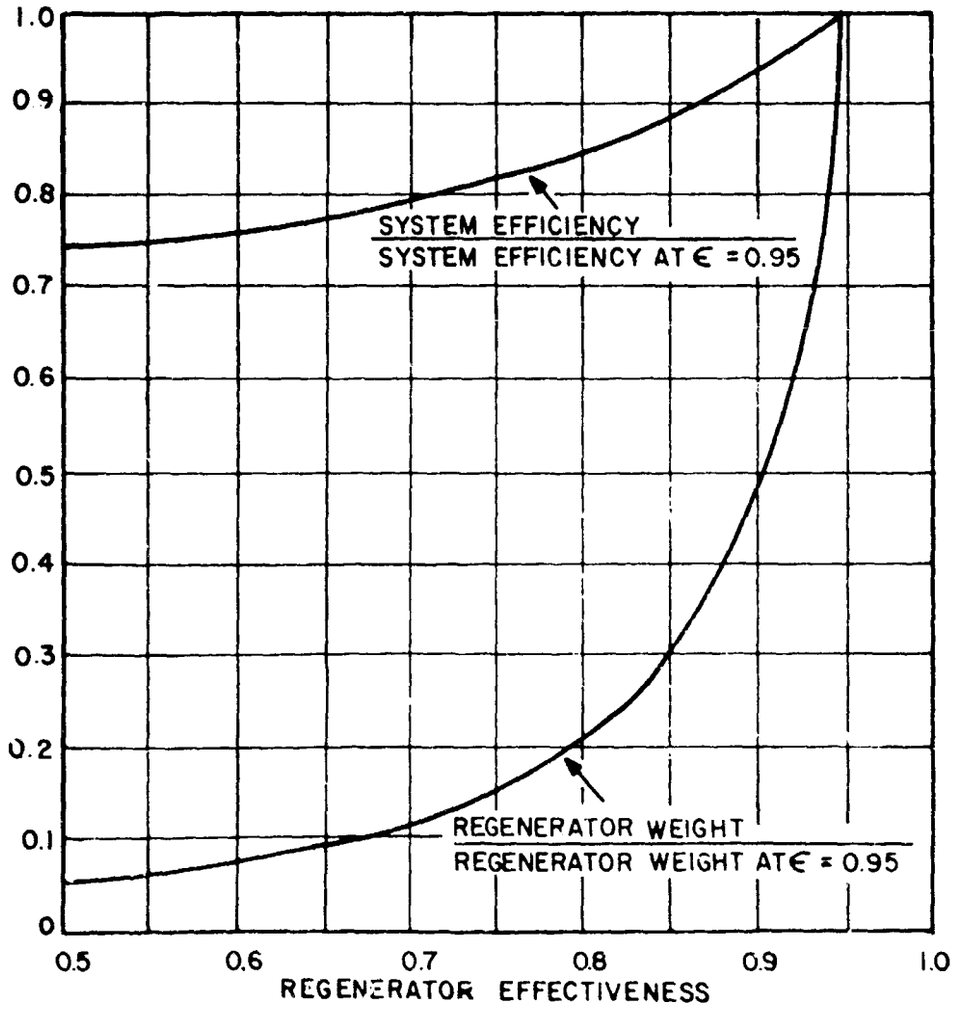

Figure 7. Effect of Regenerator Effectiveness on Regenerator Weight and System Efficiency.

*The efficiency curve of Figure 7 is taken from Figure 3-35 of Reference 8. The regenerator weight is assumed to vary with regenerator effectiveness in the same manner as the heat transfer surface area.

In addition to the components which have already been considered, the closed Brayton cycle engine requires a heat input system and a heat rejection system. A detailed analysis of these systems is given in Appendix II. The heat input system that was used as the basis for analysis of all energy conversion systems operating with an external, combustion-fired heat source is shown in Figure 8. Atmospheric air is compressed and flows through a preheater, where its temperature is increased by a specified amount. The heated air then enters a combustor, where its temperature is further increased by the injection and combustion of fuel. The hot combustion gas passes through a heat exchanger (heater), where a portion of its thermal energy is transferred to the energy converter. The combustion gas then enters the preheater, where additional thermal energy is transferred to the incoming compressed air. The combustion gas which leaves the preheater flows through a turbine, producing just enough shaft power to drive the compressor, and then is discharged into the atmosphere. The preheater is necessary to insure that most of the energy released by combustion of fuel can be transferred to the energy converter in the heat exchanger.

Possible heat sinks for waste heat that is rejected by the energy converters include: the compressed air of the heat input system, the fuel supply, and

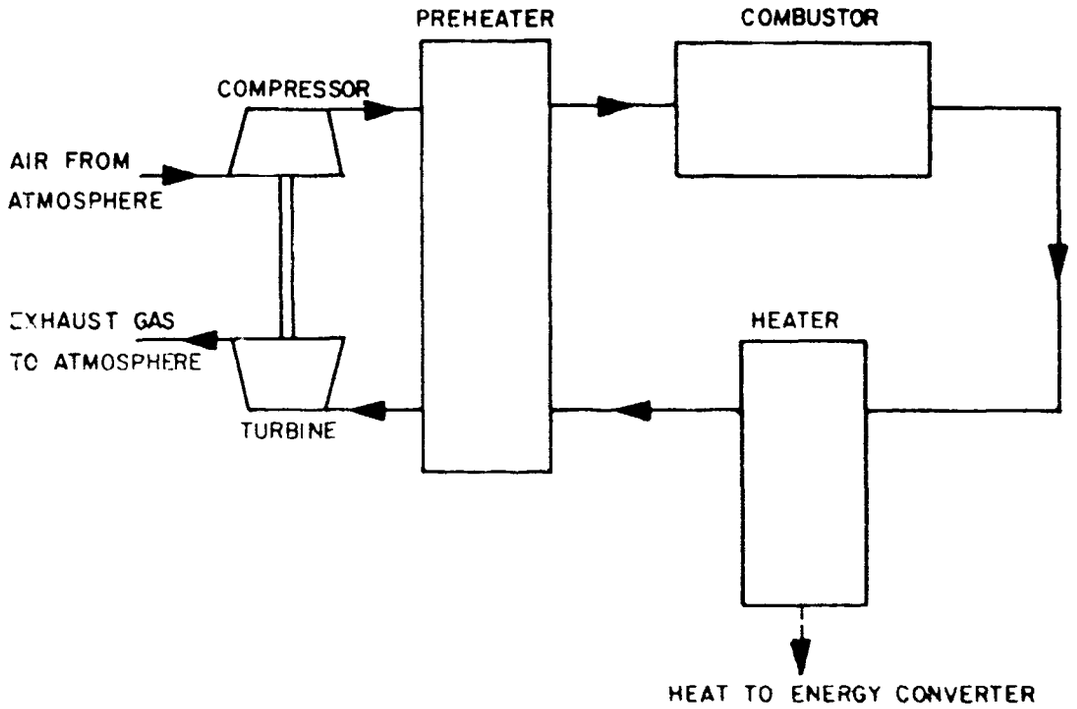

Figure 8. External, Combustion-Fired Heat Input System.

the helicopter rotor downwash air. In Appendix II, it is shown that the use of the fuel supply as a heat sink is not feasible and that a heat rejection system using the rotor downwash as a heat sink is much lighter than one that uses the compressed air of the heat input system. The waste heat exchanger that couples the energy converter to the rotor downwash air is referred to here as the cooler.

The minimum Brayton cycle temperature as shown in Figure 6 is too low to permit rejection of cycle waste heat to an air heat sink. Therefore, for the purpose of analyzing the heat input and rejection systems, a minimum cycle temperature of 190 °F was used. The maximum cycle temperature was taken to be 2040 °F. Since the ratio of maximum to minimum absolute cycle temperatures is the same as that for the Brayton cycle of Figure 6, cycle efficiencies should also remain about the same. The compressor discharge and turbine exit temperatures shown are based upon a pressure ratio of 3, a compressor efficiency of 0.83, and a turbine efficiency of 0.87. The pressure ratio of 3 was used rather than the value of 1.90 of the NASA closed Brayton cycle because the optimum regenerator effectiveness for aircraft application was expected to be less than 0.95.*

The combustion efficiency is defined here as the ratio of the heat transferred to the energy converter in the heater to the heat released in the combustor. For minimum fuel consumption, the combustion efficiency should be as close to unity as is feasible. Figure 9 shows how the combustion efficiency varies with the temperature increase of air in passing through the combustor and the temperature difference between compressed air and combustion gas at a given point in the preheater. It is desirable to have a high combustion efficiency for minimum fuel consumption, a large combustor temperature rise to minimize the heater size and weight, and a large preheater temperature difference to minimize preheater size and weight. Since weight is a predominant factor in the evaluation of energy conversion systems, a 300 °F temperature difference across the preheater and a combustor temperature rise of 3000 °F were specified. From Figure 9, the combustion efficiency is then 0.9. A combustor temperature rise of 3000 °F corresponds to about 18 percent excess air beyond that needed for stoichiometric combustion.

Cycle temperatures used in sizing the heater and preheater of the heat input system and the cooler for heat rejection to rotor downwash air are indicated in the approximate temperature–entropy diagram of Figure 10. The entropy in this figure is total entropy flow rate (i.e., entropy per unit mass times mass flow rate), so that the area under a constant pressure curve between two temperature limits ($\int TdS$) represents the actual rate of heat transfer accompanying a given temperature change. The maximum preheater temperature is 2000 °F, and the maximum temperature in the combustor and the heater is 4700 °F.

*As Figure 3-35 of Reference 8 shows, the optimum pressure ratio increases with a decrease in regenerator effectiveness.

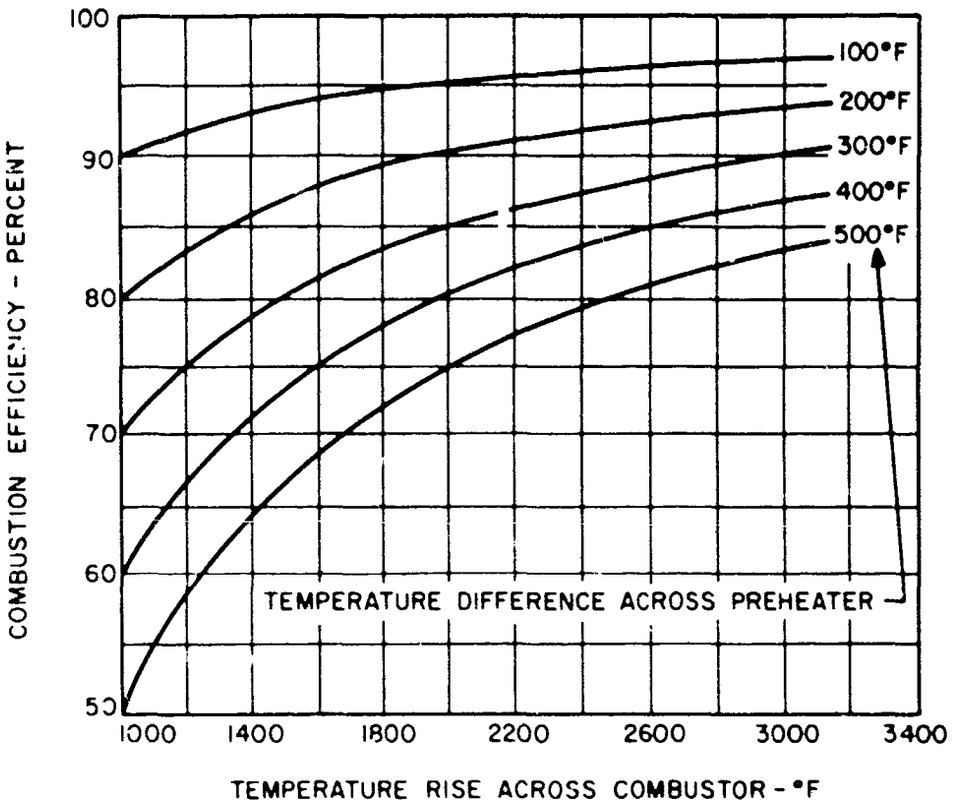

Figure 9. Effect of Combustor Temperature Rise and Temperature Difference Across Preheater on Combustion Efficiency.

Since the cycle working fluid is pressurized to 1300 psia and is at a peak temperature of 2040 °F for the combustion gas, the heat transfer coefficient of the cycle working fluid is much larger than that of the combustion gas. Therefore, most of the temperature drop between the combustion gas and the cycle working fluid will occur on the combustion gas side of the heater, and the maximum temperature of the heater wall will not be greatly in excess of 2040 °F.

An ambient air temperature of 40 °F was selected in order to present the closed Brayton cycle in its most favorable light. At higher ambient temperatures, the available temperature drop from the cycle working fluid to the air heat sink is reduced, with the result that the cooler weight undergoes a significant increase. If the closed Brayton cycle is not competitive at an ambient temperature of 40 °F, then it will surely not be competitive at higher ambient temperatures.

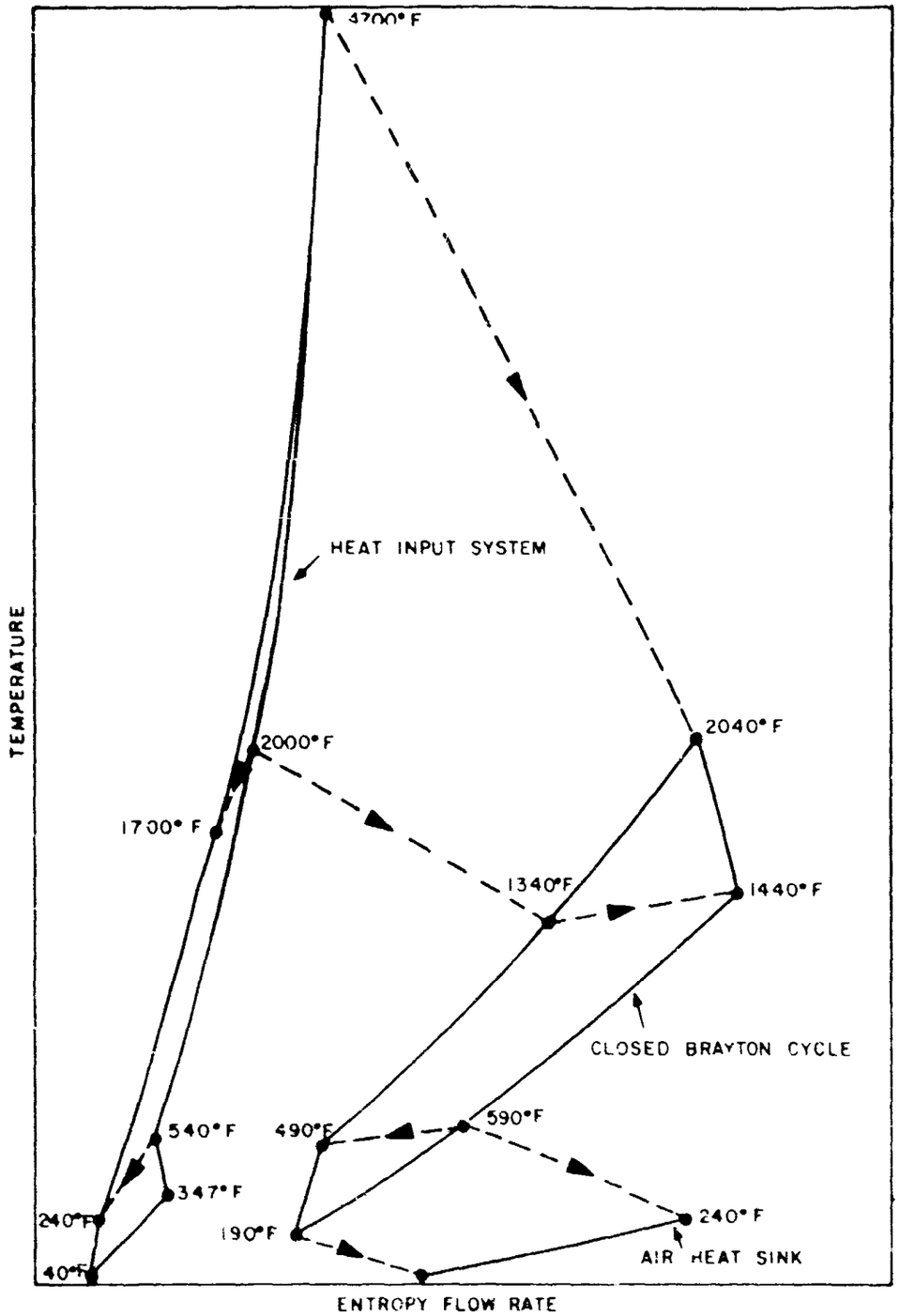

Figure 10. Temperature-Entropy Diagram for Closed Brayton Cycle and for Heat Input and Removal Systems.

Fuel weights were calculated for a 3-hr 5-min mission (the loading schedule is shown in Table II), with the assumption that the specific fuel rate of the closed Brayton cycle varies in the same manner as that of the advanced gas turbines (see Figure 1). A combustion efficiency of 90 percent was used. While the part-load specific fuel rate can be held almost constant in the closed Brayton cycle by varying the cycle pressure level, this mode of controlling the power level was not considered because of the additional weight required for a gas management subsystem and the sluggish transient response which is most probably associated with such a subsystem.

Since the engine regenerator weight increases with the regenerator effectiveness ϵ while the fuel weight decreases with ϵ, there is an optimum ϵ for minimum total system weight. In Figure 11, the engine and fuel weights are shown as a function of regenerator effectiveness at a power level of 1500 hp. Engine weight includes the weight of the heat input system, the closed Brayton cycle converter, and the cooler. The heat transfer surface in the heater, preheater, and cooler was assumed to have a thickness of 3.6 mils. The material in the heater and preheater was assumed to have the density of stainless steel. The cooler material was assumed to be titanium. The weight of the heater of the heat input system and the cooler was assumed to be independent of ϵ, since the increased heat to be transferred as ϵ gets smaller tends to be offset by an increase in the heat exchanger temperature difference. The regenerator weight and the system efficiency variation with ϵ are shown in Figure 7. The weight of other components was assumed to vary inversely as the system efficiency.

Figure 11 shows that the optimum regenerator effectiveness for minimum system weight is about 0.8. Although the weight variation at 500 hp and 10,000 hp is not shown in Figure 11, system weight at these power levels is also a minimum when $\epsilon \cong 0.8$. Consequently, all system characteristics of the closed Brayton cycle were evaluated for a regenerator effectiveness of 0.8. The system efficiency is then 30.9 percent, and the overall efficiency (system efficiency times combustion efficiency) is 27.8 percent.

Significant reductions in system weight are believed to be possible with continued development of the closed Brayton cycle. The following factors were used in estimating the weight of future closed Brayton cycle power plants:

1. The NASA regenerator design is based on a plate-fin heat exchanger configuration with a Stanton number (to which the heat transfer coefficient is proportional) of 0.014 at a Reynolds number of 1000. The configuration shown in Figure 10-71 of Reference 10 has a Stanton number of 0.030. With this configuration, the regenerator heat transfer area would be halved. While the friction factor accompanying the increase in the Stanton number goes up by a factor of almost 5, the overall pressure drop can be held constant by a comparable reduction in regenerator length and an increase in lateral dimensions. On the basis of these observations, it is concluded that future regenerators can be 50 percent lighter than the current NASA design.

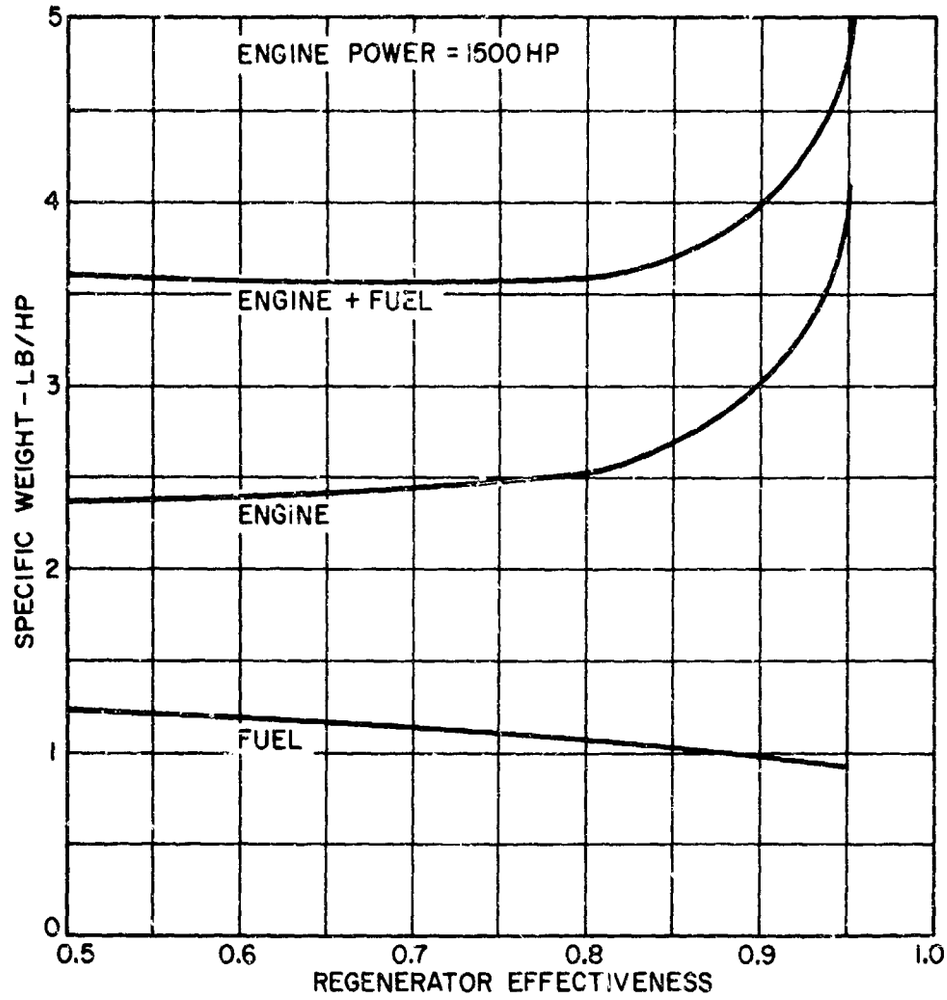

Figure 11. Variation of Engine and Fuel Specific Weights With Regenerator Effectiveness.

2. While the NASA engine is designed for at least a 10,000-hr lifetime with absolute reliability, Army aircraft requirements are less stringent, calling for a 5000-hr life with 1500 hrs between overhauls. If the system is designed for shorter life and if high-strength refractory alloys are used, substantial reductions in system weight can be expected. Ducting weight can be reduced appreciably by more compact packaging of system components. For example, by mounting the regenerator directly to the turbine exhaust duct, the heavy high-temperature duct currently used between the turbine and regenerator could be eliminated. Advances in the use of lightweight composite

structural materials and fiber-wound pressure-containing structures can yield further weight reductions.

A technique which has been successfully used in European closed-cycle gas turbines, but which has not been extensively used in the United States, may also lead to substantial reductions in weight as well as cost.[2] In this technique, high-temperature casings and ducts utilize a thin liner of high-temperature alloy which serves as a gas flow passage. The space between the liner and the outer wall is filled with insulation and is also permeated with pressurized gas. Thus, the liner is not stressed, and the relatively cool outer casing is relied upon for containment of the pressurized gas. The outer wall may then be thinner and fabricated from less expensive alloys than would be the case if the wall were at the temperature of the hot gas.

Through the use of such considerations, it was estimated that the specific weights of the turbine, compressor, ducting, and structure could be reduced to 25 percent of the values based on the current NASA design.

3. Since compressor and turbine efficiencies are currently in or approaching the range of 85 to 90 percent, it was felt that improvements in the efficiency of these components in future years will be relatively small. Therefore, it was assumed that overall system efficiencies and fuel consumption would not change significantly in future years.

4. Current weights of the heat input and heat rejection systems are based on rough calculations rather than actual hardware (see Appendix II). Meaningful projections of future weight would require design studies in depth beyond that which could be accomplished within the scope of the survey effort. Therefore, it was assumed that the weight of future heat input and heat rejection systems is the same as that calculated for the current systems.

The specific weight of current and future closed Brayton cycle converters, as determined from the above considerations, is summarized in Figures 12 and 13 at power levels of 500, 1500, and 10,000 hp. In Figure 12, the weight of the major components which comprise the engine is shown. In Figure 13, the weight of the complete energy conversion system is shown. The specific weights of the transmission were taken to be the same as those given in Table II for the advanced open-cycle gas turbines. For comparative purposes, the specific weight of the advanced open-cycle gas turbines is also given.

The data apply for the working fluid that has been proposed for the NASA closed Brayton cycle—a helium-xenon mixture with a molecular weight of 83.8. Although a closed Brayton cycle employing nitrogen as the working fluid would be preferable to helium-xenon for aircraft applications, the nitrogen system would be appreciably heavier. From Figure 4, the number of turbomachinery stages is 50 to 100 percent greater for nitrogen. Also, the lower density and specific heat of nitrogen would require larger flow rates and hence larger and heavier flow ducts.

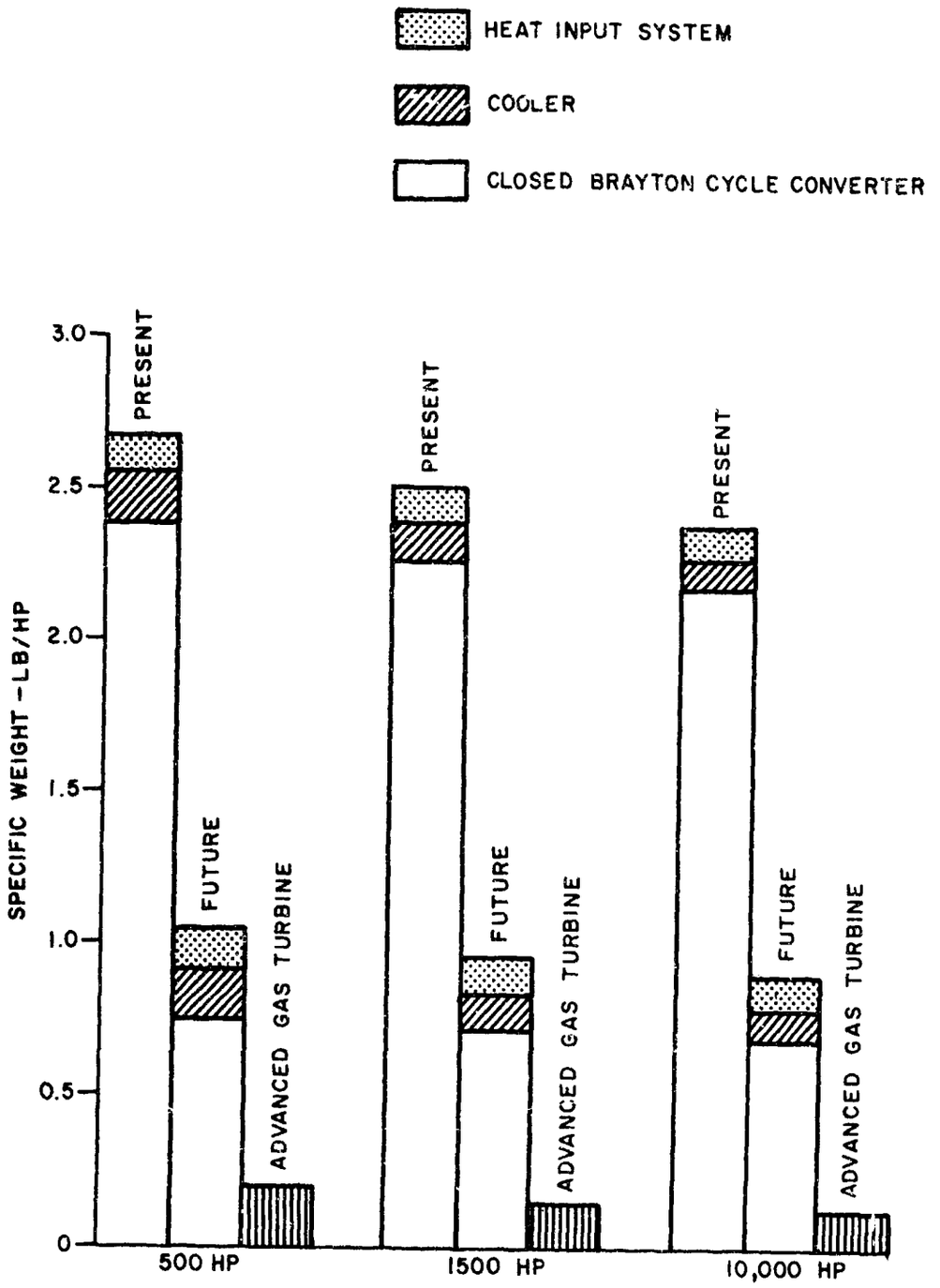

Figure 12. Specific Weight of Closed Brayton Cycle Engines.

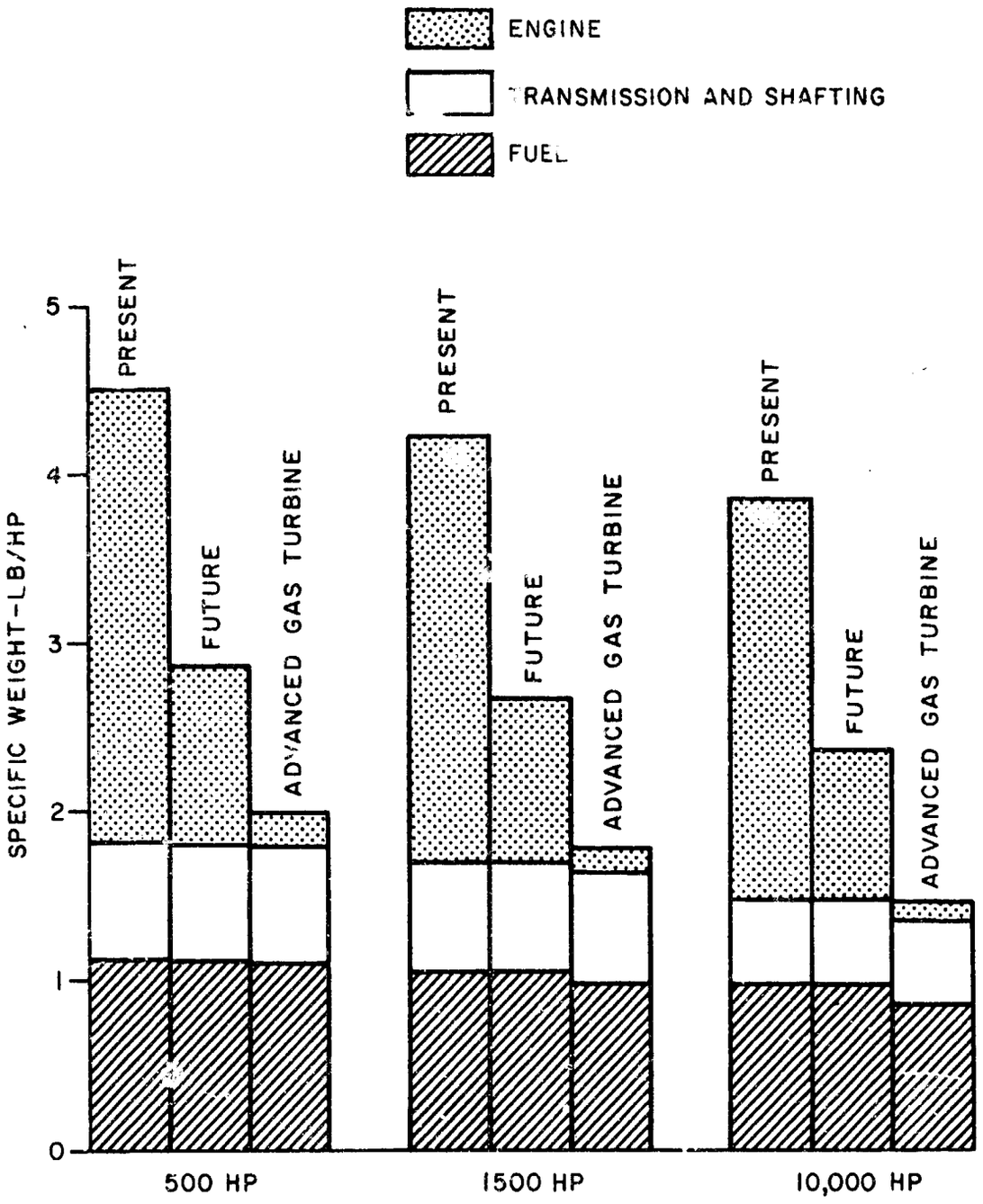

Figure 13. Specific Weight of Closed Brayton Cycle Shaft Power Systems.

Figure 12 shows that the specific weight of a closed Brayton cycle engine of the future is about 5 times that of the advanced open-cycle gas turbines. The heat input system and the cooler represent a small fraction of total engine weight, primarily because of the large temperature difference in the heater and the relatively high system efficiency.

According to Figure 13, fuel consumption for closed Brayton cycle systems and for advanced open-cycle gas turbines are comparable. However, total system weight (engine plus transmission and shafting plus fuel for the 3-hr 5-min mission defined in Table II) is about 50 percent greater for a future closed Brayton cycle system, because of the heavier closed Brayton cycle engine.

Specific Volume

The volume occupied by the closed Brayton cycle engine is in large measure dependent on the compactness of packaging of the various engine components, which is a matter of detailed design. Estimates have been made of the volume of major engine components, the sum of which can serve as a rough indication of total engine volume. These major engine components include: the turbine-compressor, the regenerator, the heater and preheater of the heat input system, and the cooler.

The turbine-compressor and regenerator volumes are based on actual data for the NASA closed Brayton cycle generator, modified to account for the effect on volume of larger shaft power outputs. The turbine-compressor volume was assumed to be constant to 500 hp and proportional to the power thereafter. The regenerator volume was assumed to increase as the shaft power to the 0.4 power to 500 hp and to be proportional to the power thereafter. Since the NASA closed Brayton cycle system has a regenerator effectiveness ϵ of 0.95 while a regenerator effectiveness of 0.8 is appropriate for an aircraft mission, the regenerator volume was reduced by the ratio of the heat transfer area required for $\epsilon = 0.8$ to that required when $\epsilon = 0.95$. (The ratio of heat transfer surface area to regenerator volume was assumed to be the same in both cases.) Using the above assumptions, the specific volume of the turbine-compressor was found to be 0.00176 ft^3/hp over the range of 500 hp to 10,000 hp. The specific volume of the regenerator was found to be 0.00322 ft^3/hp over the same power range.

The volume of the heater and preheater of the heat input system and of the cooler was obtained from previously determined values of the heat transfer surface area by assuming a constant surface area-volume ratio of 200 ft^2/ft^3. The specific volume of the combined heat input system and cooler was found to be 0.00649 ft^3/hp at 500 hp, 0.00494 ft^3/hp at 1500 hp, and 0.00422 ft^3/hp at 10,000 hp.

The specific volume for the entire engine (turbine-compressor, regenerator, heater, preheater, and cooler) is given in Table VI, along with the specific volume of the advanced gas turbines.

TABLE VI. SPECIFIC VOLUME OF CLOSED BRAYTON CYCLE ENGINES

	Shaft Power (hp)		
	500	1500	10,000
	Specific Volume (ft^3/hp)		
Advanced Gas Turbine	3.24×10^{-3}	$3.01\text{-}3.24 \times 10^{-3}$	$1.57\text{-}3.15 \times 10^{-3}$
Closed Brayton Cycle	11.39×10^{-3}	9.93×10^{-3}	9.21×10^{-3}

Although the indicated volumes for the closed Brayton cycle could undoubtedly be reduced, the extent of such reductions would require a detailed design study. Such a study was beyond the scope of the survey effort. Table VI indicates that the total volume of Brayton cycle components is three or more times that of the advanced gas turbines. The actual volume taken up by the engine will be greater than the sum of its component volumes, to an extent which will be determined by the geometrical arrangement of the components in the closed-cycle loop. Therefore, it is reasonably certain that the volume of the closed-cycle engine will be considerably greater than that of the advanced gas turbine.

Cost

Since the NASA system upon which the analysis of the closed Brayton cycle has been based is still in the early stages of development, firm cost data do not exist. The closed Brayton cycle has more components and the heat input system operates at higher material temperatures than the advanced gas turbine; both of these factors will tend to increase costs. On the other hand, the low pressure ratio of the closed Brayton cycle calls for fewer turbomachinery stages, which is an evident cost-reducing factor. Also, it may be possible to reduce costs by the use of internally insulated ducts with relatively cool external walls. When all these observations are taken into consideration, it appears likely that a closed Brayton cycle shaft power system will cost considerably more than a comparable advanced gas turbine.

Reliability

The objective of the NASA closed Brayton cycle program is a system which will function reliably in space for 10,000 hrs, and considerable progress has been made in pursuit of this goal. For aircraft application, system reliability would be expected to be lower than for the contemplated NASA space application. Whereas the NASA system generates electrical output and is hermetically sealed, an aircraft shaft output system could not be hermetically sealed. A shaft must of necessity penetrate the working fluid containment structure, and an effective dynamic seal must be provided at the penetration point. Also, the use of sealed joints at various locations in the system would be probable to facilitate access to components which require maintenance. Assuming that

such problems were successfully solved in the course of development, the reliability of closed Brayton cycle systems should be comparable to that of gas turbines.

Sensitivity to Environment

Like the open-cycle gas turbine, the closed Brayton cycle engine is moderately sensitive to ambient temperature and pressure. As the ambient temperature increases and/or the ambient pressure decreases, the heat removal capability of the cooler is reduced, which in turn will result in reduced power output and system efficiency. Performance of the closed Brayton cycle engine should not be adversely affected by acceleration and vibration. System performance will be affected by the presence of environmental foreign matter such as sand and dust to the same extent as the open-cycle gas turbine. The problem, however, is one of injection of such material by the compressor of the heat input system rather than by the main engine compressor.

Part-Load Characteristics

The efficiency of the closed Brayton cycle engine can be maintained almost constant over a wide variation in load by varying the compressor inlet pressure in proportion to the load.[2] However, high-pressure gas storage and low-pressure accumulation tanks are needed for the required changes in pressure. Also, a relatively sluggish response to load changes appears likely with this method. It has been assumed here that load changes would be achieved by variations in shaft speed and maximum cycle temperature, and that part-load characteristics would be similar to those of the advanced gas turbines.

Transient Response

Because of the thermal inertia of the various heat exchangers used in the closed Brayton cycle (i.e., the regenerator, heater, preheater, and cooler), the system should respond to transients more slowly than the open-cycle gas turbine.

Structural Considerations

The closed Brayton cycle power plant consists of several individual components that are joined together by connecting ducting, in contrast to the more or less integral structural package that is characteristic of the open-cycle gas turbine. Special consideration must be given to the relative location of the various components, whether the mounting points should be located on the engine components or on the interconnecting ducting, and to the vibration characteristics of the entire structure.

Critical Problem Areas

The most critical problem area with respect to applicability to Army aircraft propulsion is the excessive weight of the closed Brayton cycle engine. The

projected future engine weight would have to be reduced by about a factor of 5 in order to be comparable to the weight of the advanced gas turbines. It is not apparent how such a large reduction in engine weight could be achieved.

The principal problem area that would be associated with actual development of a closed Brayton cycle engine for aircraft propulsion is in the realm of high-temperature materials. A large temperature rise is necessary in the combustor in order to have a high combustion efficiency. A consequence of the large combustor temperature rise is the small fraction of excess air that is available for cooling hot combustor parts. Also, the heater will be exposed to hot combustion gases at maximum surface temperatures of 2100°F or higher. The development of heat exchanger materials that could withstand this environment for extended periods of operation constitutes a major engineering challenge.

Conclusions

Fuel consumption of the closed Brayton cycle engine is comparable to that of the advanced gas turbines. However, engine weight is a factor of 5 or more greater than that of the advanced gas turbines. Formidable materials problems are associated with the large combustor temperature rise and the high heater temperature. It is therefore concluded that the closed Brayton cycle engine is not now competitive with advanced gas turbines, nor is it likely to be competitive in the future.

RANKINE CYCLE

The Rankine cycle is a series of cyclic processes for generating shaft power from thermal energy in which the working fluid is present in both liquid and vapor phases. As Figure 14 shows, basic cycle components are: a boiler, a turbine, a condenser, and a pump. Liquid entering the boiler at maximum cycle pressure is converted by the addition of heat to a saturated or superheated vapor. The vapor expands through the turbine to minimum cycle pressure, generating shaft power in the process. After leaving the turbine, the vapor is condensed by the removal of heat in the condenser. The liquid condensate is then pumped up to maximum cycle pressure, after which it once again enters the boiler. When the vapor temperature upon leaving the turbine is appreciably higher than the condensing temperature, a regenerator may be added for the purpose of transferring heat from the turbine exit vapor to the liquid which leaves the pump prior to entering the boiler.

Maximum cycle efficiency is obtained by boiling at the highest practical temperature and condensing at the lowest practical temperature. Since the fluid pressure is directly related to temperature during phase changes, the vapor pressure/temperature relationship of a particular working fluid will strongly influence cycle temperature limits. Other factors which affect the upper temperature limit are the strength of the containment structures, the compatibility of the working fluid with the containment material, and the thermal stability of the working fluid.

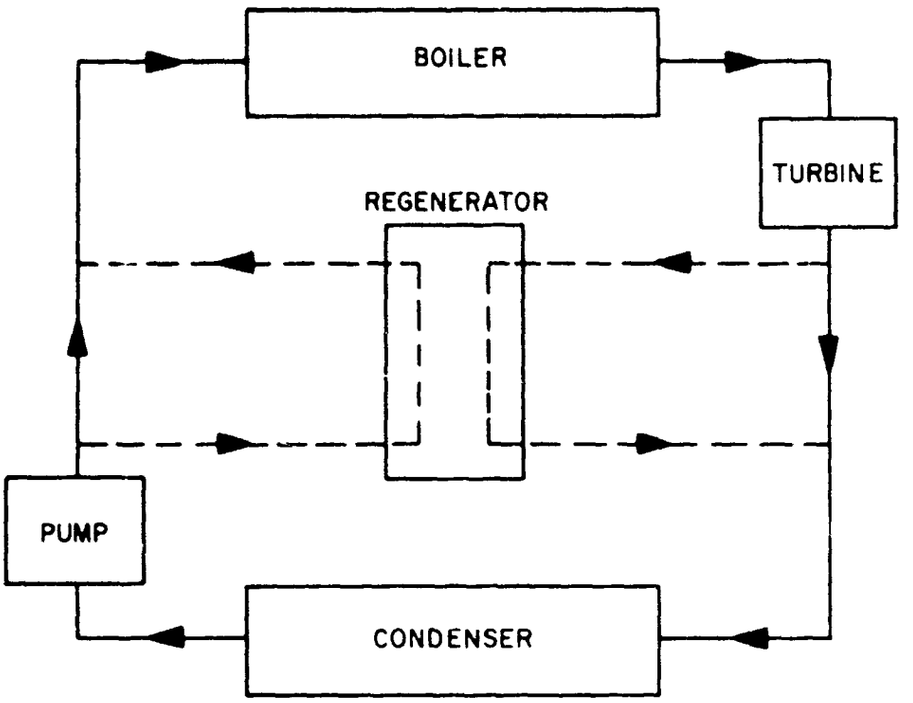

Figure 14. Rankine Cycle Components.

Current Status

Rankine cycles employing potassium, mercury, and organic working fluids have been under development for space application. The organic Rankine cycle is also being given consideration for terrestrial applications. While water is the predominant working fluid in large, central-station electrical generating plants, it has not been favorably considered for weight-sensitive applications because of high vapor pressure at moderate boiling temperatures and low condensing temperature and pressure needed for reasonably efficient performance. Significant features of the potassium, mercury, and organic Rankine cycles are presented below.

Potassium Cycle[12,13]

A potassium Rankine system to provide 300 to 400 kw of electricity in space in conjunction with a reactor heat source is under joint development by the AEC and NASA. This system is of interest because its condensing temperature (≈1200°F) is

high enough to permit waste cycle heat to be rejected in space by radiation from a relatively small surface area. The heat rejection radiator tends to be the dominant component of a space power system with respect to size and weight.

No fundamental problems have been encountered with this system, and its basic technology is well established, based on the use of refractory alloy structural materials. Cycle component technology is also well advanced.

The boiler is of the shell-and-tube type, and it is fabricated from tantalum alloy. Potassium liquid flows through the tubes, while hot lithium (the reactor coolant) flows over the outside of the tubes. Superheated potassium vapor at 150 psi and 2100°F emerges from the boiler. The shell diameter is about 9 in. and the tube length is about 7-1/2 ft. The boiler is rated at 3300 thermal kw, and it weighs about 300 lb.

The superheated potassium vapor flows through a 9-10 stage turbine which is coupled to an alternator. The turboalternator assembly rotates at 19,200 rpm and is supported by potassium-lubricated film bearings. The alternator is rated at 450 kw. The turbine efficiency is 80 to 82 percent, and the alternator efficiency is 90 to 91 percent. The turbine is fabricated from molybdenum alloy. The turboalternator weighs 1350 to 1800 lb, about 75 percent of which is attributable to the alternator.

Vapor leaves the turbine at 5.4 psi and 1220°F and enters the condenser, where it is condensed and subcooled, leaving at 985°F and 3.4 psi. The condenser weighs about 240 lb. The condensate then enters the boiler feed pump, where it is pressurized to boiler inlet requirements. The pump is an electromagnetic type with no moving parts. It weighs about 300 lb, has an efficiency of about 18 percent, and requires an electrical input of 10.8 kw.

Net output is about 350 electrical kw, and overall cycle efficiency is about 17 percent. The specific weight of the major components is given in Table VII. Since the system design characteristics are still in the process of being fully defined, the data of Table VII are quite approximate.

TABLE VII. SPECIFIC WEIGHT OF 350-KW POTASSIUM RANKINE CYCLE COMPONENTS

Component	Specific Weight (lb/kw)
Boiler	0.86
Turbine	0.96 - 1.29
Alternator	2.9 - 3.9
Condenser	0.68
Pump	0.86
Total, less Alternator	3.36 - 3.69

Mercury Cycle [14-18]

Efforts have been under way for about 12 years to develop a mercury Rankine cycle space power system. Current efforts are concentrated on the 35-kw SNAP-8 system. Throughout its history, the mercury boiler has represented the most formidable development problem. The problem arose primarily from difficulty in getting mercury to wet the boiler heat transfer surfaces. The possible contamination of mercury with the organic fluid lubricant used in the SNAP-8 bearings has been thought to be a contributor to this problem, as well as the presence of gaseous impurities. The problem is now believed to have been solved by the use of tantalum boiler tubes, since mercury readily wets this material.

The mercury boiler is a tube-in-shell type, with 7 composite-wall tubes (tantalum inside, stainless steel outside) about 30 ft long inside a shell about 6 in. in diameter. The shell-tube structure is coiled into a 4-ft-diameter helix. Mercury is boiled and superheated in the tubes by the flow of hot NaK (the reactor coolant for SNAP-8) through the shell. Superheated mercury at 1290°F and 240 psi leaves the boiler. The boiler is rated at about 500 thermal kw and weighs about 500 lb (including 17 lb of mercury and 107 lb of NaK).

Upon leaving the boiler, the mercury vapor enters a 4-stage turbine which is coupled to a 56-kw alternator. The turboalternator assembly rotates at 12,000 rpm, and it has organic-liquid-lubricated ball bearings. The turbine efficiency is 58 percent, and the alternator efficiency is about 87 percent. The turboalternator assembly weighs 702 lb, of which about 25 percent is attributable to the turbine.

The mercury vapor leaving the turbine enters the condenser at 670°F and 14.5 psi, where it is condensed and subcooled to 490°F at 14.1 psi. The condenser is of the tube-in-shell type, with the mercury condensing in 73 tapered tubes. The heat of condensation is removed by the flow of NaK on the shell side. The condenser is 50 inches long, with a maximum diameter of 7 inches. The condenser weight is about 140 lb (which includes 20 to 30 lb of mercury and 30 lb of NaK).

Condensate enters the centrifugal boiler feed pump, where its pressure is increased to 358 psi prior to entering the boiler. The pump is motor-driven, and the pump-motor assembly is supported by organic-liquid-lubricated ball bearings. The assembly is 2-1/2 ft long, is 8 in. in diameter, and weighs 150 lb. Overall efficiency is 14 percent, and the input power is 2.8 kw.

The output is 26 electrical kw, and the overall cycle efficiency is about 7 percent. SNAP-8 growth potential studies have shown that through component design modifications and system optimization, the net power output can be increased to 103 kw at an overall efficiency of 17 percent. The specific weight of current SNAP-8 components is given in Table VIII, along with an estimate of total component specific weight for the upgraded system.

TABLE VIII. SPECIFIC WEIGHT OF SNAP-8 POWER CONVERSION COMPONENTS

Component	36 kw SNAP-8		103 kw SNAP-8
	Specific Weight (lb/kw)		
Boiler	13.9	11.1 (without NaK)	
Turbine	4.9		
Alternator	14.6		
Condenser	3.9	3.1 (without NaK)	
Pump	4.2		
Ducting & Insulation	5.3		
Structure	9.7		
Total, less Alternator	41.9	38.3 (without NaK)	9.4 (est.)

Organic Cycle[20-23]

The use of an organic fluid in the Rankine cycle is of interest for the following reasons: the maximum cycle temperature is 650° to 700°F and the working fluid is noncorrosive, thus permitting the use of relatively inexpensive construction materials such as mild steel; in the turbine, the vapor always expands into the superheated region, eliminating blade erosion problems associated with moisture impingement; at low-power levels, volume flow rates are relatively large, permitting the design of reasonably efficient turbines; with a regenerator, overall cycle efficiencies are in the range of 12 to 20 percent, even at low power levels.

The organic working fluid is subject to thermal decomposition, but studies have confirmed that for peak cycle temperatures not in excess of 700°F, operating times of thousands of hours can be expected without adverse effects on system performance. For power levels up to 10 to 20 kw, Dowtherm A (a eutectic mixture of biphenyl and phenyl ether) is a preferred working fluid. The freezing point of Dowtherm A is 54°F. At higher power levels and where a lower freezing point is desired, the compound pyridine (also called CP-32) may be preferable. CP-32 freezes at -40°F. Both Dowtherm A and CP-32 are flammable.

Two representative organic Rankine power systems will now be described. The first is a space power plant called ORACLE. A 12-kw breadboard model of ORACLE has been built and tested. The second is a 150-kw ground power plant for which a preliminary design has been completed.

1. ORACLE

The most significant feature of ORACLE is that it employs a jet condenser, which permits condensation pressures as low as 0.1 psia. Overall system efficiency at a condensing pressure of 0.1 psi is about twice that for

systems which condense at 1 psi. In the jet condenser, vapor at low pressure mixes with subcooled liquid at high pressure. In the process, the vapor condenses and its pressure is raised to 50 to 60 percent of the inlet liquid pressure. The 12-kw ORACLE operates at a condensing pressure of 0.5 psi. A second unit rated at 6 kw with a condensing pressure of 0.1 psi is planned.

In the once-through boiler, Dowtherm liquid is converted to saturated vapor at 700°F and 107 psi. The vapor flows through a single-stage turbine rated at 14.2 kw shaft power and 73 percent efficiency. The turbine is coupled to a 92-percent efficient alternator operating at 24,000 rpm, and it yields 12 electrical kw. The vapor leaves the turbine at 599°F and 0.65 psi, and it enters a 90-percent effectiveness regenerator. After leaving the regenerator, the vapor at 297°F and 0.59 psi enters the jet condenser, where it mixes with about ten times the weight flow rate of liquid Dowtherm at 225°F and 145 psi and is condensed. The liquid leaving the jet condenser is at 260°F and 133 psi. It flows through a radiator (needed for a space power plant), where the liquid temperature is lowered to 225°F. The liquid then enters a pump mounted on the turbine shaft, which operates at 65 percent efficiency. About one-tenth of the pump discharge flow at 145 psi flows through the regenerator and then the boiler. The remainder is directed into the jet condenser. The predicted overall system efficiency is 17.7 percent. Actual measured efficiency averaged about 14.2 percent. Weight data for an 18-kw ORACLE for space application are given in Table IX. This system has a condensing pressure of 0.1 psi and an overall system efficiency of about 22 to 24 percent.

TABLE IX. WEIGHT DATA FOR 18-KW ORACLE

Component	Weight (lb)	Specific Weight (lb/kw)
Turbine-Alternator-Pump Assembly	122	6.8
Regenerator	350	19.4
Boiler, Jet Condenser, Pipes, & Insulation	166	9.2
Dowtherm Inventory	269	14.9
Start System	242	13.4
Controls	120	6.7
Structure	40	2.2
Total	1309	72.7

2. 150-kw Power Plant

This system differs conceptually from ORACLE in that it is designed for terrestrial application, CP-32 rather than Dowtherm is used, a jet condenser is not used, and fan-driven air is the heat sink. Boiler exit conditions are 600 psi and 700°F. The condenser conditions are 10 psi and 190°F. The turbine speed is 12,000 rpm. The efficiency of the alternator is 90.5 percent. Overall system efficiency is about 20 percent. With design improvements, efficiency might be increased to 26 percent. The weight of major system components is shown in Table X.

TABLE X. WEIGHT OF 150-KW ORGANIC CYCLE COMPONENTS

Component	Weight (lb)	Specific Weight (lb/kw)
Turbine-Alternator-Pump	400	2.6
Regenerator	150	1.0
Condenser	400	2.6
CP-32 Inventory	240	1.6
Structure & Piping	190	1.3
Air Fan & Motor	230	1.5
Total, less Air Fan & Motor	1380	9.2

Application to Aircraft Propulsion

The application of the potassium, mercury, and organic Rankine cycles to aircraft propulsion will now be considered. Such systems must provide a shaft output in the 500-hp to 10,000-hp range, must be supplied with thermal energy from an externally fired combustion system, and must utilize the atmosphere as a heat sink. The heat input and heat rejection systems are conceptually the same as those used for the closed Brayton cycle.

Potassium Cycle

Factors involved in the evaluation of the potassium Rankine cycle are discussed below.

Specific Weight

Since the alternator efficiency is 90 percent, the net shaft output of the 350-kw potassium Rankine cycle is (350 kw/0.9) (1.341 hp/kw) = 521 hp. Also, the system efficiency for shaft power is 0.17/0.9 = 0.189=18.9 percent. In the NASA system, substantial amounts of shaft power are needed to drive the pump that circulates lithium from the reactor to the boiler, the pumps that circulate NaK between the condenser and the radiator, and the auxiliary pump that circulates NaK for cooling the alternator. The power required for these pumps is estimated to be 70 hp.

For a shaft power application, estimated alternator windage losses of 30 hp would not be present. Therefore, the gross shaft output in an aircraft propulsion system would be increased by 70 hp + 30 hp = 100 hp to a total of 621 hp. The net shaft power would be 610 hp, since about 11 hp is required to drive the boiler feed pump. The cycle efficiency would then increase to 0.189 (610/521) = 0.222 = 22.2 percent.

The estimated specific weight of potassium Rankine cycle components, established from the above considerations, is given in Table XI. It was assumed that the weight of ducting, insulation, and structure was 30 percent of the sum of the boiler, condenser, turbine, and pump weights. The system efficiency was taken to be 23 percent at 500 hp, and the efficiency was assumed to increase with power level in the manner indicated in Table XI. The specific weight at 500 hp was assumed to be the same as that calculated at 610 hp. The specific weight at higher power levels was assumed to vary inversely with cycle efficiency.

TABLE XI. SPECIFIC WEIGHT OF POTASSIUM RANKINE CYCLE COMPONENTS

Shaft Power - hp	500	1500	10,000
System Efficiency - %	23	24	26
Component	Specific Weight (lb/hp)		
Boiler	0.492	0.471	0.435
Condenser	0.388	0.372	0.343
Turbine	0.550	0.526	0.486
Pump	0.492	0.471	0.435
Ducts, Insulation, & Structure	0.576	0.551	0.509
Total	2.50	2.40	2.21

The heat input system is identical to that used for the closed Brayton cycle (see Figure 8), and it operates at a combustion efficiency of 90 percent. The heat rejection system is also the same as that for the closed Brayton cycle.

The temperature distribution in the heater and cooler of the potassium Rankine cycle is shown in Figure 15. In the heater, combustion gas from the heat input system is cooled from 4700°F to 2000°F while heating the potassium working fluid from 985°F to 2100°F. In the process, the potassium passes from the subcooled to the saturation to the superheated state. In the cooler, saturated potassium condenses at 1220°F and then is subcooled to 985°F, while the rotor discharge air is heated from 40°F to 240°F.

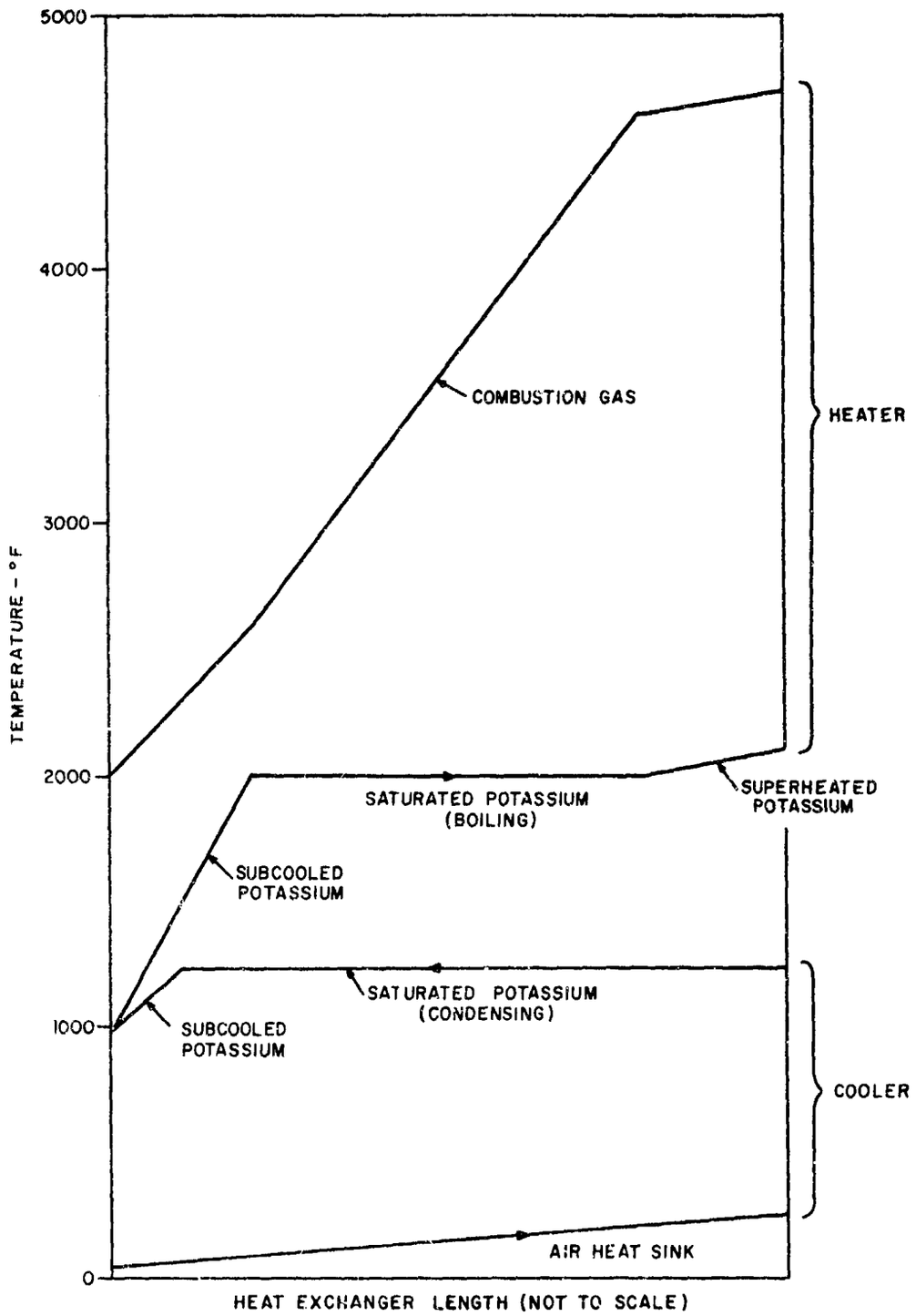

Figure 15. Temperature Distribution in Heater and Cooler of Potassium Rankine Cycle.

The weight of the boiler tubes and shell and of the condenser tubes and shell has already been included in the boiler and condenser weights (see Table XI). The weight of additional gas-side (in the boiler) and air-side (in the condenser) heat transfer surfaces must also be determined. Presumably, this added surface will be achieved by the use of external fins on the boiler and condenser tubes.

Since the heat transfer properties of the potassium working fluid are markedly different in the subcooled, boiling, and superheated regimes, each of these regimes must be treated separately in the evaluation of gas-side heat transfer requirements. In the subcooled and boiling zones, the heat transfer coefficient of the potassium is 30 to 50 times that of the combustion gas. Thus, most of the temperature drop will occur in the combustion gas, and the heat transfer surface temperature will be within 100° F of the potassium temperature.

In the superheater section, the heat transfer coefficient is about the same as the value of 100 Btu/hr-ft^2 -°F that has been assumed for the combustion gas. In order for the wall temperature in the superheat zone to be within 100° F of the potassium temperature, the heat transfer coefficient of the combustion gas will have to be reduced to about 4 Btu/hr-ft^2 -°F. The reduction would be accomplished by the use of a large flow area and hence low velocities on the gas side of the boiler tubes in the superheating section.

The specific weight of the added heat transfer surface area on the gas side of the boiler tubes was found to be 0.027 lb/hp at 500 hp. 0.026 lb/hp at 1500 hp, and 0.024 lb/hp at 10,000 hp. No added gas-side heat transfer surface is required in the superheater section. The extra gas-side heat transfer surface area was considered to be part of the heat input system.

The weight of the remainder of the heat input system (compressor, turbine, combustor, and preheater) was assumed to be proportional to the air flow rate through the system. Since the combustor inlet and outlet temperatures are the same as those of the closed Brayton cycle heat input system, the flow rate is proportional to the heat input rate, which in turn varies inversely as the cycle efficiency. Hence, the remainder of the heat input system's specific weight at a given power level was obtained by multiplying the specific weight of corresponding components in the closed Brayton cycle heat input system by the ratio of the closed Brayton and Rankine cycle efficiencies. These specific weights were found to be 0.108 lb/hp at 500 hp, 0.103 lb/hp at 1500 hp, and 0.0955 lb/hp at 10,000 hp.

The air-side heat transfer surface of the condenser was assumed to constitute the cooler. Cooler specific weights were estimated by assuming that all of the potassium condensate was at 1220°F. The error induced by this assumption is small, since only about 6 percent of the heat removed is removed from the subcooled potassium. The source of cooling air is again the rotor downwash. The cooler specific weights were found to be 0.095 lb/hp at 500 hp, 0.068 lb/hp at 1500 hp, and 0.056 lb/hp at 10,000 hp.

The system weight data that have just been presented are representative of present-day technology. Considerable reductions in weight and increases in cycle efficiency can be anticipated with future development. First of all, the current NASA potassium Rankine cycle engine development is based on the achievement of a lifetime of 30,000 to 50,000 hrs, while the desired lifetime of Army aircraft engines is about 5000 hrs. The reduced lifetime requirement will permit higher stresses for a specified creep rate, and hence thinner, lighter system components. It is estimated that engine weight could be reduced by a factor of 2 because of the reduced lifetime requirement. An additional weight reduction factor of 2 is believed to be likely as future development proceeds, as a consequence of reduced design conservatism, lower permissible reliability of an aircraft power plant in comparison with a space power system, and the use of lightweight composite materials and internally insulated walls.

The efficiency of future systems can be improved by about 15 percent by lowering the condensing temperature from 1220°F to 1100°F. System efficiencies are then 26.6 percent at 500 hp, 27.8 percent at 1500 hp, and 30.0 percent at 10,000 hp. However, the condensing pressure is then only 2.4 psi, which will probably require a larger, lower pressure drop condenser. Also, a larger boiler which develops more superheat to prevent excessive wetness in the turbine exhaust vapor will probably be needed, along with a larger cooler because of the reduced condensate-air temperature difference. The increase in Rankine cycle component weight resulting from these factors will tend to offset the weight reductions resulting from the improvements in cycle efficiency. Hence, the weights of the boiler, condenser, turbine, pump, and cooler are assumed not to be affected by the drop in condensing temperature. However, the weight of the heat input system was assumed to vary inversely with the increased cycle efficiencies that result from the lower condensing temperature.

Fuel consumption was calculated using the cycle efficiencies that have been proposed above for present and future technology and for a combustion efficiency of 90 percent. Part-load specific fuel consumption and the mission load-time schedule were assumed to be the same as those of the advanced gas turbines (see Figure 1 and Table II). Transmission weights were also assumed to be the same as those of the advanced gas turbines (see Table II).

Figures 16 and 17 give the specific weight of potassium Rankine cycle engines and complete propulsion systems (engine, transmission, and fuel) at power levels of 500 hp, 1500 hp, and 10,000 hp. Specific weights for current and future technology systems, as established from the above considerations, are compared with the advanced gas turbine specific weights.

From Figure 16, the projected future weight of the potassium cycle engine is more than three times the weight of a comparable advanced gas turbine. The potassium engines would still be substantially heavier than the

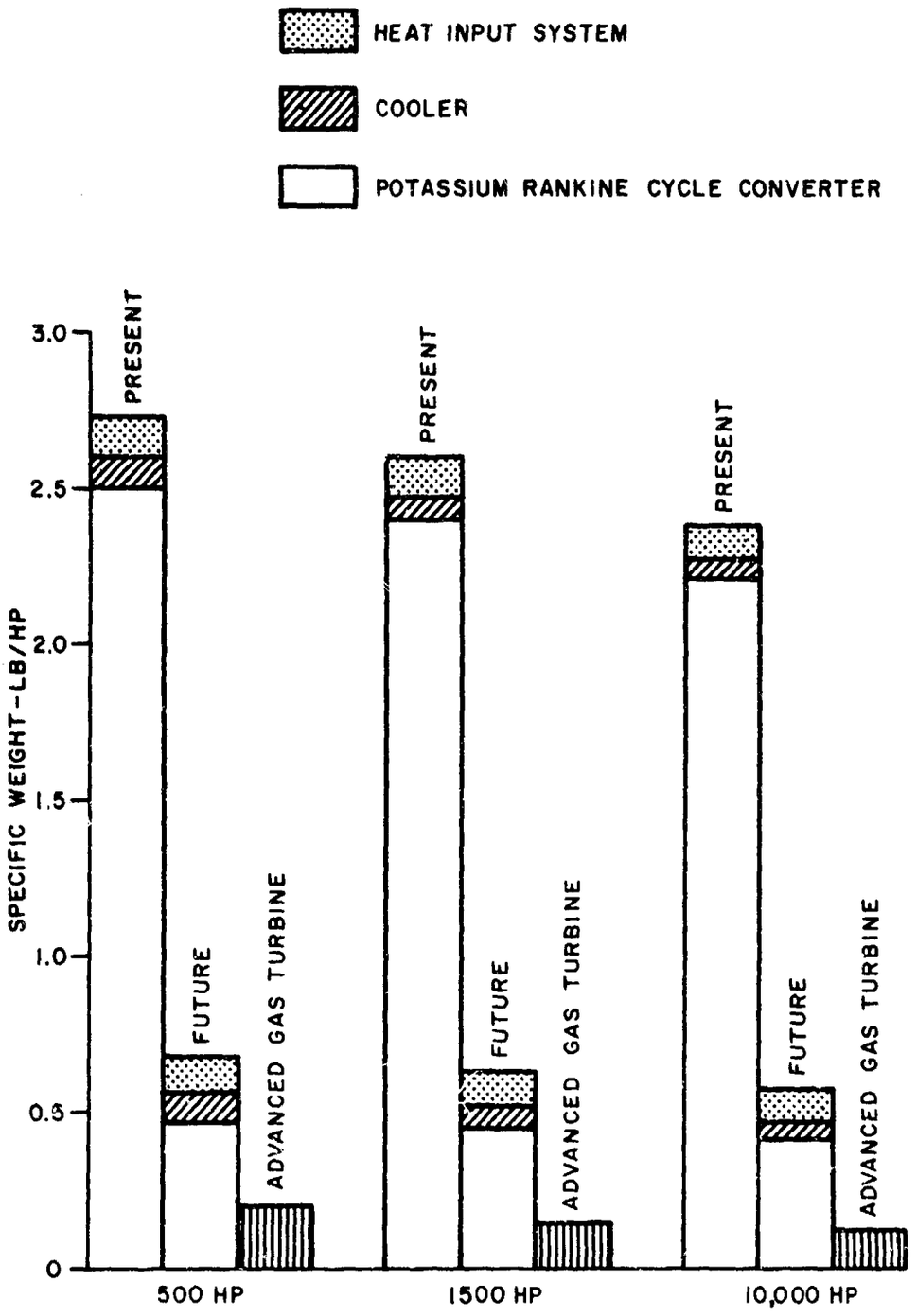

Figure 16. Specific Weight of Potassium Rankine Cycle Engines.

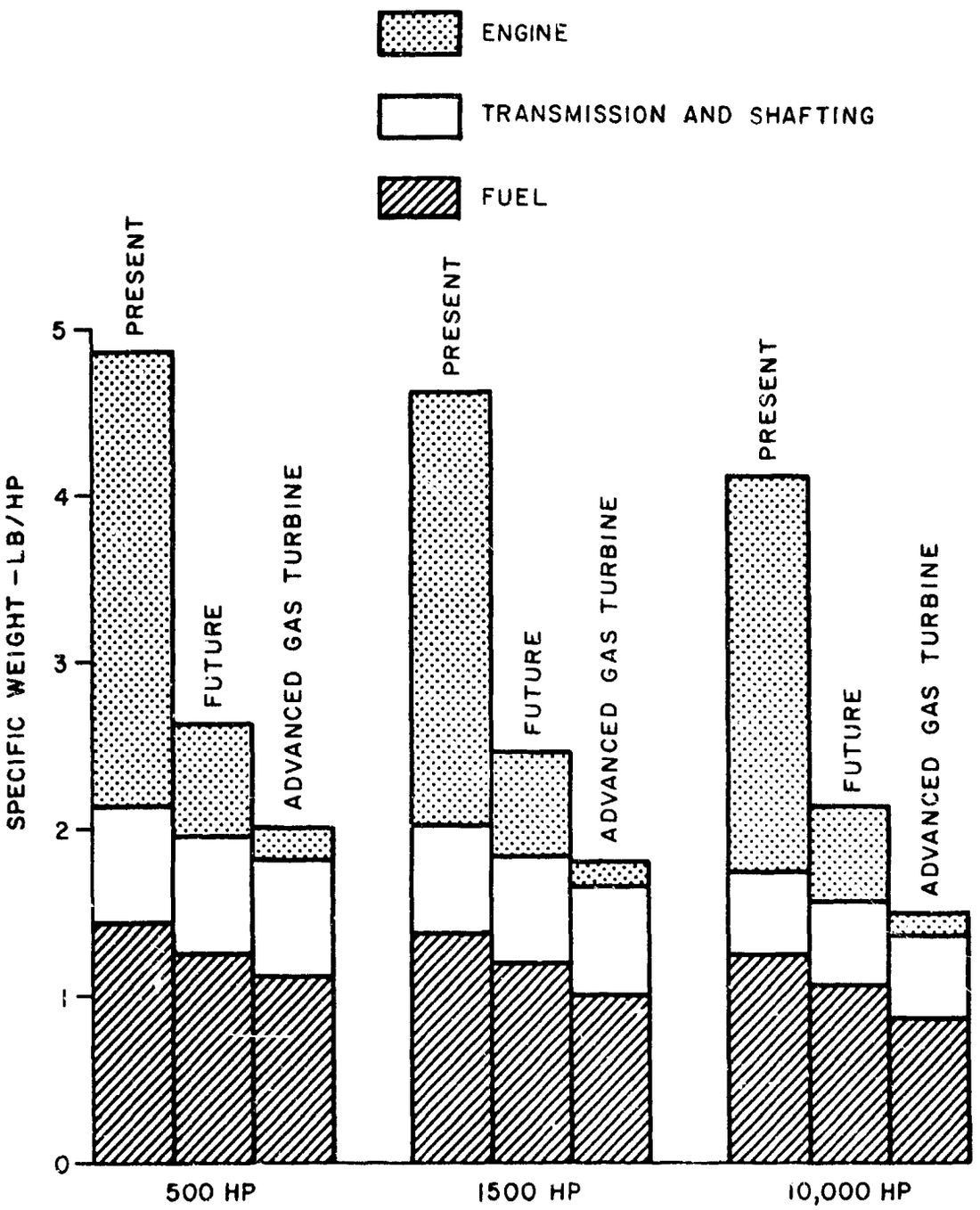

Figure 17. Specific Weight of Potassium Rankine Cycle Shaft Power Systems.

advanced gas turbines even if the heat input system and cooler weights were negligible. From Figure 17, the total projected future potassium Rankine cycle system weight (engine, transmission plus shafting, and fuel) exceeds that of the advanced gas turbines by about 30 percent. Fuel consumption of the future potassium systems is 15 to 20 percent greater than that of the advanced gas turbines. Most of the difference in total system weights, however, results from the heavier potassium Rankine cycle engine.

Specific Volume

The volume of the major potassium Rankine cycle engine components (boiler, condenser, pump, and turbine) was calculated from NASA data for the 350-kw generator. The total component volume of 14.95 ft^3 was divided by the shaft output of 610 hp obtainable for aircraft application to obtain a specific volume of 0.0246 ft^3/hp. This value was assumed to be constant over the range of 500 hp to 10,000 hp. The specific volume of the heater and preheater of the heat input system and of the cooler was estimated from previously determined values of heat transfer surface area on the assumption that the ratio of heat transfer surface area to volume was 200 ft/ft^3. The specific volume of these components for present engines was found to be 0.00248 ft^3/hp at 500 hp, 0.00234 ft^3/hp at 1500 hp, and 0.00212 ft^3/hp at 10,000 hp. For future engines, the estimated specific volume of these components is 0.00218 ft^3/hp at 500 hp, 0.00212 ft^3/hp at 1500 hp, and 0.00195 ft^3/hp at 10,000 hp.

The total specific volume of the boiler, condenser, pump, turbine, heater, preheater, and cooler is given in Table XII, along with the specific volumes of the advanced gas turbines. The actual engine volume will also include the volume of ducting plus the combustor, turbine, and compressor of the heat input system, and it will also depend on how the various components are arranged with respect to each other. Hence, the potassium engine volume given in Table XII represents a lower limit.

It is evident from Table XII that the volume of the potassium Rankine cycle engines substantially exceeds that of the advanced gas turbines.

Cost

Since the potassium Rankine cycle is in the developmental stage, meaningful cost data are not available. However, the extensive use of molybdenum- and tantalum-base alloys in high-temperature components indicates that engine cost will be relatively high.

Reliability

Since a prime design objective of the NASA potassium Rankine cycle generator is 30,000 to 50,000 hrs of unattended operation in space, the fully developed system should be highly reliable. Individual components have successfully operated for thousands of hours, but long-term operation

TABLE XII. SPECIFIC VOLUME OF POTASSIUM RANKINE CYCLE ENGINES

	Shaft Power (hp)		
	500	1500	10,000
	Specific Volume (ft^3/hp)		
Advanced Gas Turbine	3.24×10^{-3}	$3.01\text{-}3.24 \times 10^{-3}$	$1.57\text{-}3.15 \times 10^{-3}$
Potassium Rankine Cycle-Present	27.1×10^{-3}	26.9×10^{-3}	26.7×10^{-3}
Potassium Rankine Cycle-Future	26.8×10^{-3}	26.7×10^{-3}	26.6×10^{-3}

has not yet been demonstrated for a complete system. For a nonhermetically sealed system such as will be required for a shaft power rather than electrical power output, seals could present a problem. However, considerable progress has been made in the development of dynamic seals which provide a positive pumping head in a direction opposite to that of the leakage flow. Any small leak which resulted in the loss of potassium at a significant rate would result in power plant failure. Since hot liquid potassium will burn upon exposure to air, a leak would also introduce a fire hazard.

Sensitivity to Environment

Since the temperature difference between the condensing potassium and the coolant air is on the order of 1000°F, the condensation rate will be relatively insensitive to changes in ambient temperature. However, the mass flow rate of air in the heat input system, and hence the heat input rate, will be affected by ambient temperature in the same manner as for a gas turbine. The heat input system will be affected by sand and dust ingestion to the same extent as a gas turbine. Engine operation should be relatively insensitive to vibration. However, acceleration could produce adverse pressure gradients in the liquid leg of the condenser, which in turn could have a disruptive effect on overall engine operation.

Part-Load Characteristics

Rankine cycle electrical generators are usually designed to operate at constant output, with the electrical output being divided between the actual load requirement and parasitic resistors. The resistors dissipate electrical energy that is not utilized by the load. Part-load characteristics of a shaft power potassium Rankine cycle have not been explored. For purposes of estimating fuel consumption, it was assumed that part-load characteristics were similar to those of the advanced gas turbines.

Transient Response

Transient response of the potassium Rankine cycle should be poorer than that of gas turbines because of the thermal inertia associated with the heat input and removal systems, as well as greater weight and hence thermal inertia of the other cycle components.

Structural Considerations

The Rankine cycle consists of several components connected by intervening ducting rather than a single integral structure such as is characteristic of the gas turbine. The mechanical design will therefore have to consider whether the ducting or the components should bear structural support loads. Also, the condenser should be so located as to facilitate cooling with rotor downwash air.

Critical Problem Areas

The development of shaft seals that will limit shaft leakage of working fluid to tolerable values and which exhibit long-term reliability is a critical problem in the development of any shaft power output Rankine cycle. The question of two-phase flow stability under varying acceleration also requires careful evaluation. The development of materials suitable for use in the heater at temperatures in excess of 2100° F and in a combustion gas environment represents another critical problem area. Perhaps the most critical problem is the excessive size and weight of the potassium Rankine cycle engine. It is not apparent how engine weight can be reduced sufficiently to be competitive with the advanced gas turbines.

Conclusions

The fuel consumption and engine weight of the potassium Rankine cycle currently exceed those of advanced gas turbines. This situation will also persist in the foreseeable future. None of the other characteristics offer any advantage over those of gas turbines. Therefore, it is concluded that the potassium Rankine cycle is not presently competitive with the advanced gas turbine, and it is not likely to be competitive in the foreseeable future.

Mercury Cycle

Factors involved in the evaluation of the mercury Rankine cycle are discussed below.

Specific Weight

The mercury Rankine cycle generator that is currently under development by NASA has a net electrical output of 36.2 kw and an overall efficiency of 7.07 percent. The gross electrical output is 55.9 kw in order to meet the power needs of the various pumps that are required for circulating

coolant through the alternator, for circulating NaK to the waste heat radiator, for system controls, and for alternate windage losses.

For the aircraft propulsion application under consideration, the alternator, the electrical controls, and the auxiliary pumps are not needed. Since the alternator efficiency is 87 percent, the gross shaft output is 55.9 kw/0.87 = 64.4 kw = 86.4 hp. It is assumed here that the latter figure represents the attainable net shaft power from the NASA mercury Rankine cycle engine. The corresponding overall efficiency is 12.6 percent. At higher power levels, the overall efficiency can be expected to increase because of higher turbine efficiency.

The specific weight of major mercury Rankine cycle components is given in Table XIII. The indicated system efficiencies represent estimates of the improvements in efficiency that can be expected to accompany an increase in power level. The indicated specific weights were derived from those of the 36-kw SNAP-8 generator in Table VIII, on the assumption that specific weight varies inversely as system efficiency.

Characteristics of future mercury Rankine cycle engines were derived in the following manner. It was assumed that refinements in turbine design could increase the turbine efficiency and hence system efficiency by 8 percent. Boiling was assumed to occur at 1120° F and 350 psi instead of 1040° F and 240 psi, and condensing was assumed to occur at 605° F and 7.2 psi instead of 670° F and 14.5 psi. These cycle changes are the same as those proposed for modification EGS-8 to the basic SNAP-8 design.[16,17] As a result of these changes, the Carnot cycle efficiency based on the boiling and condensing temperatures increases by 32 percent. It was assumed that system efficiency would improve by a similar percentage. Therefore, for future systems, the system efficiency was assumed to increase by a factor of 1.08 (1.32) = 1.43. At the same time, component specific weight was assumed to decrease by this same factor.

The NASA mercury Rankine cycle generator is designed for 10,000 hrs of unattended operation, while 1000 to 5000 hrs should be adequate for aircraft application. It was assumed that because of higher allowable stresses and lower corrosion for the shorter operating time, as well as reduced design conservatism and the future availability of stronger, more corrosion-resistant alloys, the weight of future system components could be further reduced by a factor of 4. An additional reduction factor of 2 in the weight of ducting, insulation, and structure was assumed to be achievable through more compact packaging and the elimination of unnecessary structural supports.

The heat input and rejection systems were the same as those used for the closed Brayton cycle, and a combustion efficiency of 90 percent was also used. The temperature distribution in the heater and cooler of the mercury Rankine cycle is shown in Figure 18. Combustion gas enters the heater at 3730° F and is cooled to 1030° F. Subcooled mercury enters the heater at 490° F, is heated and boiled at 1030° F, and then is superheated

TABLE XIII. SPECIFIC WEIGHT OF MERCURY RANKINE CYCLE COMPONENTS				
Shaft Power - hp	86.4	500	1500	10,000
Turbine Efficiency - %	58	62	64	68
System Efficiency - %	12.6	13.5	13.9	14.8
Component	Specific Weight (lb/hp)			
Boiler	7.20	6.70	6.54	6.15
Condenser	2.00	1.86	1.81	1.71
Turbine	3.18	2.96	2.88	2.71
Pump	2.72	2.43	2.46	2.32
Ducts & Insulation	3.44	3.20	3.12	2.96
Structure	6.29	5.85	5.70	5.36
Total	24.83	23.00	22.51	21.21

to 1290° F. In the cooler, mercury condenses at 670° F and is subcooled to 490° F, while rotor downwash air is heated from 40° F to 240° F. Upon leaving the heater, the combustion gas enters the preheater of the heat input system, where its temperature drops to 540° F. In the process, compressed air in the preheater is heated from 240° F to 730° F (the combustor inlet temperature). Both the preheater and the air side of the cooler are fabricated from titanium.

The specific weights of the heat input and removal systems are determined according to the methods of Appendix II. The weight of the gas-side heat transfer surface area only is calculated for the heater and cooler, since the weight of the mercury side has already been included in the boiler and condenser weights. Extra gas-side heat transfer is required only in the subcooled and boiling sections of the heater. In the superheating section, the gas-side temperature drop is deliberately made very large in order to keep the wall temperature relatively close to the mercury vapor temperature. This is accomplished by the use of wide spacings between superheater tubes to reduce the heat transfer coefficient of the combustion gas to a value below that of the superheated mercury vapor. The cooler specific weight was calculated by assuming that all the condensate is at 670° F, since only about 4 percent of the total heat removed is used to subcool the mercury.

The specific weights of the combustor, turbine, and compressor of the heat input system were taken to be equal to the weights of these components in the closed Brayton cycle times the ratio of Brayton to Rankine cycle efficiencies. The preheater weight was determined in the same manner, but with an additional multiplying factor equal to the ratio of NTU's (number of heat transfer units) for the Rankine and Brayton cycles.

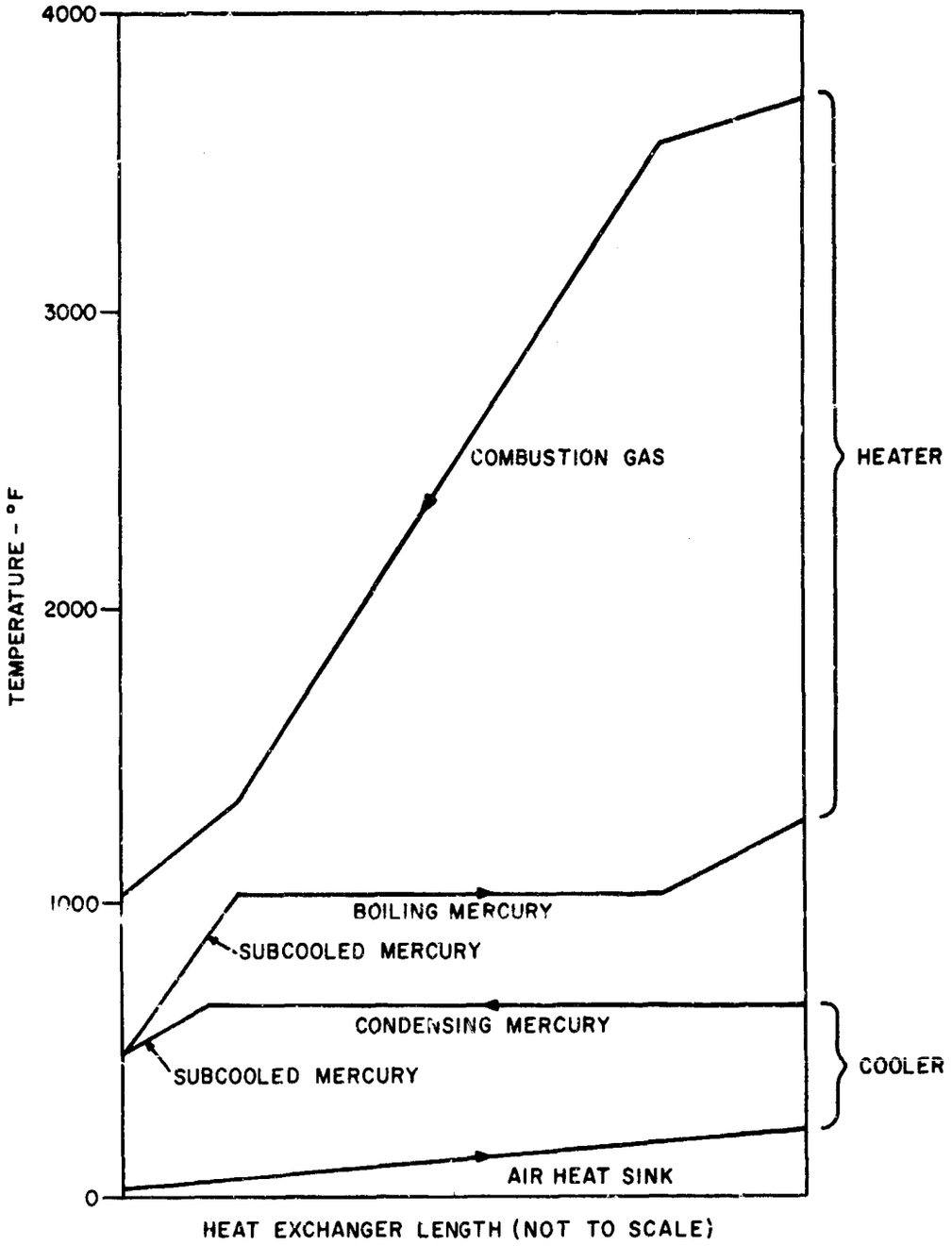

Figure 18. Temperature Distribution in Heater and Cooler of Mercury Rankine Cycle.

The specific weight of the heat input system (heater, preheater, combustor, turbine, and compressor) was found to be 0.1735 lb/hp at 500 hp, 0.1687 lb/hp at 1500 hp, and 0.1525 lb/hp at 10,000 hp. The specific weight of the cooler (air side) was found to be 0.1700 lb/hp at 500 hp, 0.1642 lb/hp at 1500 hp, and 0.1525 lb/hp at 10,000 hp.

The specific weight of the heat input system for future engines was found by assuming that the specific weight varied inversely as system efficiency. The specific weight of the cooler for future engines was found by assuming that the specific weight varied inversely as the system efficiency and directly as one minus the system efficiency.

Fuel consumption was calculated on the basis of the load-time schedule of Table II. The specific fuel consumption was assumed to vary with load in the same manner as shown in Figure 1 for the advanced gas turbines. Transmission and shafting specific weights were taken to be the same as those given in Table II for the advanced gas turbines.

Specific engine weights for the mercury Rankine cycle are given in Figure 19. Engine weight includes that of the components of Table XIII plus the heat input system and cooler weights. Total system weight (engine, transmission and shafting, and fuel) is shown in Figure 20. The high weight of the mercury Rankine cycle is evident. Even for the projected future, the mercury engine is about 20 times heavier than the advanced gas turbine. From Figure 20, the estimated future fuel consumption for the mercury Rankine cycle is about 60 percent greater than that for the advanced gas turbines, and the total estimated future system weight is about 3 times greater.

Specific Volume

The total volume of the boiler, condenser, pump-motor, and turbine of the NASA mercury Rankine cycle generator is 21.8 ft^3. The boiler alone occupies 18.8 ft^3. (This is the enclosed volume when the boiler shell is coiled into a helix 4 ft in diameter and 1-1/2 ft in length.) The specific volume for a shaft output of 86.4 hp is 0.25 ft^3/hp. This figure was assumed to be constant over the range of 500 hp to 10,000 hp for both present and future technology.

The specific volume of the heat input system and cooler was estimated from the heat transfer area on the assumption that the area-volume ratio was 200 ft^2/ft^3. The volume of the heat input system plus the cooler for present technology was found to be 0.0068 ft^3/hp at 500 hp, 0.0068 ft^3/hp at 1500 hp, and 0.0062 ft^3/hp at 10,000 hp. For future technology, the corresponding figures are 0.0046 ft^3/hp at 500 hp, 0.0045 ft^3/hp at 1500 hp, and 0.0042 ft^3/hp at 10,000 hp.

The total specific volume of the mercury Rankine cycle engines (boiler, condenser, pump, turbine, heat input system, and cooler) is given in Table XIV, along with the specific volume for the advanced gas turbine.

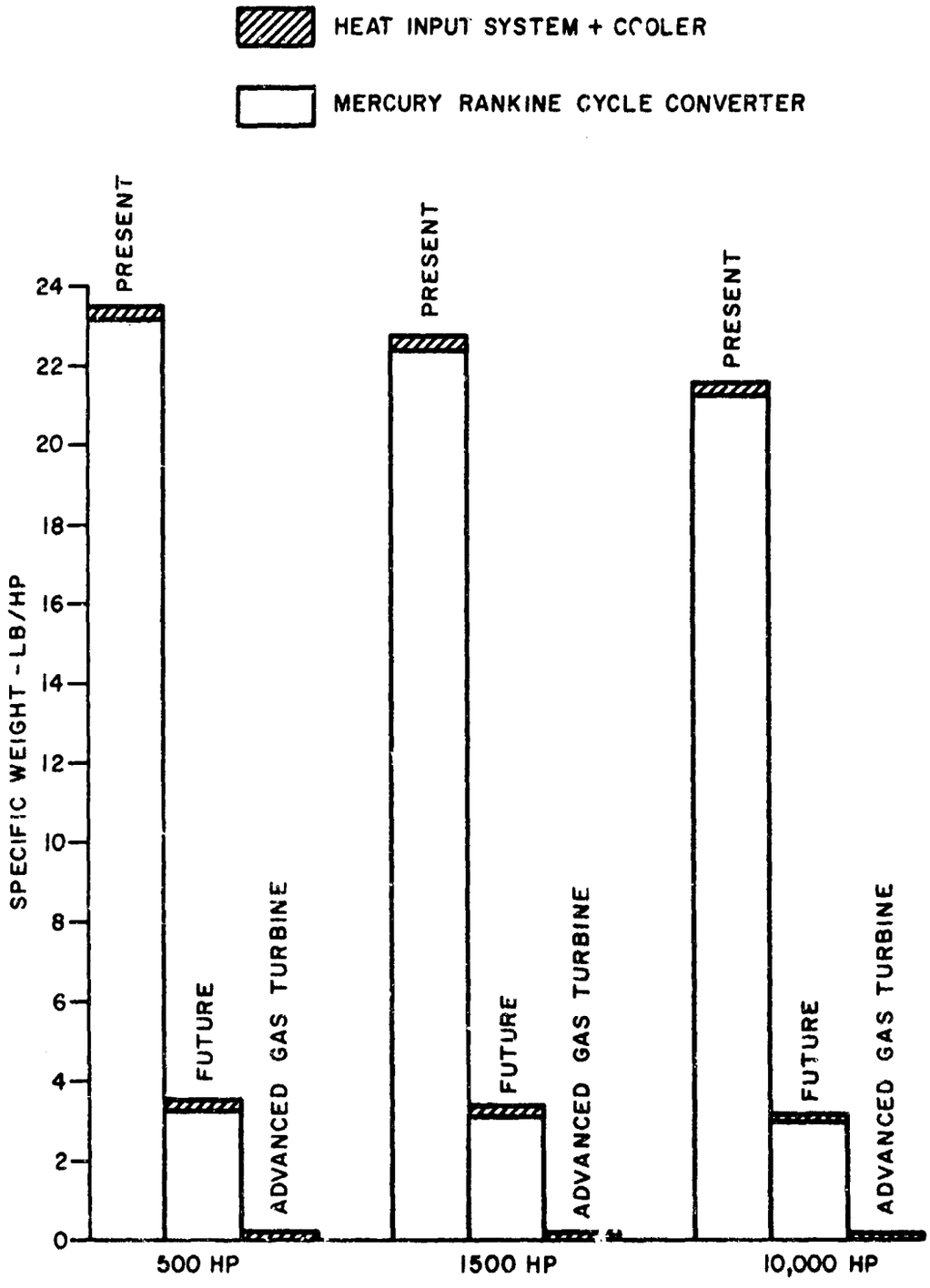

Figure 19. Specific Weight of Mercury Rankine Cycle Engines.

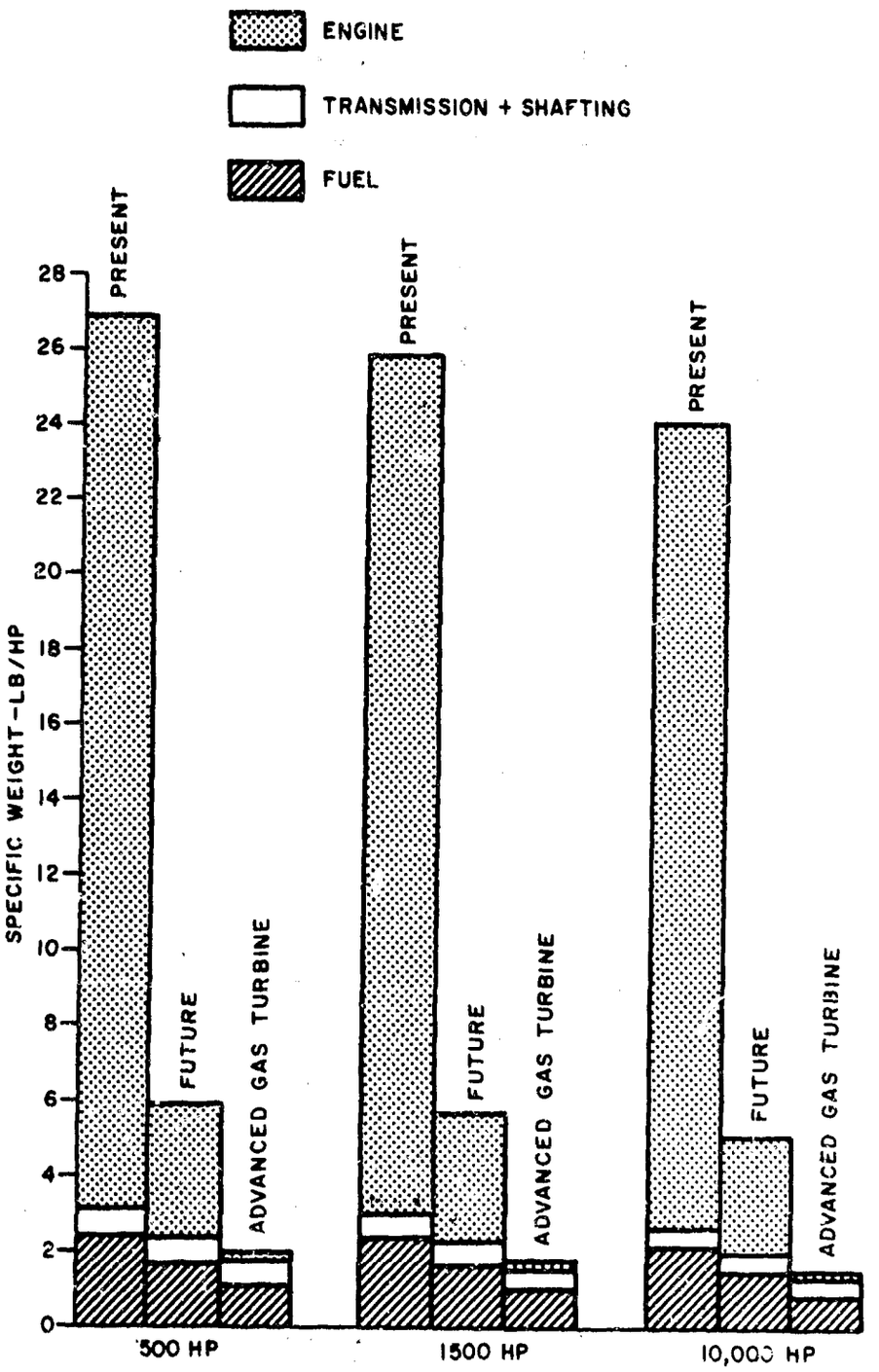

Figure 20. Specific Weight of Mercury Rankine Cycle Shaft Power Systems.

TABLE XIV. SPECIFIC VOLUME OF MERCURY RANKINE CYCLE ENGINES

	Shaft Power (hp)		
	500	1500	10,000
	Specific Volume (ft^3/hp)		
Advanced Gas Turbine	3.24×10^{-3}	$3.01\text{-}3.24 \times 10^{-3}$	$1.57\text{-}3.15 \times 10^{-3}$
Mercury Rankine Cycle-Present	257×10^{-3}	257×10^{-3}	256×10^{-3}
Mercury Rankine Cycle-Future	255×10^{-3}	254×10^{-3}	254×10^{-3}

It can be seen that the mercury engine volumes are 80 or more times larger than those of the advanced gas turbines. As has been pointed out, most of the mercury cycle volume resides in the boiler. Although the actual volume occupied by the boiler shell is much less than the enclosed volume of the shell in the coiled configuration, it is nonetheless clear that the mercury Rankine cycle engine is not competitive with advanced gas turbines on a volume basis.

Cost

The use of tantalum and complex fabrication techniques in the boiler indicates that the cost of a mercury Rankine cycle engine is likely to be high.

Reliability

The NASA mercury Rankine cycle generator is being designed for at least 10,000 hrs of unattended operation and, hence, when fully developed, should exhibit good reliability. However, reliability in a shaft power engine will depend on the effectiveness of shaft seals. The leakage of mercury at any significant rate would soon render the engine inoperative.

Sensitivity to Environment

Because of its lower condensing temperature, the mercury Rankine cycle will exhibit greater sensitivity to changes in temperature of cooling air than the potassium Rankine cycle. The effect of ingestion of sand and dust by the heat input system will be similar to that of sand and dust ingestion by a gas turbine. The condensation process could be disrupted by acceleration, and possibly by vibration as well.

Part-Load Characteristics

No information was obtained for this engine.

Transient Response

Transient response should be considerably slower than that of gas turbines because of the large mass and hence the thermal inertia of engine components.

Structural Considerations

The various engine components should be arranged in a configuration of maximum compactness that integrates readily with an aircraft airframe. In particular, the condenser cooler must be located so as to facilitate cooling by rotor downwash air. The vibration characteristics of the engine also require consideration.

Critical Problem Areas

Stable, reproducible boiling of mercury has been a continuing problem in the NASA mercury Rankine cycle program for several years. Although the use of tantalum boiler tubes has greatly alleviated the problem, the matter is still of some concern. Possible adverse effects of acceleration on the condensing process also require investigation. The problem of heater materials is largely alleviated because of the relatively low peak cycle temperature of 1290°F. Protection of the combuster against combustion gases remains a major problem, although the gases are at a temperature of 3600°F in the mercury cycle compared to 4600°F in the potassium cycle. The development of satisfactory dynamic and static mercury seals will be a substantial effort, although considerable progress in this area has been achieved. Again, the most critical problem area is the excessive engine size and weight, for which no viable design or development is apparent.

Conclusions

The mercury Rankine cycle engine is not competitive with the advanced gas turbine on the basis of any of the evaluatory criteria that have been considered.

Organic Cycle

Factors involved in the evaluation of the organic Rankine cycle are discussed below.

Specific Weight

Information has been compiled on two basic types of organic Rankine cycles: the ORACLE and a 150-kw conceptual design. The ORACLE concept uses Dowtherm as the working fluid and relies on the jet

condenser to achieve condensing pressures as low as 0.1 psi with attendant high cycle efficiency. The 150-kw concept uses CP-32 as the working fluid and uses a conventional condenser at a condensing pressure of 6.1 psi.

The attainment of reasonable cycle efficiency with an organic working fluid requires a regenerator to transfer heat from the dry turbine exhaust vapor to pressurized condensate prior to the entrance of the condensate into the boiler. When the turbine exhaust pressure is very low (as will be the case with a jet condenser), the heat transfer coefficient of the vapor entering the regenerator is small. Consequently, the regenerator will be large and heavy, and the regenerator will contain a large inventory of liquid working fluid. For this reason, the efficiency gain resulting from the use of a jet condenser and a low condensing pressure is accompanied by a disproportionate increase in engine weight. Preliminary calculations indicated that a 1500-hp ORACLE-type Rankine cycle engine based on future technology would have a specific weight of 10.9 lb/hp and a cycle efficiency of 29.8 percent at a condensing pressure of 0.1 psi. At a condensing pressure of 0.5 psi, the same engine would have a specific weight of 7.90 lb/hp and a cycle efficiency of 22.0 percent. A 1500-hp engine using CP-32 with a conventional condenser would have a projected future specific weight of 0.94 lb/hp and a cycle efficiency of 29.7 percent. Therefore, the 150-kw organic Rankine cycle engine with CP-32 as the working fluid and a conventional condenser was used as the basis for further evaluation.

The net available shaft power of the 150-kw engine was obtained by dividing the 150-kw electrical output by the electrical conversion efficiency of 87 percent and adding the 6 kw of power required to drive the fan used for condensing the organic vapor. The shaft power is then (150 kw/0.87)+6 kw= 179 kw x 1.341 hp/kw=240 hp. In the design study, the boiler exit vapor was throttled from a pressure of 600 psi to 500 psi, prior to entering the turbine. If the vapor had not been throttled, it is estimated that about 20 percent more power could have been obtained. It was assumed that the additional power would be available, so that the total shaft output was 1.2 (240 hp) = 288 hp. The cycle efficiency corresponding to this shaft power level is 28.8 percent.

At higher power levels, the turbine efficiency was assumed to be larger than the value of 75.7 percent used for the 288-hp engine. The cycle efficiency then increased in proportion to the increase in turbine efficiency. The specific weight of all engine components except the condenser was assumed to vary inversely as the cycle efficiency. The condenser's specific weight was assumed to vary inversely as the efficiency and directly as one minus the efficiency. The resulting component specific weights are given in Table XV.

The temperature distribution in the heater and cooler of the organic Rankine cycle engine is shown in Figure 21. The heater temperature distribution is actually that of the ORACLE system with Dowtherm working fluid and a jet condenser. The heater specific weight calculated on the basis of this

TABLE XV. SPECIFIC WEIGHT OF ORGANIC RANKINE CYCLE COMPONENTS

Shaft Power - hp	288	500	1500	10,000
Turbine Efficiency - %	75.7	76	78	81
Cycle Efficiency - %	28.8	29.0	29.7	30.8
Component	**Specific Weight (lb/hp)**			
Turbine-Pump	0.347	0.346	0.337	0.324
Regenerator	0.520	0.517	0.505	0.486
Condenser	0.870	0.856	0.764	0.636
Structure & Piping	0.660	0.658	0.640	0.616
CP-32	0.834	0.832	0.809	0.780
Total	3.231	3.209	3.055	2.842

temperature distribution does not differ substantially from that corresponding to the heater temperature distribution for the cycle with CP-32 as the working fluid. The temperature distribution in the cooler is representative of the CP-32 cycle. Because of the low condensing temperature, cooler size and weight are quite sensitive to the ambient temperature. Therefore, an ambient air temperature of 100° F was used instead of the 40° F which was previously used, in order not to arrive at an overly optimistic estimate of cooler weight.

In the heater, combustion gas is cooled from 3400° F to 700° F while heating and then boiling the organic fluid at 700° F. The combustor inlet temperature is 400° F, and the combustion efficiency is 90 percent. In the cooler, the organic liquid condenses at 189° F, while rotor downwash air is heated from 100° F to 158° F. Because of the low cooler temperatures, aluminum was specified for the air-side heat transfer surface. The assumptions previously made about the dependence of the heat input system and cooler weight for the mercury Rankine cycle were also used here. The heat input system weights were found to be 0.0886 lb/hp at 500 hp, 0.0866 lb/hp at 1500 hp, and 0.0835 lb/hp at 10,000 hp. The air-side cooler specific weights were found to be 0.468 lb/hp at 500 hp, 0.344 lb/hp at 1500 hp, and 0.296 lb/hp at 10,000 hp.

For estimates of future engine specific weight, it was assumed that titanium was the material used for fabricating all components but the condenser. The condenser was assumed to be fabricated from aluminum. It was assumed that the weight of engine components varied inversely as the density of the material of construction. With the use of titanium instead of stainless steel, component weights are then 55.2 percent of the values given in Table XV. Similarly, the weight of the aluminum condenser is 33.8 percent of the value given in Table XV. In addition, it was assumed that a more compact configuration, an overhaul time of 1000 hr instead of 10,000 hr, and a reduced design conservatism would permit another 50-percent reduction in system weight. It was assumed that the

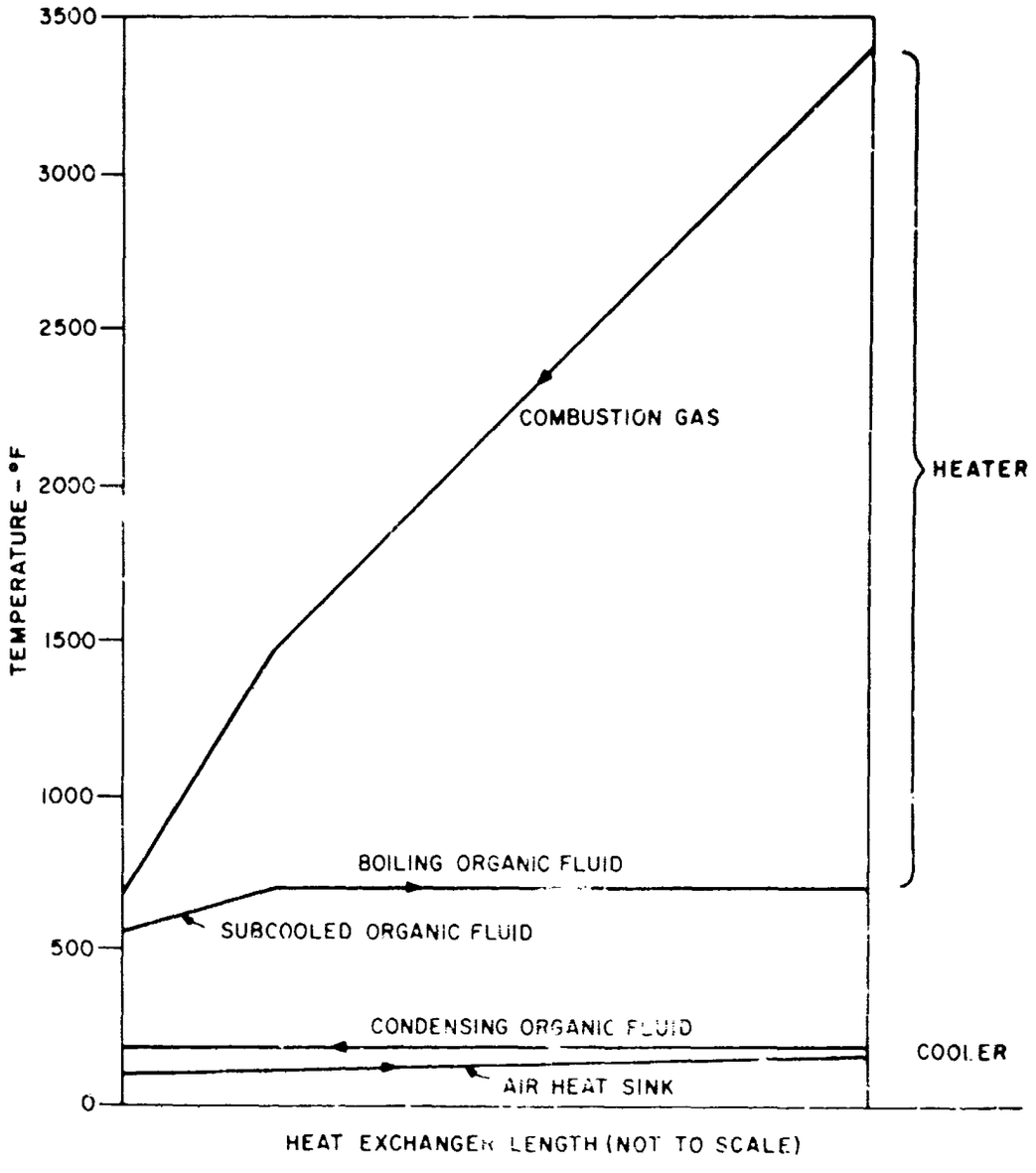

Figure 21. Temperature Distribution in Heater and Cooler of Organic Rankine Cycle.

cycle efficiency and the heat input and removal system weights would not change significantly with continued development.

Again, fuel consumption was based on the load-time schedule of Table II, and the variation of specific fuel consumption with load was assumed to

vary in the same manner as the curves of Figure 1. Transmission and shafting specific weights were taken to be the same as those given in Table II for the advanced gas turbines.

The calculated organic Rankine cycle engine specific weight based on the above assumptions is given in Figure 22, and the total system specific weight (engine, transmission plus shafting, and fuel) is given in Figure 23. From Figure 22, the estimated future engine weight is more than 7 times greater than that of the advanced gas turbines. From Figure 23, total system weight exceeds that for the advanced gas turbine by about 70 percent. This difference results principally from the large specific weight of the organic Rankine cycle engine.

Specific Volume

The overall package dimensions of the 150-kw CP-32 Rankine cycle generator are 4 ft x 6 ft x 7 ft, for a total volume of 168 ft^3. However, the total volume of major components is about 22 ft^3, divided in the following manner: regenerator, 1.68 ft^3; condenser, 12.0 ft^3; pump and turbine, 2 ft^3 (estimated); and boiler, 6 ft^3 (estimated). The total specific volume of these components for a net shaft output of 288 hp is 0.0764 ft^3/hp. This figure was assumed to be constant over the range of 500 hp to 10,000 hp. The specific volume of the heat input system and the air-side of the cooler was estimated from heat transfer surface area data on the assumption of an area-volume ratio of 200 ft^2/ft^3. The sum of the component and heat input-output system specific volumes was taken to be a lower limit of engine specific volume, which would not change significantly with future development. The specific volume of the organic Rankine cycle engines is given in Table XVI, along with specific volume of the advanced gas turbines. The organic Rankine cycle specific volumes are seen to be 30 or more times those of the advanced gas turbines.

Cost

Factors favoring low cost of the organic Rankine cycle engines are low-temperature operation, permitting the extensive use of titanium and aluminum as construction materials, and a single-stage turbine. Factors favoring high cost are the high engine weight and the large number of components. The costs of the organic engine and advanced gas turbine are expected to be comparable.

Reliability

The combination of low peak cycle temperature (700° F) and a noncorrosive working fluid favors the development of a highly reliable system, although the high combustion gas temperature (3400° F) presents a severe materials problem in the combustor. On the other hand, the relatively large maximum turbine inlet pressure of 600 psi will accentuate shaft sealing problems. Reliability comparable to the gas turbine can probably be achieved.

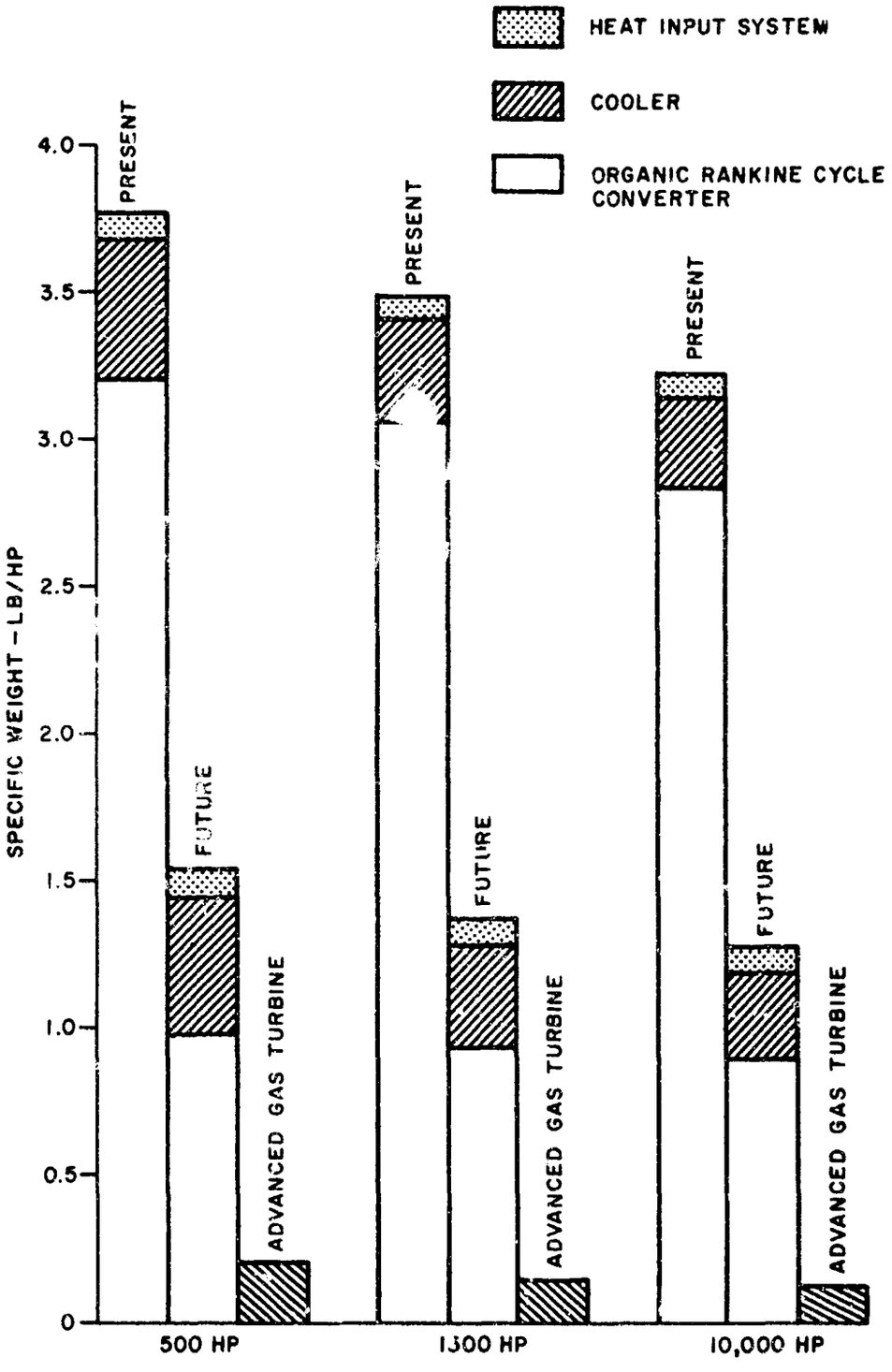

Figure 22. Specific Weight of Organic Rankine Cycle Engines.

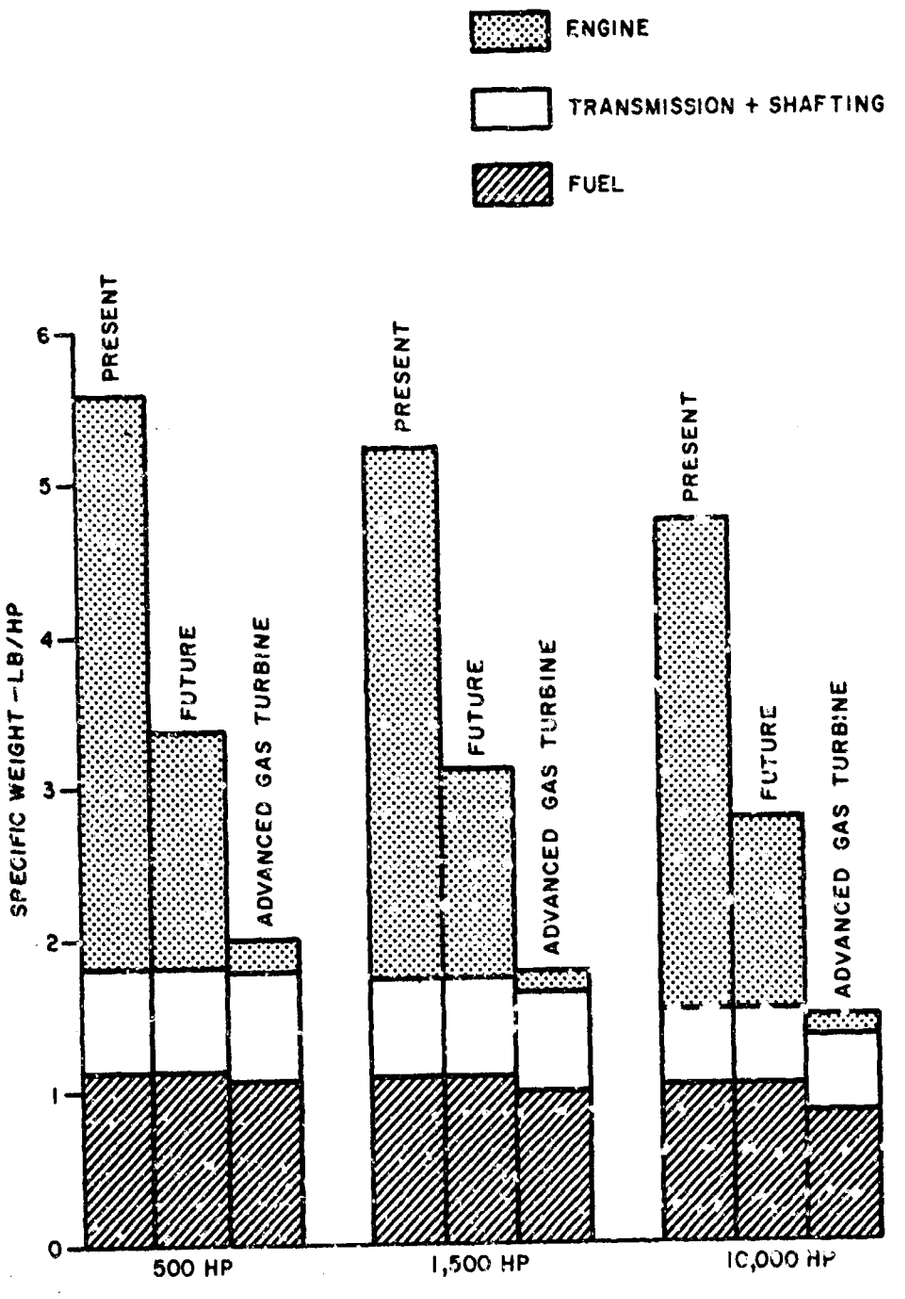

Figure 23. Specific Weight of Organic Rankine Cycle Shaft Power Systems.

TABLE XVI. SPECIFIC VOLUME OF ORGANIC RANKINE CYCLE ENGINES

	Shaft Power (hp)		
	500	1500	10,000
	Specific Volume (ft^3/hp)		
Advanced Gas Turbine	3.24×10^{-3}	$3.01\text{-}3.24 \times 10^{-3}$	$1.57\text{-}3.15 \times 10^{-3}$
Organic Rankine Cycle	100.4×10^{-3}	94.2×10^{-3}	91.7×10^{-3}

Sensitivity to Environment

Because of the low condensing temperature of 189°F, performance of the organic Rankine cycle engine will be quite sensitive to the ambient temperature. Performance will also be affected by variations in the temperature of inlet air to the heat input system. The ingestion of sand and dust into the heat input system would affect engine performance to the same extent as in a gas turbine. The system can probably be designed to withstand aircraft vibrations, but, as is the case with all Rankine cycle engines, the possible disruptive effect of acceleration on the condensing process is a matter of concern.

Part-Load Characteristics

No information on part-load characteristics was obtained.

Transient Response

Transient response should be poorer than that of gas turbines because of the large engine weight and hence large thermal inertia of the organic Rankine cycle engine.

Structural Considerations

The same structural considerations which apply to the other Rankine cycle engines are also applicable here: the need for compact orientation of engine components, consideration of methods for supporting the engine to the airframe, vibration characteristics of the structure, and the need to locate the cooler to facilitate cooling with rotor downwash air.

Critical Problem Areas

With the exception of the combustor, the low peak cycle temperature virtually eliminates materials as a critical problem area. Combustor

materials and cooling techniques, shaft seals, and condenser operation under adverse acceleration constitute the major technical problem areas. Again, however, the most critical stumbling blocks are engine size and weight.

Conclusions

The organic Rankine cycle engine is likely to be several times heavier than a comparable advanced gas turbine in the foreseeable future. This observation, coupled with the fact that fuel consumption is somewhat greater than that predicted for advanced gas turbines, indicates that the organic Rankine cycle engine is not competitive with advanced gas turbines. Although the materials problem is greatly eased by low peak cycle temperature, serious materials problems nonetheless remain in the combustor of the heat input system.

INTERCOOL-REHEAT CYCLE

Gains in the specific fuel consumption and specific horsepower of gas turbines have generally been sought by increases in compressor pressure ratio and turbine inlet temperature. In current advanced gas turbine designs, turbine inlet temperatures as high as 2500°F have been postulated. However, the performance gains possible at such temperatures are tempered by the design complexities resulting from the use of cooled blades, the reduced fraction of excess air available for cooling the combustor liner, the performance losses associated with the bleeding off of compressor air for blade cooling, and the reduction of design margins necessitated by pushing materials toward maximum temperature and stress limits.

Significant improvements in specific fuel consumption can also be achieved by the use of a regenerator to transfer heat from hot turbine exhaust gas to the compressor discharge air. However, engine specific weight and volume usually suffer because of the weight and bulk of the regenerator.

The intercool-reheat cycle represents an attempt to achieve the performance potential of the turbine-blade-cooled, high-temperature Brayton cycle without recourse to either very high turbine inlet temperatures or the use of regenerators. Instead, very high compression ratios are used as an alternate approach to the achievement of good engine performance.

Cycle Characteristics

The ideal intercool-reheat cycle is shown as solid lines in the temperature-entropy diagram of Figure 24. Ambient air at temperature T_1 and pressure p_1 is isothermally compressed to pressure p_2 and temperature $T_2 = T_1$. The air is then isentropically compressed to pressure p_3 and temperature T_3, and it expands isothermally to pressure p_4 and temperature $T_4 = T_3$. An isentropic expansion to

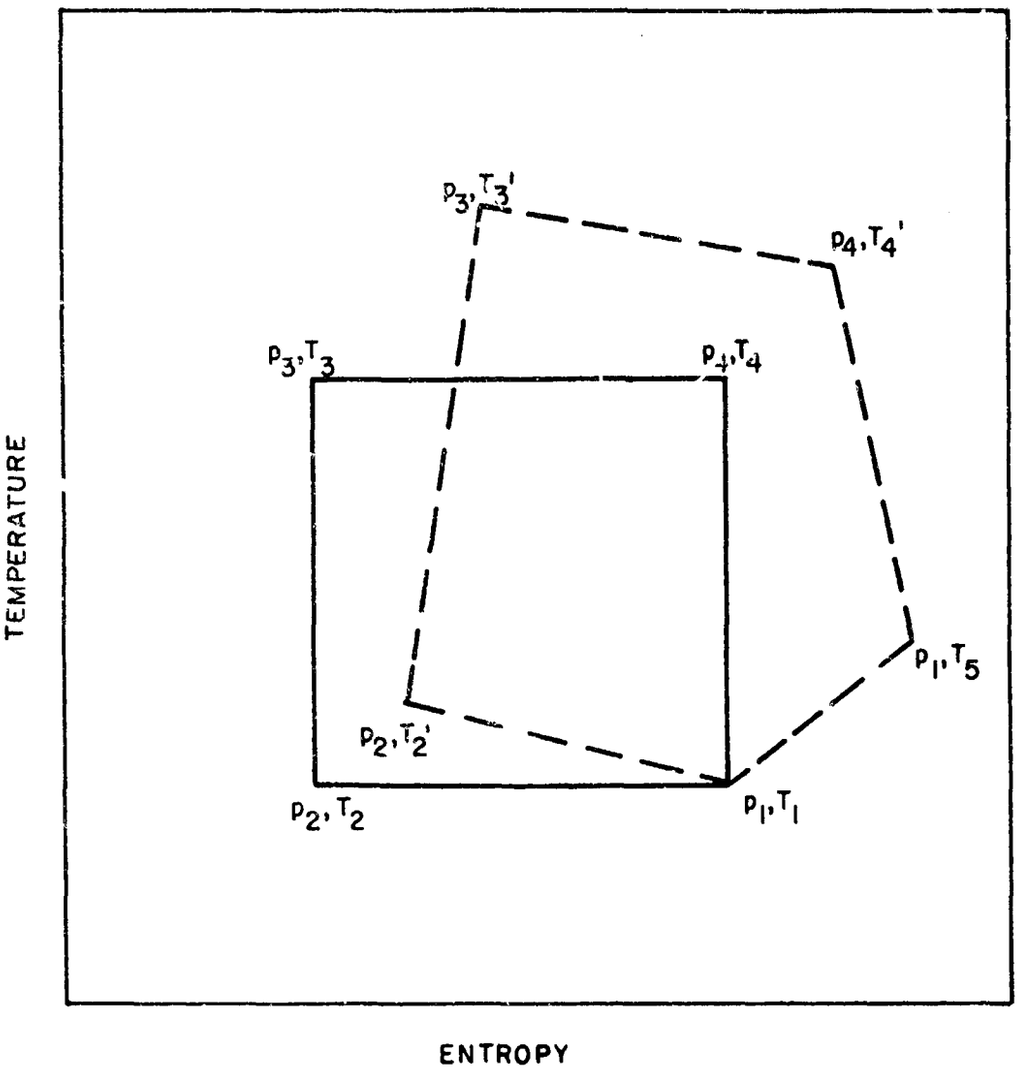

Figure 24. Intercool-Reheat Cycle Diagrams.

pressure p_1 and temperature T_1 completes the cycle. The isothermal compression is accomplished by intercooling between compressor stages with ambient air. The isothermal expansion is accomplished by reheating between turbine stages with interstage combustors.

The efficiency of the ideal intercool-reheat cycle is the same as the efficiency of the Carnot cycle with maximum and minimum temperatures of T_3 and T_1. The ideal cycle efficiency is plotted as a function of the pressure ratio $P_1 = p_2/p_1$ and

the total pressure ratio $P=p_3/p_1$ in Figure 25. For a given P, the ideal cycle efficiency decreases continuously with an increase in P_1, becoming equal to zero when $P_1 = P$. There is an optimum P_1 for which the specific power (power per unit mass flow rate) is a maximum. The optimum P_1 increases with P and, as shown in Appendix I, approaches a limiting value of $P_1=33.2$ as P approaches infinity.

The locus of points for which the specific power is a maximum is shown as a dashed curve in Figure 25. For example, when P=100, the optimum P_1 is 6.7 and the corresponding ideal cycle efficiency is 54 percent. This figure may be compared with the maximum efficiency of 73 percent which occurs when $P_1=1$ (and the specific power is zero).

The actual intercool-reheat cycle is indicated by the dashed lines of Figure 24. The cycle pressures are the same at the various state points, but the temperatures are different. The isothermal compression and expansion processes have been replaced by polytropic processes for which both heat transfer and temperature changes occur. The isentropic compression and expansion processes have been replaced by adiabatic processes for which both temperature and entropy changes occur.

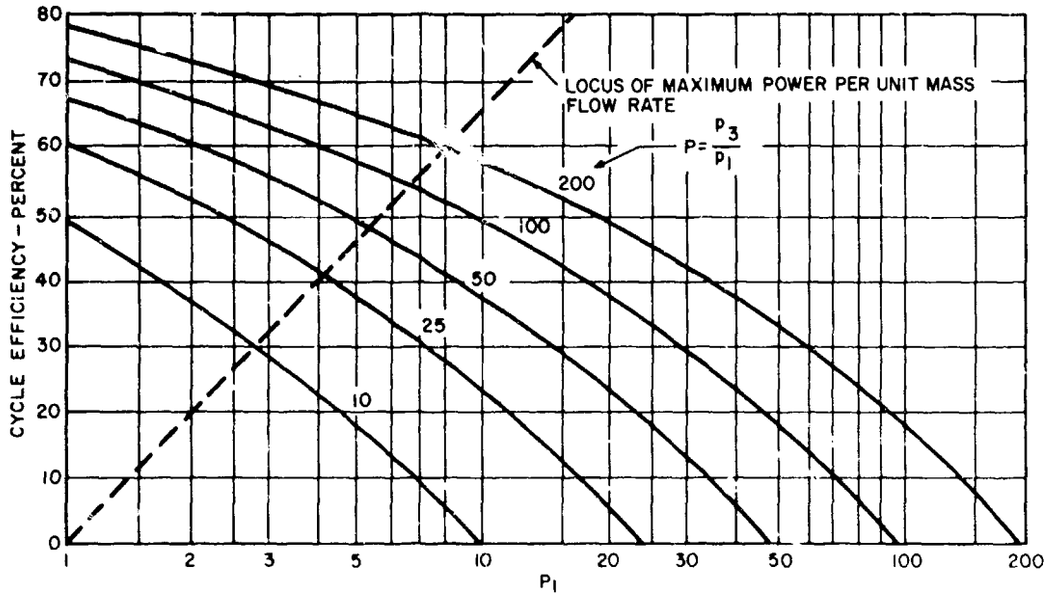

Figure 25. Ideal Efficiency of Intercool-Reheat Cycle.

Parameters that define the characteristics of the actual intercool-reheat cycle include: polytropic compressor efficiency η_{c1}; adiabatic compressor efficiency η_{c2}; polytropic turbine efficiency η_{t1}; adiabatic turbine efficiency η_{t2}; and the pressure ratios $P_1 = p_2/p_1$, $P_2 = p_3/p_2$, and $P = P_1 P_2 = p_3/p_1$. All calculations for the intercool-reheat cycle used the following values for compressor and turbine efficiencies: $\eta_{c1} = 0.80$, $\eta_{c2} = 0.85$, $\eta_{t1} = 0.85$, and $\eta_{t2} = 0.90$.

Figure 26 shows the variation of cycle efficiency with P_1 and P for isothermal compression ($T'_2 = T_1$) and isothermal expansion ($T'_3 = T'_4$). The existence of an optimum P_1 that yields maximum efficiency for a given P is evident. The optimum value of P_1 varies over the relatively narrow range of 6 to 10 as P varies from 100 to 800. Maximum cycle efficiency varies from 20 percent at P=100 to 44.4 percent at P=800.

The selection of P_1 for maximum cycle efficiency results in a higher peak cycle temperature T_3 than when a value larger than the optimum value is selected for P_1. Figure 27 shows the variation of the maximum cycle temperature and cycle efficiency with the overall pressure ratio P. Curves are shown for the pressure ratio P_1 corresponding to maximum cycle efficiency and for $P_1 = 20$. Again, $T'_2 = T_1$ and $T'_3 = T'_4$, and the ambient temperature is 80° F. It can be seen that operation at $P_1 = 20$ instead of the optimum P_1 for maximum cycle efficiency can substantially reduce the peak cycle temperature with a relatively modest loss of efficiency. For example, for an overall pressure ratio of 400, the maximum cycle efficiency is 37 percent and the corresponding peak cycle temperature is 1390°F; while at $P_1 = 20$, the cycle efficiency is 30 percent and the peak cycle temperature is 930°F.

Since the intercool-reheat cycle is open, continuously ingesting ambient air, and since ambient air is the heat sink, there must be some temperature rise of initially compressed air in order that heat of compression may be transferred to the heat sink. Thus, in the real cycle the initial compression must be polytropic, with an increase in the temperature of compressor discharge air.

The undesirable aspect of having $T'_2 > T_1$ is that for specified pressure ratios P_1 and P_2, the peak cycle temperature T'_3 increases. However, the increase in T'_3 produces the desirable effect of an increase in cycle efficiency. Also, the intercooling heat load is reduced as the temperature T'_2 after polytropic compression is allowed to increase.

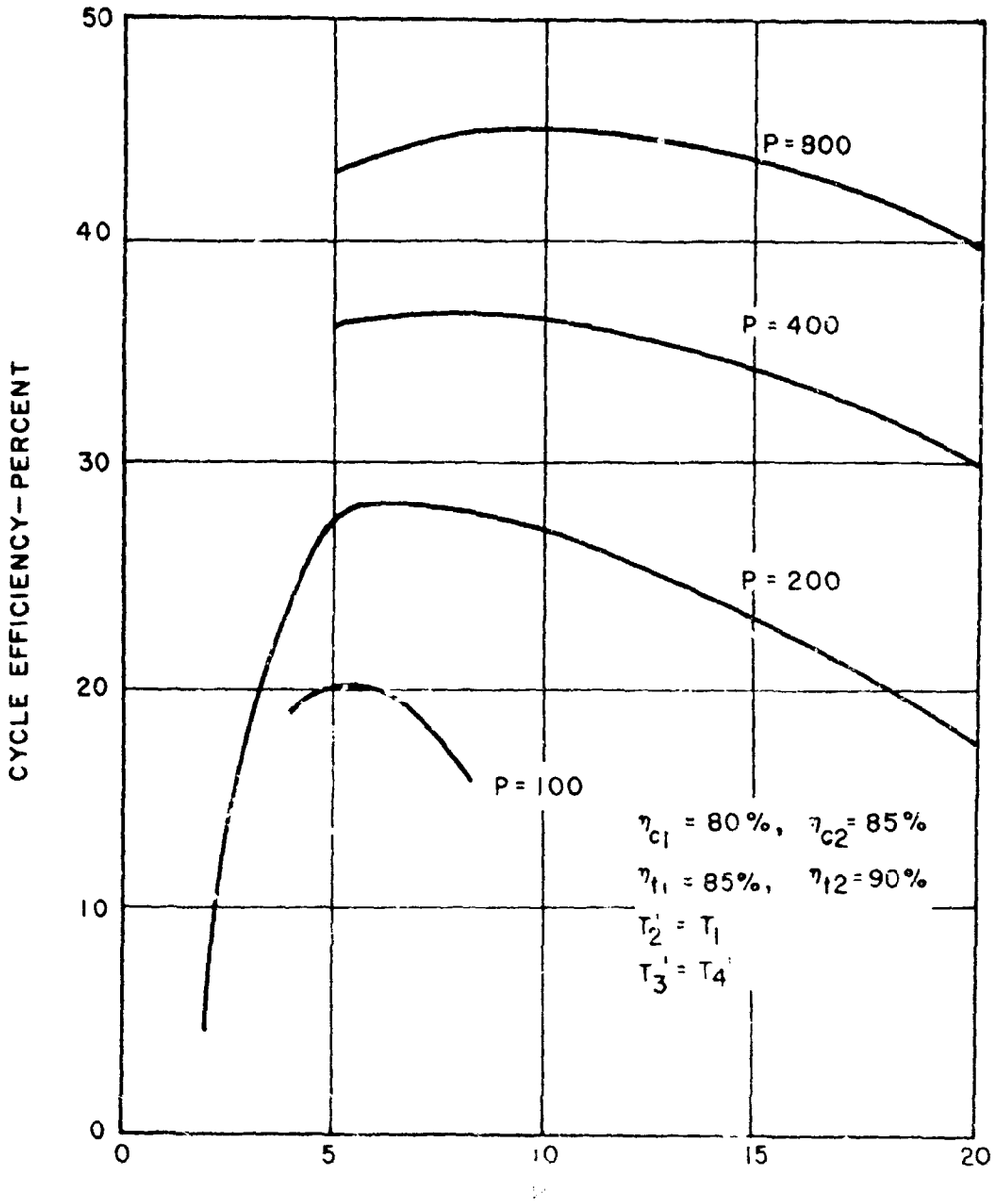

Figure 26. Efficiency of Intercool-Reheat Cycle.

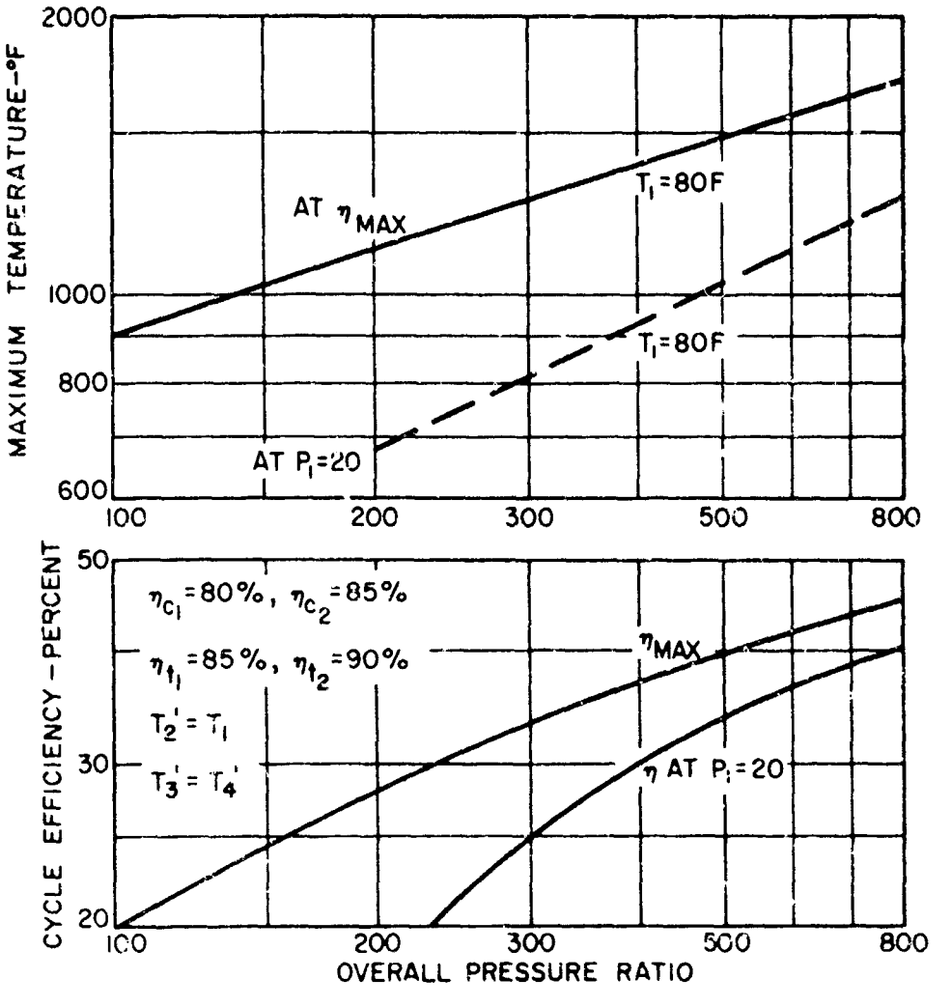

Figure 27. Efficiency and Maximum Temperature for Intercool-Reheat Cycle.

The effect of T_2' on cycle efficiency and maximum cycle temperature T_3' is shown in Figure 28 for an overall pressure ratio P of 400, isothermal reheat, and an ambient temperature T_1 of 80° F. Two sets of curves are shown, one for a polytropic compression ratio P_1 of 8 (this value of P_1 yields maximum cycle efficiency for P=400 and $T_3' = T_4'$) and one for $P_1 = 20$. It can be seen that for a given maximum cycle temperature, the cycle efficiency is virtually independent of P_1 but that T_2' is considerably higher for $P_1 = 20$ than for $P_1 = 8$. The higher value of T_2' increases the available ΔT in the intercooler and hence reduces intercooler heat transfer surface area, size and weight.

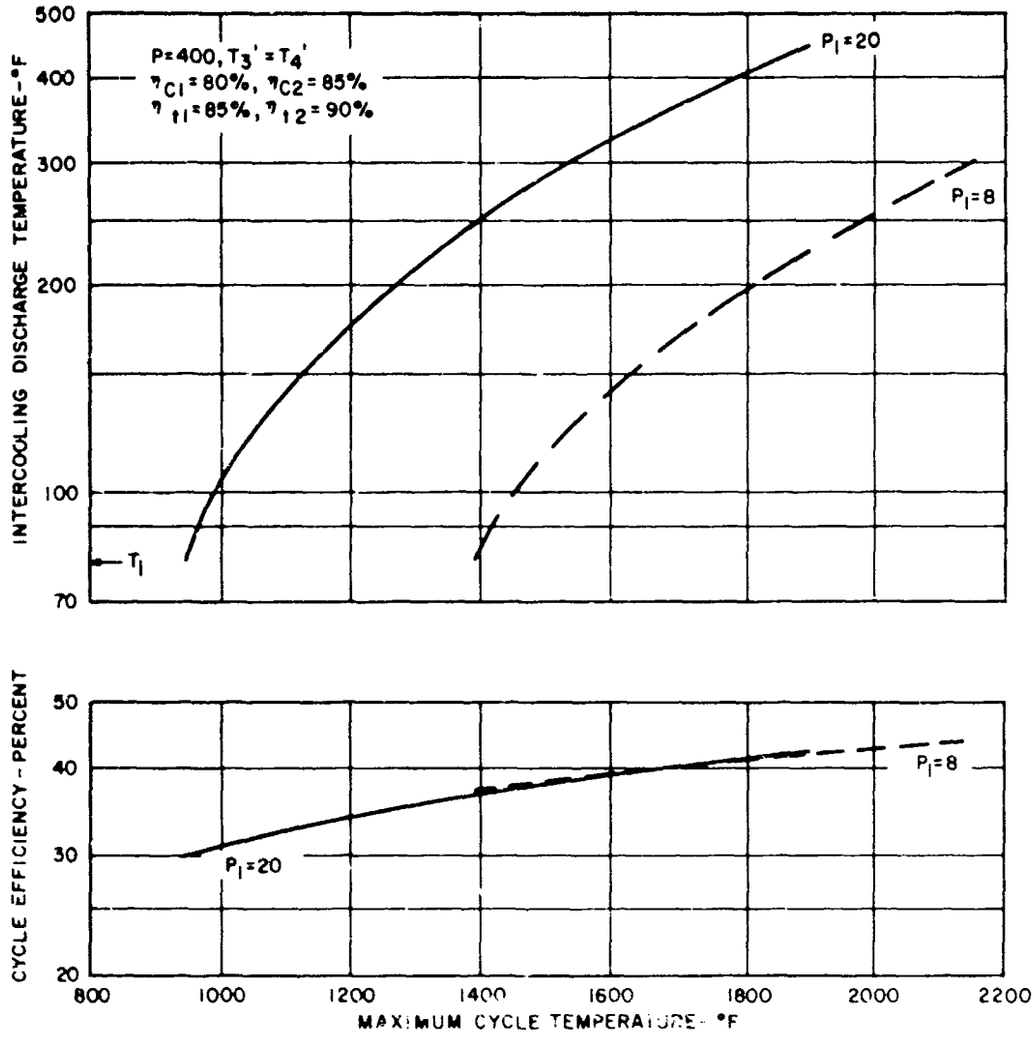

Figure 28. Effect of Intercooling Discharge Temperature on Cycle Efficiency and Maximum Cycle Temperature.

For purposes of further analysis, an intercool-reheat cycle was considered with isothermal reheat, pressure ratios P_1 and P_2 each equal to 20, an ambient temperature T_1 of 80°F, and a maximum cycle temperature T_3' of 1520°F. Then $P = P_1 P_2 = 400$ and $T_3' = T_4'$. From Figure 28, the cycle efficiency is 38.3 percent and the temperature T_2' after polytropic compression is 300°F. The specific power

for these conditions is 196 hp/lb/sec. For a 10,000-hp engine, the flow area at the discharge end of the adiabatic compressor is about 9.7 $in.^2$, if a flow velocity of 100 ft/sec is assumed.

Application to Aircraft Propulsion

The various factors involved in evaluation of the intercool-reheat cycle for aircraft propulsion are discussed below.

Specific Weight

In order to provide a finite temperature difference at the intercooler inlet, intercooling should not be initiated until the incoming cycle air has been adiabatically compressed to raise its temperature a few degrees above ambient. It was assumed that the initial temperature rise during adiabatic compression was 20°F and that the ambient heat sink air would be heated from 80°F to 180°F. The specific weight of the intercooler was then calculated according to the method described in Appendix II, assuming that aluminum was used as the construction material. The resulting intercooler specific weights were 0.166 lb/hp at 500 hp, 0.126 lb/hp at 1500 hp, and 0.114 lb/hp at 10,000 hp.

On the basis of the information presented in Appendix II, the cross-sectional areas required to intercept sufficient rotor downwash air for intercooling were found to be 5.05 ft^2 at 500 hp, 18.9 ft^2 at 3000 hp, and 106.7 ft^2 at 20,000 hp. The cross-sectional areas were calculated for 3000-hp and 20,000-hp levels in order to provide sufficient cooling air for two 1500-hp engines and two 10,000-hp engines respectively. The calculated areas represent less than 1 percent of the total area swept out by the rotors.

The required pressure ratio of 400 would be achieved by feeding the output from the polytropic compressor with a pressure ratio of 20 to the adiabatic compressor with a pressure ratio of 20. An axial polytropic compressor is preferable to a centrifugal compressor, because the ideal of continuous intercooling can be approached more closely with the larger number of stages which is usually characteristic of axial compression.

The weights of the engine turbines and compressors were estimated by taking into consideration the influence of peak cycle temperatures and pressures on the weights of advanced gas turbine components. The weight of the low-pressure (polytropic) compressor should be comparable to or less than that of an advanced gas turbine compressor. While the mass flow rate may be somewhat greater and supplementary surface area for intercooling may be required, these factors are countered by the higher density of compressed air, whose exit temperature is 300°F. Also, because of the low exit temperature, it may be possible to use lightweight aluminum or aluminum composites for many of the low-pressure compressor components. It was assumed that the weight of the low-pressure compressor was the same as that of a compressor for an advanced gas turbine.

The low-pressure (adiabatic) turbine should be somewhat lighter than its advanced gas turbine counterpart because of its low turbine inlet temperature (1520° F) and consequently its lighter gas density. It was assumed that the low-pressure turbine weight was 0.8 times the weight of the turbine in an advanced gas turbine.

Because of the high pressures encountered, most of the weight of the high-pressure (adiabatic) compressor should be accounted for by its outer casing. The casing weight will be proportional to its volume, assuming constant material density. The compressor diameter will vary approximately as the inlet absolute temperature and inversely as the square root of the inlet pressure.[1] For the high-pressure compressor, the inlet conditions are 760°R and 20 atmospheres. For the advanced gas turbine compressor, inlet conditions are 540°R and 1 atmosphere. Then the diameter of the high-pressure compressor is calculated to be 0.314, or about one-third the diameter of the compressor of a comparable advanced gas turbine. If a constant length-diameter ratio is assumed, the length of the high-pressure compressor would also be one-third the length of its advanced gas turbine counterpart.

For a fixed design stress, the casing thickness will be proportional to the product of the gas pressure and the casing diameter (which is assumed to be approximately equal to the compressor diameter). The casing volume, which is proportional to the product of its length, diameter, and thickness, will then vary as the product of the diameter cubed times the pressure. Since the diameter of the high-pressure casing is about one-third that of the advanced gas turbine compressor and since its pressure is about 20 times greater, the high-pressure casing volume will be about $(1/3)^3 (20) = 0.74$ times that of the advanced gas turbine compressor. If the casing materials are assumed to have the same density, then the casing weight (and hence most of the high-pressure compressor weight) should bear the same relationship to the casing weight of the reference compressor as do the casing volumes. If it is further assumed that the casing weight of the reference compressor represents 25 percent of the total reference compressor weight, the weight of the high-pressure compressor will be $0.74 (0.25) = 0.185$, or about 0.2 times the weight of the compressor in a comparable advanced gas turbine.

Application of the same considerations to the high-pressure (polytropic) turbine leads to the conclusion that its weight is about 0.2 times the turbine weight in a comparable advanced gas turbine. However, the presence of the reheaters must also be accounted for. It is assumed that these would be annular combustors located between and in line with the turbine stages, and that their presence will double the effective turbine weight. Thus, the total high-temperature turbine weight was assumed to be $2 (0.2) = 0.4$ times the turbine weight of a comparable gas turbine.

One final assumption was that in the advanced gas turbines the compressor represents 75 percent of total engine weight and the turbine represents 25 percent.* The estimate of total intercool-reheat cycle engine weight was then compiled as follows:

Low-pressure compressor wt	= reference compressor wt	= 0.75 (reference engine wt)
Low-pressure turbine wt	= 0.8 (reference turbine wt)	= 0.20 (reference engine wt)
High-pressure compressor wt	= 0.2 (reference compressor wt)	= 0.15 (reference engine wt)
High-pressure turbine wt	= 0.4 (reference turbine wt)	= 0.10 (reference engine wt)
Total engine wt		= 1.20 (reference engine wt)

Thus, the conclusion is that the intercool-reheat engine will weigh about 20 percent more than a comparable advanced gas turbine. The specific weight of a 10,000-hp engine then would be 1.2 (0.125 lb/hp) = 0.150 lb/hp. The intercooler specific weight of 0.114 lb/hp must be added to obtain a total engine specific weight of 0.264 lb/hp for a 10,000-hp engine. For a 1500-hp engine, the total engine specific weight calculated on the same basis is 0.298 lb/hp. For a 500-hp engine, the calculated specific weight is 0.406 lb/hp.

Fuel consumption was calculated using an overall efficiency of 38 percent, using the load-time schedule in Table II, and assuming that the fractional change in specific fuel consumption with load is the same as that of the advanced gas turbines (see Figure 1). Transmission and shafting specific weights were assumed to be the same as those of the advanced gas turbines. The total system specific weight (engine, transmission and shafting, and fuel) for intercool-reheat cycle engines and advanced gas turbines is compared in Figure 29.

Figure 29 indicates that the total specific weight of intercool-reheat engine and advanced gas turbine are comparable in magnitude. While the specific weight of the intercool-reheat engine exceeds that of the advanced gas turbine by a factor of 2 or more, this difference tends to be offset by the lower fuel consumption of the intercool-reheat engine.

Figure 29 shows the total system weight for the intercool-reheat engine to be less than that of the advanced gas turbine at 500 hp and 1500 hp. This is a consequence of the assumption that the component and cycle efficiencies are the same over the range of 500 hp to 10,000 hp. Actually, efficiencies would be expected to drop off substantially at power levels below 10,000 hp because of the small size of the high-pressure compressor and turbine, and total

*The combustor weight was assumed to be a small fraction of the total engine weight and was neglected in the analysis.

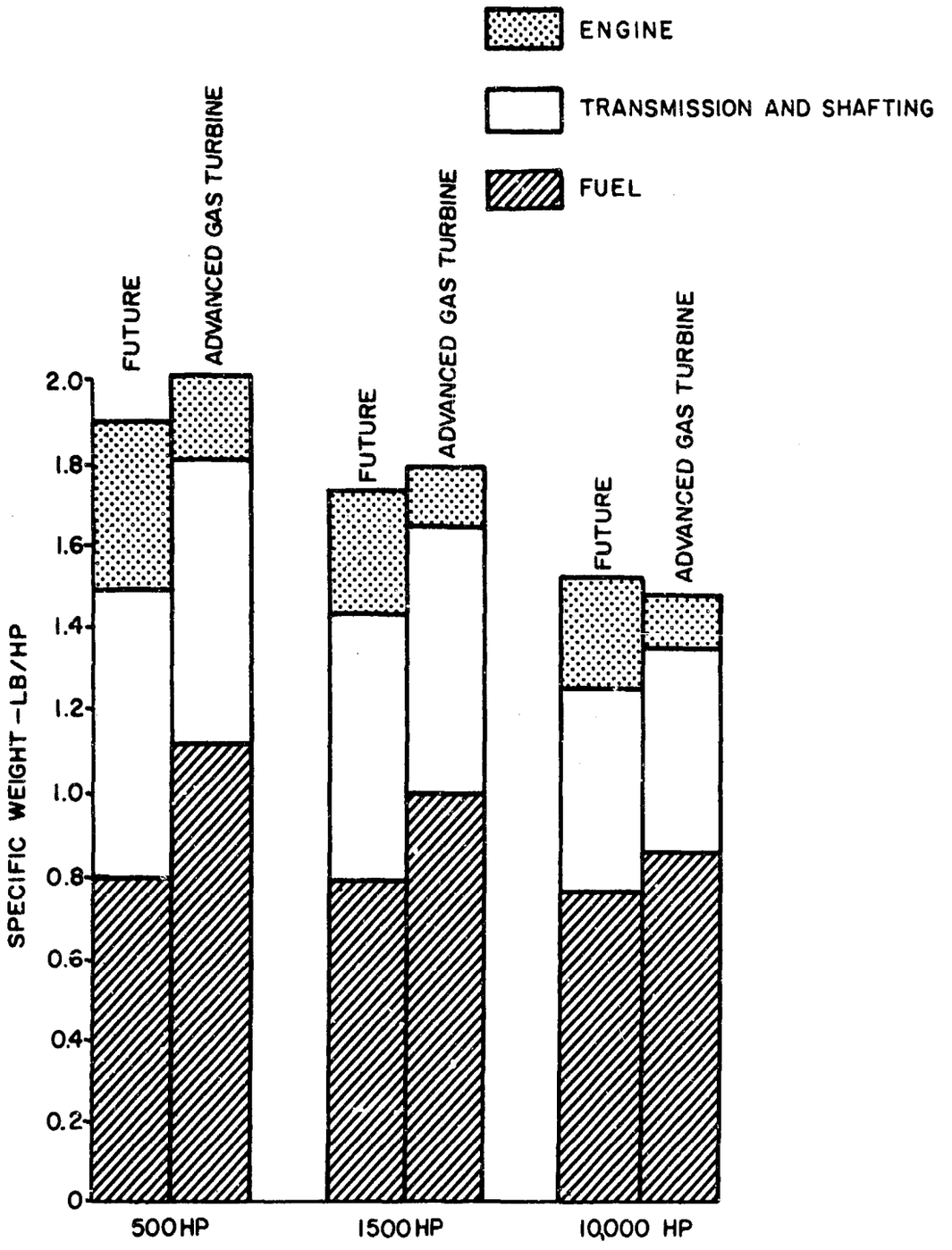

Figure 29. Specific Weight of Intercool-Reheat Cycle Shaft Power Systems.

system weights would probably exceed those of the advanced gas turbines at the 500 and 1500 hp levels.

Specific Volume

It was estimated that the volume of main engine components would bear about the same relationship to advanced gas turbine volume as does weight. Thus, the total specific volume of the compressors and turbines comprising the intercool-reheat engine was taken to be 1.2 times the specific volume of the advanced gas turbines. The intercooler specific volume was estimated from heat transfer surface data on the assumption of a surface-volume ratio of 200 ft^2/ft^3. The resulting intercooler specific volumes were 0.00822 ft^3/hp at 500 hp, 0.00624 ft^3/hp at 1500 hp, and 0.00524 ft^3/hp at 10,000 hp. The total estimated engine specific volume (rotating components plus intercooler) is given in Table XVII, along with the specific volume of the advanced gas turbines.

TABLE XVII. SPECIFIC VOLUME OF INTERCOOL-REHEAT CYCLE ENGINES

	Shaft Power (hp)		
	500	1500	10,000
	Specific Volume (ft^3/hp)		
Advanced Gas Turbine	3.24×10^{-3}	$3.01\text{-}3.24 \times 10^{-3}$	$1.57\text{-}3.15 \times 10^{-3}$
Intercool-Reheat Cycle	12.11×10^{-3}	$9.86\text{-}10.13 \times 10^{-3}$	$7.53\text{-}9.42 \times 10^{-3}$

The total engine volumes are seen to be 3 to 4 times greater than that of the advanced gas turbines. Most of the excess volume is attributable to the intercooler.

Cost

It is expected that the cost of an intercool-reheat engine would be similar to or less than that of a comparable advanced gas turbine because of lower material temperatures and the avoidance of the need for cooled turbine blades. While thick-walled casings will be required for the high-pressure compressor and turbine, the casing costs should not be excessive because of the relatively small volumes of these components.

Reliability

Although the intercool-reheat engine has more components than an advanced gas turbine, the adverse effect of this fact on reliability is countered by the

lower operating temperature and the avoidance of blade cooling schemes. Significant differences in reliability between the two engine types are not expected.

Sensitivity to Environment

The intercool-reheat cycle will be more sensitive to ambient temperature and pressure than the advanced gas turbine because ambient air is used as the heat sink for the heat of compression which is removed from the polytropic compressor. With respect to sand and dust ingestion and vibration and acceleration, the sensitivity of the two engine types should be comparable.

Part-Load Characteristics

Part-load characteristics should be similar to those of the advanced gas turbines.

Transient Response

The intercool-reheat engine may not respond to transients quite as rapidly as an advanced gas turbine because of the larger number of interacting components and the greater engine weight.

Structural Considerations

The use of four rather than two pieces of rotating machinery will require more bearings and probably more structure support at points where the engine is mounted to the airframe. The vibration characteristics of the engine and in particular the intercooler will require careful examination. Also, passages will have to be provided for directing rotor downwash air through the intercooler.

Critical Problem Areas

A number of unique problems will be encountered in the design and development of an intercool-reheat cycle engine. The polytropic compressor must permit the ready removal of the heat of compression without adverse effects on compressor efficiency or pressure ratio. The intercooler will require careful design to avoid excessive pressure drops, particularly on the ambient air side. The adiabatic compressor must exhibit good efficiency despite its small size, and it must be capable of withstanding internal pressures of several hundred atmospheres without excessive back leakage. The polytropic turbine design requires similar considerations. In addition, the reheat combusters must be compact and capable of efficient operation at several hundred atmospheres. High-pressure fuel injection systems will also be required. The adiabatic turbine is relatively conventional and should present few problems.

Conclusions

The intercool-reheat cycle engine appears to be competitive with advanced gas turbines with respect to overall system weight (engine, transmission and shafting, and fuel). While the engine is heavier, this weight penalty tends to be offset by the lower fuel consumption of the intercool-reheat engine. The intercool-reheat cycle compares reasonably well with the advanced gas turbine with respect to most other characteristics. The relatively large volume of the intercooler is perhaps the most unfavorable characteristic of the intercool-reheat engine.

The favorable performance of the intercool-reheat engine is achieved with a peak cycle temperature of about 1500°F, thus avoiding the materials and cooling problems of the advanced gas turbines. Because of the small size of the adiabatic compressor and polytropic turbine, the most favorable performance will probably be achieved at the 10,000-hp level, where dimensions of the high-pressure rotating components should be adequate to permit reasonable component efficiencies. Penalties to be paid for the performance of the intercool-reheat engine include: overall pressure ratios of several hundred, a more complex system, and the need for reheat and intercooling.

It is concluded that the favorable system characteristics revealed in this preliminary evaluation warrant a more detailed study of the intercool-reheat cycle. The purpose of such a study would be to determine and optimize system design and performance characteristics on a much firmer basis than was possible within the scope of this preliminary effort. Should such a study confirm the favorable characteristics of the intercool-reheat cycle, development could then be initiated in some of the critical problem areas cited above.

DIRECT-CONVERSION ELECTRICAL GENERATORS

Four direct-conversion electrical generators have been included in this survey: fuel cells, MHD (magnetohydrodynamic) converters, thermionic converters, and thermoelectric converters. In each case, an electric motor is required to convert the electricity produced to the desired shaft output. The characteristics of conventional and superconducting motors are discussed in Appendix III. In this section, results and data derived in Appendix III are applied without comment in the evaluation of the direct electrical generators for aircraft propulsion.

FUEL CELLS[23-37]

Fuel cells have been under development since the early 1950's. Principal applications thus far have included: space power systems for the Gemini and Apollo manned space flight programs, portable generators and land vehicle propulsion for the military, and commercial power generation. The major incentive for fuel cell development is the high thermal efficiency that can be achieved with this device, even at relatively low temperatures and power levels. (For example, the efficiency of the 2-kw Apollo fuel cell power plant operating at 400° to 500° F is well over 50 percent.) Other considerations favoring the fuel cell are its basic simplicity and ruggedness (no moving parts in the cell stacks) and its quietness of operation. Offsetting these factors are the relatively high fuel cell specific weight (lb/kw), the need for heat and reaction product removal systems as well as startup and control systems, the deleterious effect of reactant impurities on performance, the chemical reactiveness of the fuel cell reactants and/or electrolyte, and high costs due to use of noble metal catalysts (i.e., platinum).

In a fuel cell, a chemical fuel is electrochemically oxidized to yield electricity, heat, and reaction products. A fuel cell schematic is shown in Figure 30. The cell consists of five major components: a central compartment filled with electrolyte is flanked on either side by electrodes (an anode and a cathode), which in turn are flanked by fuel and oxidant compartments. In the cell of Figure 30, hydrogen is the fuel and oxygen is the oxidant. Both are fed continuously into the fuel cell from external tanks. The electrolyte is an aqueous solution of potassium hydroxide. At the anode-electrolyte interface, hydrogen gas reacts with negative OH ions (which have migrated through the eletrolyte from the cathode) to form water plus free electrons. The free electrons flow through an external load to the cathode, where they react at the cathode-electrolyte interface with oxygen gas and water to form OH ions. Chemically, the reactions are

$$\text{Anode:} \quad H_2 + 2\,OH^- + 2\bar{e} \rightarrow 2H_2O$$

$$\text{Cathode:} \quad 1/2O_2 + H_2O + 2\bar{e} \rightarrow 2\,OH^-$$

The overall reaction is

$$H_2 + 1/2\,O_2 \rightarrow H_2O$$

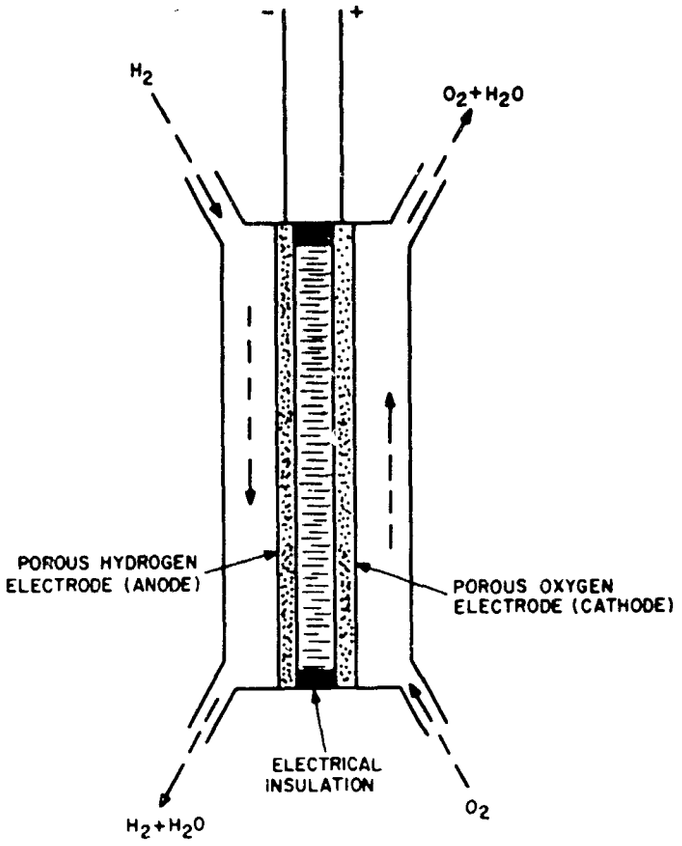

Figure 30. Fuel Cell.[23]

Water, the reaction product, and heat, resulting from the inefficiency of conversion of the heat of reaction to electricity, must be continuously removed. Water removal is usually accomplished by evaporation into the hydrogen gas compartment. The water vapor may then be transported to a condenser by circulation of excess hydrogen, or removed by a "static removal" technique.[26] Heat may be removed by conduction or by circulation of a liquid coolant through coolant passages.

The heat of reaction (Btu/lb) may be represented in the form of joules/coulomb (i.e., volts), since a definite flow of electric charge is associated with the electrochemical oxidation of each pound of fuel. For the hydrogen-oxygen fuel cell, the heat of reaction is equivalent to 1.48 volts. The thermal efficiency η of the cell (fraction of the heat of reaction which is converted to electricity) is simply

$$\eta = V/1.48$$

where V is the net output voltage of a single cell.[24] For a hydrogen-oxygen fuel cell, the maximum (open circuit) voltage is 1.23 volts. Therefore, the maximum thermal efficiency is 1.23/1.48 or 0.83.

As indicated in Figure 31, the output voltage V (and hence efficiency) diminishes continuously as increasing current is drawn from the cell. The voltage loss is referred to as polarization and is a consequence of three factors: (1) a chemical kinetics limitation on reaction rates at the electrodes (activation polarization), (2) internal cell resistance (ohmic polarization), and (3) a limitation on the rate at which reactants can diffuse through the porous electrode structure to the active reaction sites at the electrode-electrolyte interfaces (concentration polarization). The portion of the voltage-current density curve over which each type of voltage loss is predominant is indicated in Figure 31.

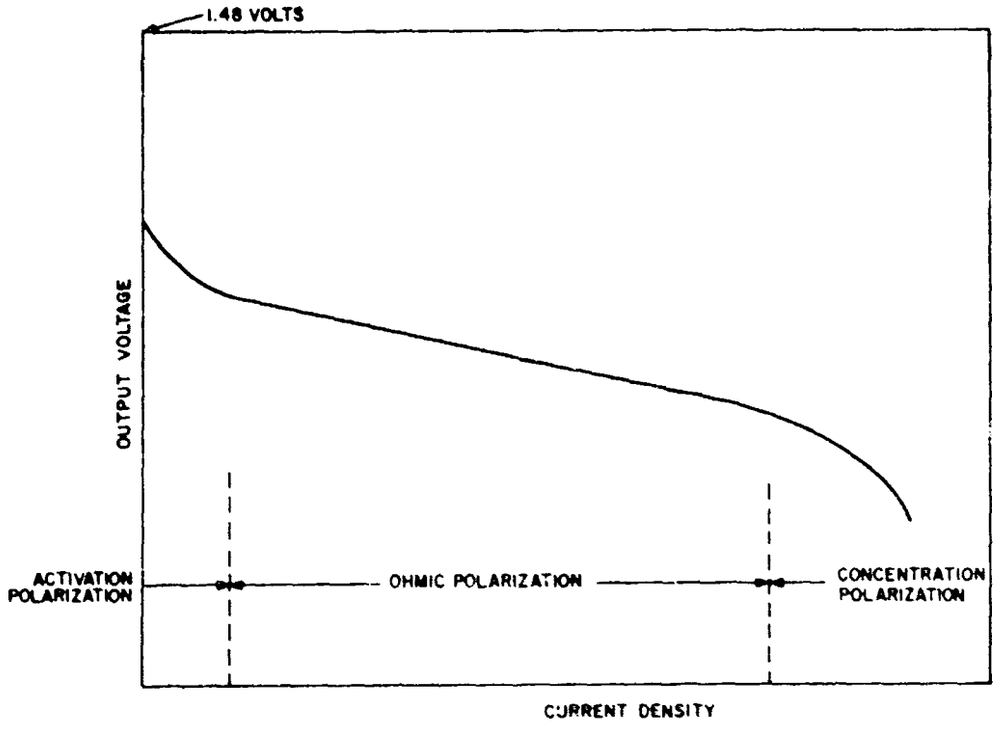

Figure 31. Fuel Cell Output Voltage Versus Current Density.[24]

The optimum current density and power density for which the total fuel cell system weight and volume, including reactants, are a minimum are dependent on total operating time. Where the operating time is hundreds of hours, as for the Gemini and Apollo space flights, reactant weight is dominant, and the operating point on the volt-current density curve is selected at about 1 volt in order to have high thermal efficiency. However, the resultant low current density ($\approx$200 amp/ft^2) results in a heavy power plant (120 lb/kw for the 2-kw Apollo unit). For short

missions of 1 hour or less, power plant weight is dominant and a high-current-density, low-voltage operating point will minimize the system weight. For example, a 10-kw unit has been designed for 15-minute operation. The fuel cell operates at about 0.5 volt and 2000 amp/ft^2 and weighs about 2.4 lb/kw.[25]

It is apparent that, for any mission, a fuel cell system with the "flattest" volt-current density curve is the most desirable. As shown in Figure 32, the curve is flattened by operation both at higher temperature and at higher reactant pressures.

The volt-current density curve for fuel cells results in useful performance characteristics. The part-load efficiency exceeds that at the design point, since a reduction in load causes the operating point to move to a lower current density, higher voltage (thus, more efficient) condition. Further, considerable overloads can be tolerated for short times at the expense of efficiency. For example, a 2-kw hydrogen-oxygen fuel cell has operated at 4.5 kw continuously for up to 5 minutes.[26]

Fuel cells can also exhibit good transient response, and lifetimes of thousands of hours are achievable. The 2-kw fuel cell just referred to can adjust to large step changes in load in less than 100 milliseconds, and it has operated for 3000 hours.

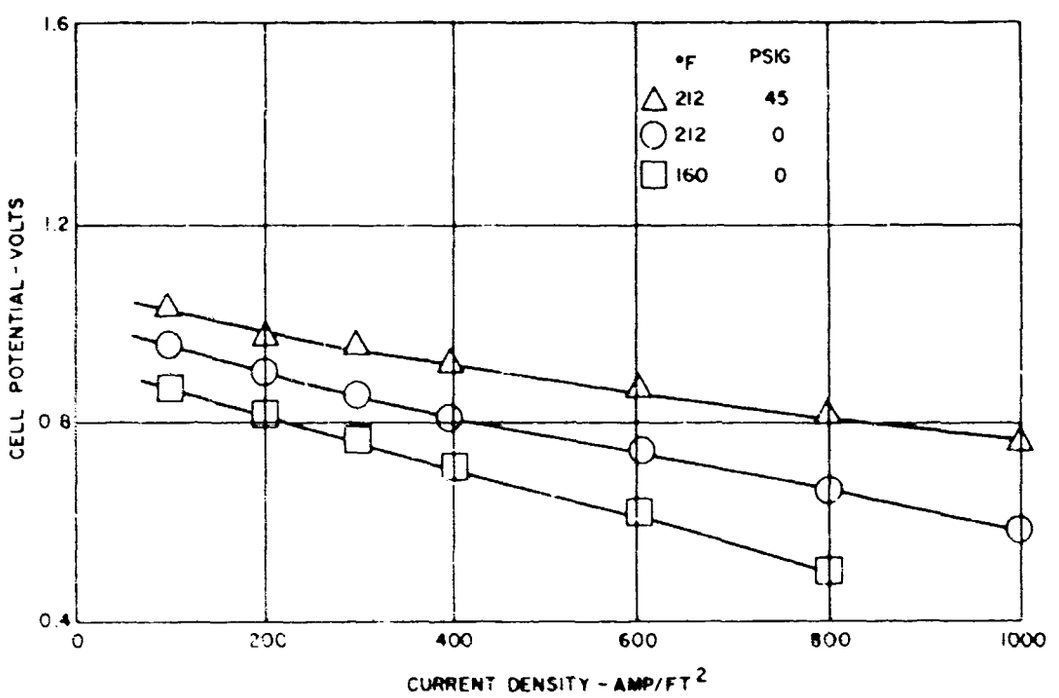

Figure 32. Effect of Temperature and Pressure on Voltage–Current Density Curve.[32]

However, the voltage during this time dropped to 27 volts from an initial output of almost 30 volts.

Current Status[27-36]

The principal distinguishing features of fuel cells are: fuel and oxidant to be reacted, operating temperature, and the electrolyte.

The simplest, most efficient type is the hydrogen-oxygen fuel cell. Three H_2-O_2 cells have been under development for space application. The first type operates at about 200°F and uses an aqueous solution of 35 wt percent potassium hydroxide (KOH) as the electrolyte, which is retained in a porous asbestos matrix. The second type operates at about 400°F and uses an aqueous solution of 85 percent KOH as the electrolyte. The third type operates at about 100°F and uses a water-saturated ion-exchange membrane as the electrolyte. Hydrogen fuel cells can also be operated with air as the oxidant, but a CO_2 scrubber is needed to prevent its reaction with alkaline electrolytes. At low current densities ($\approx$200 amp/ft^2), the consequence of operating with air instead of oxygen is about a 10-percent loss of efficiency. However, at higher current densities, voltage losses due to concentration polarization increase rapidly and efficiency drops off sharply.

Fuel cells utilizing inorganic fuels such as hydrazine (N_2H_4) and ammonia with air have also been considered. Hydrazine gives better performance than ammonia, but it is quite expensive. 300-watt and 5-kw hydrazine-air units have been developed by the Army for field application, and a 40-kw unit is under development for research purposes.[27] The units operate at low temperature (<200° F) and utilize liquid hydrazine hydrate as the fuel (64 percent N_2H_4, 36 percent H_2O) and a 35-wt percent KOH aqueous electrolyte. The fuel consumption rate is about 1.4 lb/kw-hr.

Much research has also gone into hydrocarbon-air fuel cells. Some of these cell types can utilize the hydrocarbon fuel directly, while in other cases the hydrocarbon must be "reformed" to yield free hydrogen, which is then fed to the cell anodes. The hydrocarbon-air units are considerably less efficient and heavier than fuel cells operating with pure hydrogen fuel. Depending on the particular cell type, alkaline, acid, or molten carbonate electrolytes may be used.

Table XVIII gives typical fuel characteristics for hydrocarbon (CITE), hydrogen, and hydrazine fuels.

TABLE XVIII. TYPICAL CHARACTERISTICS OF FUEL CELL FUELS [27]

Fuel	Heat Val (kw-hr/lb)	Heat Val (kw-hr/gal)	Cost (cents/lb)	Thermal Eff (%)	Specific Fuel Consump (lb/kw-hr)	Specific Fuel Consump (gal/kw-hr)	Cost (cents/kw-hr)
CITE	5.6	31.0	3.5	30	0.6	0.105	2.1
Hydrogen	14.9	8.4	50.0*	60	0.1	0.195	5.0
Hydrazine	1.6	13.5	50.0	45	1.4	0.165	70.0

*More recent studies indicate that hydrogen produced on a large scale may be available for less than 4 cents/lb.[37]

If hydrogen were used as a fuel, it would normally be supplied in a high-pressure gas tank or a cryogenically cooled container. Recent studies indicate that a third means for storing hydrogen, in metal hydride form, may be feasible.[37] The metal hydride would dissociate, yielding free hydrogen, when heated to its dissociation temperature. Magnesium hydride dissociates at 550° F under 1 atmosphere of pressure. With the addition of a small amount of nickel catalyst, dissociation rates are sufficiently rapid to meet hydrogen fuel cell feed requirements. A hydrided iron-titanium alloy dissociates under 1 atmosphere at 70° F at a satisfactory rate. A metal hydride hydrogen storage system is appreciably lighter and smaller than a gas storage system, and it is moderately heavier than a liquid (cryogenic) storage system, as indicated in Table XIX. Characteristics of several fuel cell types are given in Table XX.

TABLE XIX. COMPARISON OF HYDROGEN STORAGE SYSTEMS[37]

Hydrogen Wt (lb)	Storage System	Carrier and Fuel Wt (lb)	Contained Volume (ft^3)
45	Gas at 2000 psi	2250	66
45	Liquid	353	10.2
45	MgH with Ni catalyst (40% voids)	692	10.8

The minimum specific weight of high-efficiency H_2-O_2 fuel cells is currently about 30 lb/kw. Protracted development would be needed to reduce the specific weight to 15 to 20 lb/kw. On the other hand, specific weights of 2 lb/kw currently appear to be feasible for low-efficiency fuel cells (item 5, Table XX). With continued development, a specific weight of 1 lb/kw is conceivable. However, this is an open-cycle, high-current-density cell which utilizes expendable water for

TABLE XX. FUEL CELL CHARACTERISTICS

Fuel-Oxidant	Net Power (kw)	Thermal Eff (%)	Current Density (amp/ft^2)	Volts/cell	Temp. (°F)	Specific Wt (lb/kw)	Specific Vol (ft^3/kw)	Ref
1. H_2-O_2	0.4	79	65		200	222	3.32	31
2. H_2-O_2	0.2	66	200	>0.9	200	150	2.42	26
3. H_2-O_2	2.0	66	200	>0.9	200	84.5	3.11	26
4. H_2-O_2	5.0	66	200	≈0.98	200	30.0	0.45	26
5. H_2-O_2	10.0	46	1550	0.68	230	1.7*	0.32	25
6. H_2-air	2.0	56	167	0.83	160	19.1*		29
7. N_2H_4-air	40.0					21.2	0.38	27
8. JP-4-air	1.5	22				100		33
9. Multi-fuel-air	15.0	20+				113		33
10. JP-125-air	5.6	27	130	0.83	180	199	6.24	28
11. Methanol-air	0.1	27	71	0.4		200		34

*Weight of fuel cell stack only.

cooling and expendable hydrogen for removal of cell water. Cell lifetime may be limited and reactant and water coolant weight may be high. N_2H_4-air systems have a current specific weight of about 20 lb/kw; an improvement of a factor of 2 in specific weight is conceivable.

Hydrocarbon-air systems are currently characterized by low efficiency (25 percent) and high specific weight (100 to 200 lb/kw). Specific weights may be expected to drop by a factor of 2 to 3 as plant size increases from current levels to 500 kw. Future projections of hydrocarbon-air fuel cell weight predict specific weights of 10 lb/kw for a 100-kw unit and 5 lb/kw for a 500-kw unit by 1980.[27] Efficiency may increase to 40 percent.

Major problems encountered in fuel cell development are: the use of expensive catalysts, voltage degradation with time due to accumulation of impurities in electrodes, materials compatibility, and heat and water removal systems. These problems are yielding to continued research and development.

Application to Aircraft Propulsion

The applicability to aircraft propulsion of fuel cells with four different combinations of fuel and oxidant will be considered. These combinations are: hydrogen-air, hydrocarbon-air, hydrazine-air, and hydrogen-oxygen. Only the open-cycle hydrogen-oxygen cell is considered because of its unusually low specific weight (see item 5, Table XX).

Specific Weight

Since fuel cells have a significant overload capacity, system characteristics have been determined for fuel cells rated at 60 percent of the nominal full load. For example, a fuel cell rated at 300 hp would be used to meet the same requirements as a 500-hp gas turbine. From Table II, the load-time schedule indicates that an engine will operate at 60 percent of full load for 2 hrs, 70 percent of full load for 15 min, and 85 percent of full load for 35 min. Thus, a fuel cell rated at 60 percent of full load would operate at (85/60) (100) = 142 percent of its rated load for 35 min. A 2-kw fuel cell has successfully operated at 225 percent of rated load for up to 5 min.[26] On the basis of an efficiency-load curve for fuel cells based on the 1964 state of the art[26] and the load-time schedule of Table II, it was established that total fuel consumption was equal to fuel consumed after operation for 2.12 hrs at the rated load (60 percent of the nominal full load). The specific weights of hydrogen-air, hydrocarbon-air, hydrazine-air, and hydrogen-oxygen fuel cells are discussed below.

1. The efficiency of a typical 5-kw hydrogen-oxygen fuel cell is about 66 percent. If the cell were operated on air, the efficiency would probably drop to 56 percent. The overall efficiency, taking into account auxiliary power requirements, would be about 46 percent. This fuel cell has a specific weight of 30 lb/kw, or 18 lb/kw when rated at 60 percent of full load. In terms of hp, the specific weight is 13.4 lb/hp. The efficiency should increase with plant size, and the specific weight should decrease with plant size, because then larger, more efficient auxiliaries can be used. Significant improvements in efficiency and specific weight can be expected in the future as design and engineering improvements are applied and as lighter, more efficient auxiliaries come into use. It was assumed that such improvements can reduce specific weights based on current technology by about a factor of 2. (This assumption was used for all the fuel cell types which were considered.)

   The hydrogen fuel was assumed to be stored as a cryogenic liquid because, as is shown in Appendix III, the weight of the liquid storage mode is less than for storage of hydrogen in other forms. The weight of the storage system plus liquid hydrogen is 7.85 lb/lb of hydrogen for a system with a capacity of 45 lb of hydrogen. The storage system weight should decrease significantly with an increase in capacity because of the resulting reduction in the surface-volume ratio. A reduction of a factor of 2 in storage system weight is

predicted for the future because of anticipated improvements in thermal insulation and the availability of lightweight turbomachinery for refrigeration in place of reciprocating machinery.

Estimated characteristics of hydrogen-air fuel cells based on present and future technology as delineated above are presented in Table XXI for the power range of 500 hp to 10,000 hp.

TABLE XXI. CHARACTERISTICS OF HYDROGEN-AIR FUEL CELLS

	PRESENT			FUTURE		
Power - hp	500	1500	10,000	500	1500	10,000
Efficiency - %	50	51	53	60	63	63
Specific Weight - lb/hp						
Fuel Cell	10.8	10.2	9.0	5.40	5.10	4.50
Fuel	0.210	0.206	0.198	0.175	0.169	0.166
Fuel + Storage	1.260	0.825	0.396	0.525	0.338	0.249

2. The specific weight of low-kw hydrocarbon-air fuel cells is typically about 100 lb/kw = 74.6 lb/hp. When rated at 60 percent of full load, the specific weight is 44.7 lb/hp. The system efficiency for these systems is about 25 percent. The projected characteristics of hydrocarbon-air fuel cells in the 500-hp to 10,000-hp range are presented in Table XXII.

TABLE XXII. CHARACTERISTICS OF HYDROCARBON-AIR FUEL CELLS

	PRESENT			FUTURE		
Power - hp	500	1500	10,000	500	1500	10,000
Efficiency - %	25	27	30	30	33	40
Specific Weight - lb/hp						
Fuel Cell	30	25	15	15	12	
Fuel	1.17	1.08	0.98	0.98	0.89	0.73

3. The specific weight of a 40-kw hydrazine-air fuel cell is about 20 lb/kw = 14.9 lb/hp. When rated at 60 percent of full load, the specific weight is 8.94 lb/hp. The fuel consumption rate at an

efficiency of 45 percent is 1.4 lb/kw-hr = 1.042 lb/hp-hr (see Table XVIII). The projected characteristics of hydrazine-air fuel cells in the 500-hp to 10,000-hp range are given in Table XXIII.

TABLE XXIII. CHARACTERISTICS OF HYDRAZINE-AIR FUEL CELLS

	PRESENT			FUTURE		
Power - hp	500	1500	10,000	500	1500	10,000
Efficiency - %	40	42	45	45	47	50
Specific Weight - lb/hp						
Fuel Cell	8	7	6	4	3.5	3
Fuel	2.48	2.36	2.21	2.21	2.12	1.99

4. The last fuel cell type to be considered is the hydrogen-oxygen cell that operates on the open cycle.[25] In this fuel cell, product heat evaporates extra water, which is then vented. Similarly, product water is removed by evaporation into excess hydrogen vapor, which is then vented. The specific weight of a 10-kw fuel cell is 1.7 lb/kw = 1.27 lb/hp. When rated at 60 percent of full load, the specific weight is 0.762 lb/hp. When optimized for a 15-min mission, the optimum conditions for minimum fuel cell plus fuel weight are 1550 amp/ft^2 and 0.68 volt. The corresponding system efficiency is 46 percent. These conditions were used as the basis for analysis of the aircraft mission, although for longer operating times the optimum current density decreases and the optimum voltage increases.

   Fuel in this case is considered to include the hydrogen (including excess for product water removal), oxygen, their respective storage systems, and water for product heat removal. In this design, the hydrogen and oxygen are assumed to be stored at 6000 psi in filament-wound composite tanks. The hydrogen tank weight is 11.0 lb/lb of hydrogen. The oxygen tank weight is 0.55 lb/lb of oxygen. The specific weight for the aircraft mission is 6.64 lb/hp for the hydrogen, oxygen, and storage tanks, and 6.17 lb/hp for the water that is carried along for heat removal.

   For future systems of this type, a system efficiency of 50 percent was assumed, and liquid hydrogen storage was used with the same future ratios of storage system weight to hydrogen weight as were used to estimate future fuel consumption of hydrogen-air fuel cells. A reduction of 25 percent in fuel cell weight was postulated through the use of thinner plates and more compact packaging; a 20-percent reduction in the weight of the heat removal system was assumed

through the use of thinner, lighter wicks. The projected characteristics of the open-cycle hydrogen-oxygen fuel cell, as established from the above considerations, are presented in Table XXIV for the power range of 500 hp to 10,000 hp.

TABLE XXIV. CHARACTERISTICS OF OPEN-CYCLE HYDROGEN-OXYGEN FUEL CELLS

	PRESENT			FUTURE		
Power - hp	500	1500	10,000	500	1500	10,000
Efficiency - %	46	46	46	50	50	50
Specific Weight - lb/hp						
Fuel Cell	0.76	0.76	0.76	0.57	0.57	0.57
Fuel + Storage	12.81	12.81	12.81	8.12	7.80	7.20

The total system specific weight (fuel cell, motor-transmission, and fuel) for the various fuel cell types based on present technology is shown in Figure 33. Similar data based on future technology are given in Figure 34. The motor-transmission specific weights were obtained from data given in Appendix III. Except for the motor used with the 500-hp system based on present technology, all of the motors are of the superconducting type.

Figure 34 indicates that the lightest fuel cell systems projected for the future are the hydrogen-air and hydrazine-air fuel cells. Even so, these are three times heavier than the advanced gas turbine systems. The total fuel weight of the hydrogen-air fuel cell is quite low, even allowing for the added weight of the hydrogen storage system. The open-cycle hydrogen-oxygen fuel cell is much lighter than any of the other types (although heavier than an advanced gas turbine), but it suffers from excessive fuel consumption because of the need for an oxygen supply, excess hydrogen for product water removal, and extra water for product heat removal.

Specific Volume

The specific volumes of current hydrogen-oxygen and hydrazine-air fuel cells that are rated at 60 percent of full load are in the range of 0.13 to 0.22 ft^3/hp. These specific volumes are 40 to 70 times greater than the specific volumes of the advanced gas turbines. The specific volume of hydrocarbon-air fuel cells is on the order of 1.3 ft^3/hp, which is several hundred times greater than that of the advanced gas turbines.

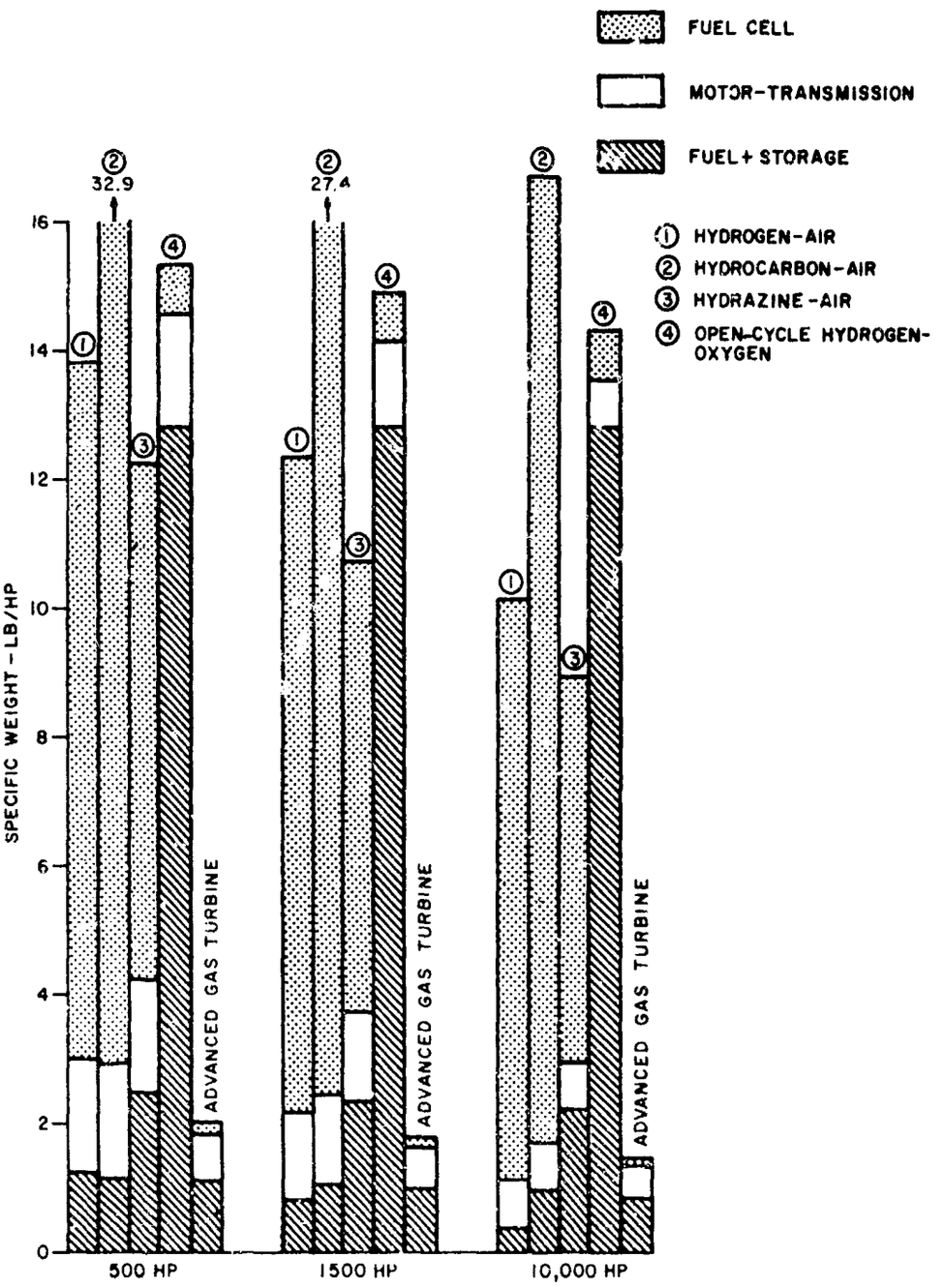

Figure 33. Specific Weight of Fuel Cell Shaft Power Systems – Present Technology.

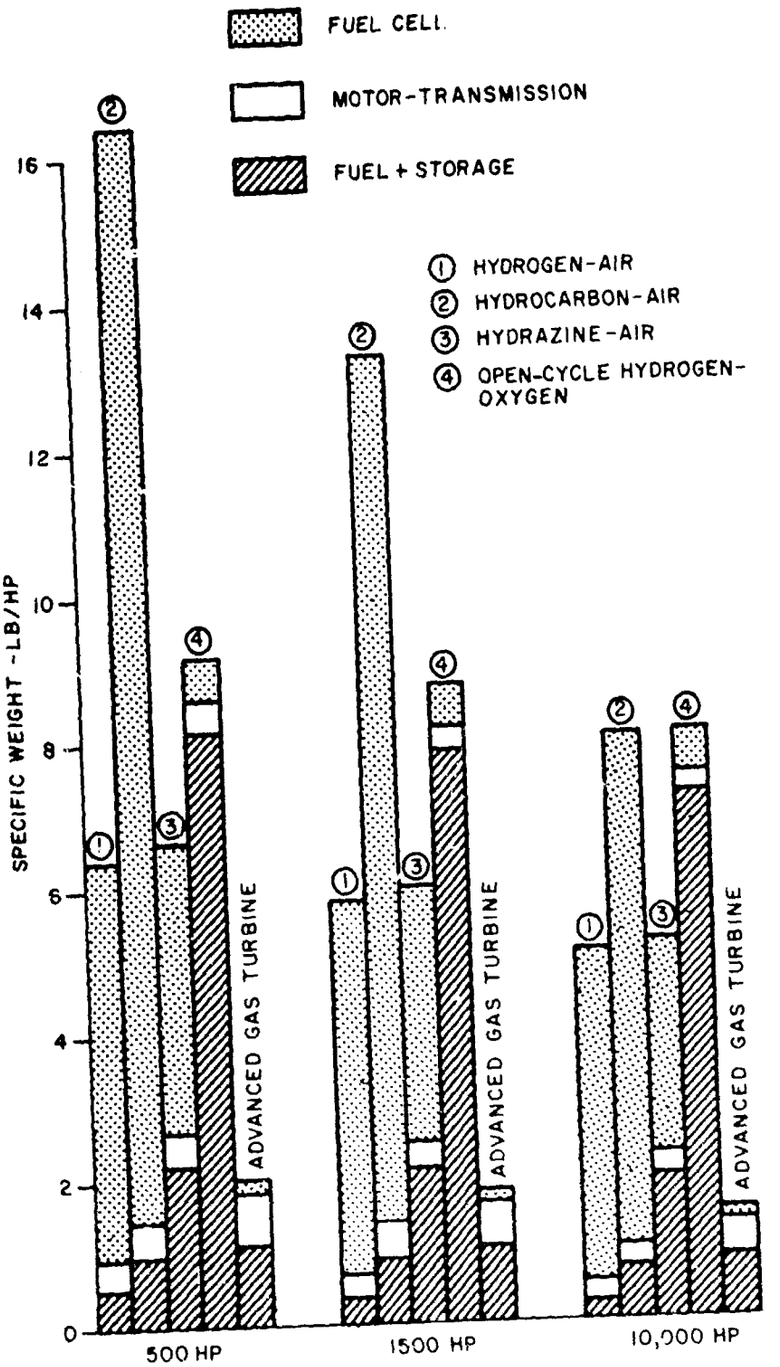

Figure 34. Specific Weight of Fuel Cell Shaft Power Systems – Future Technology.

Cost

Fuel cells are currently quite costly, primarily because noble metals such as platinum and palladium are used as catalysts. The need for a catalyst is lessened as the fuel cell's operating temperature is increased, and at high operating temperatures the catalyst may be eliminated. However, as temperatures rise, the reactants and electrolyte become more corrosive, and costly construction materials may be required for corrosion protection. It has been estimated that the initial production cost of fuel cells would be about $5000/kw = $3740/hp.* If the fuel cells were rated at 60 percent of full load, the cost would be $2240/hp. If a nonnoble catalyst were used, the cost could drop to $630/hp. These cost figures may be compared with estimated costs of $22/hp to $76/hp for advanced gas turbines (see Table II).

Cost data for CITE (hydrocarbon), hydrogen, and hydrazine fuels are given in Table XVIII. Fuel costs per hp-hr, as calculated from the Table XVIII data, are: CITE, 1.57¢/hp-hr; hydrogen, 0.3-3.73¢/hp-hr; and hydrazine, 52¢/hp-hr. The cost of JP-4 jet fuel, such as would be used in the advanced gas turbines, is about 0.8¢/hp-hr at a specific fuel consumption of 0.5 lb/hp-hr. Fuel cell fuel costs are seen to be high in comparison to the cost of gas turbine fuel, although hydrogen could conceivably be cheaper if projected large-scale production costs are achieved. (The figure of 0.3¢/hp-hr for hydrogen is based on a unit cost of 4¢/lb compared to current estimates of 50¢/lb.)

Reliability

Fuel cells have exhibited good reliability and have operated successfully for thousands of hours. However, some voltage degradation is to be expected during long operating periods from the accumulation of impurities on the electrodes. This degradation can be controlled by periodic purging of the fuel and oxidant. The ultimate goal of the Army for fuel cells for ground vehicles or ground power generation is a 10,000-hr life with 5000 hrs between overhauls.*

Sensitivity to Environment

Fuel cell operation is affected by ambient temperature, which will affect the rate at which product heat can be removed. For fuel cells that use ambient air as the oxidant, operation could be strongly affected by solid contaminants as well as moisture and carbon dioxide in the air. Filters, dehumidifiers, and CO_2 scrubbers are necessary for efficient operation over a long period. Fuel cells are inherently rugged devices, and they withstand vibration and acceleration without difficulty.

Part-Load Characteristics

Fuel cells exhibit excellent part-load characteristics, since the voltage (and hence the efficiency) increases as the load decreases.

*Personal communication with T. Kirkland, MERDC, Ft. Belvoir, Va.

Transient Response

The transient response of fuel cells is fairly good. The power level of a 2-kw unit has been increased from 422 watts to 4340 watts in 20 msec. The return from 4340 watts to 422 watts was accomplished in 62 msec.[26]

Structural Considerations

Since the fuel cell is essentially a chemical reactor, corrosion protection plays an important role in the selection of construction materials. The fuel cell is basically an assemblage of thin plates that are bolted together. Proper alignment and structural rigidity are essential for proper operation. Fuel cell weight may be reduced appreciably by the use of lightweight metals such as magnesium for structural purposes. For moderate-temperature fuel cells, the use of metal-coated plastic structural parts may also be considered.

Critical Problem Areas

The most critical problem area is that of reducing the high specific weight of fuel cell systems while retaining high efficiency. Approaches to this goal include operation at higher temperature and pressure and reduction in the weight of fuel cell auxiliaries. (In some systems, the auxiliaries may constitute as much as two-thirds of the total fuel cell weight.) The expensive catalysts constitute another critical problem area, which may be lessened through operation at higher temperatures and the development of nonnoble metal catalysts. The degradation of voltage with time, while currently at acceptable levels, should be further lessened and, if possible, eliminated. Materials compatibility is an important problem area for fuel cells that operate at elevated temperatures. The removal of product heat and water is an ever-present problem, which grows in difficulty with the fuel cell power level.

The high weight of fuel cells is a consequence of the relatively low power density required for good efficiency. This situation results in large measure from the fact that the reactants must migrate to the surfaces of the fuel cell electrodes, where the basic chemical reactions take place. If a fuel cell concept could be devised wherein reaction sites were distributed through the electrode volume rather than located on the surface, radical increases in power density and reductions in fuel cell weight could be expected.

Conclusions

Fuel cells are not suitable for aircraft propulsion applications because of excessive total system size and weight.

MAGNETOHYDRODYNAMIC (MHD) CONVERTER

MHD refers to the direct generation of electricity as the consequence of flow of an electrically conductive fluid across a magnetic field. Serious efforts to develop practical MHD generators have been under way for about six years.

In contrast to fuel cell, thermionic, and thermoelectric electric generators, an MHD generator is readily scaled up to meet increasing power requirements and, in fact, should be rated at a minimum of about 200 kw for reasonable performance. Power levels of 200 kw and up are readily achieved in a single unit capable of output potentials of several hundred volts. MHD generators have been considered for space application, for central station power, and for the production of large-amplitude, short-duration power pulses.

The most significant characteristic of an MHD generator is its capability for operation at high temperature. This is possible because the generator is a simple gas flow duct, with no need for high-speed turbomachinery such as is characteristic of gas turbines. When the MHD fluid is gaseous, the high-temperature operating capability is an absolute necessity, since the electrical conductivity of the gas upon which power generation depends is not significant at lower temperatures.

A schematic of an MHD power generation duct is shown in Figure 35. A conductive fluid flows through the duct, intersecting lines of magnetic force (magnetic field B) that are normal to the fluid flow direction. An electric potential difference then develops between the electrodes. If the electrodes are connected to an external load, current will flow and power will be dissipated in the load. In general, the voltage and current will have components both normal and parallel to the fluid flow direction. The relative magnitude of these components depends on a quantity

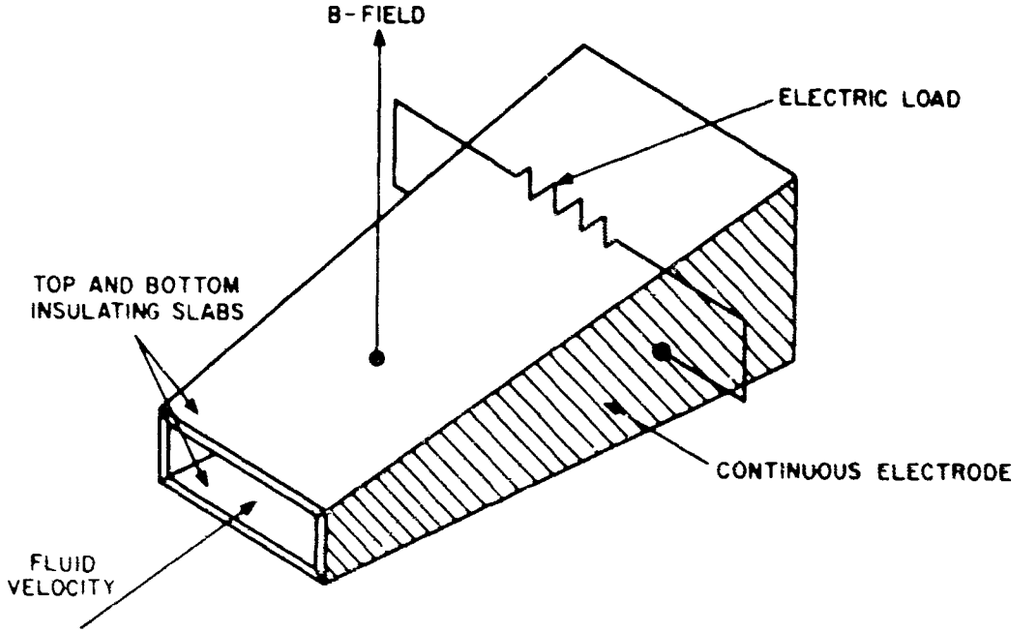

Figure 35. MHD Power Generation Duct.[38]

called the Hall parameter, which varies directly as the magnetic field and inversely as the fluid density.[38] A Faraday generator uses the normal component of current, and the axial flow of current along the electrodes is prevented by segmenting the electrodes and interspersing insulating segments. A Hall generator uses the parallel component of current. The normal component is then shorted out by the use of segmented electrodes that extend completely around the flow duct. The axial current flows between the electrodes at each end of the flow duct. The features of segmented-electrode Faraday and Hall generators are shown in Figures 36 and 37.

Current Status

The MHD generating duct is equivalent in function to the rotating turbine-generator portion of a conventional power generation system. Electricity is produced at the expense of pressure and enthalpy drops in the MHD working fluid. The MHD duct can be incorporated into three basic thermodynamic cycles: the open cycle, the closed gas cycle, and the closed liquid metal cycle.

Open Cycle

In the open cycle, a chemical fuel and an oxidant are burned in a combustion chamber to form combustion gases at a pressure of several atmospheres and

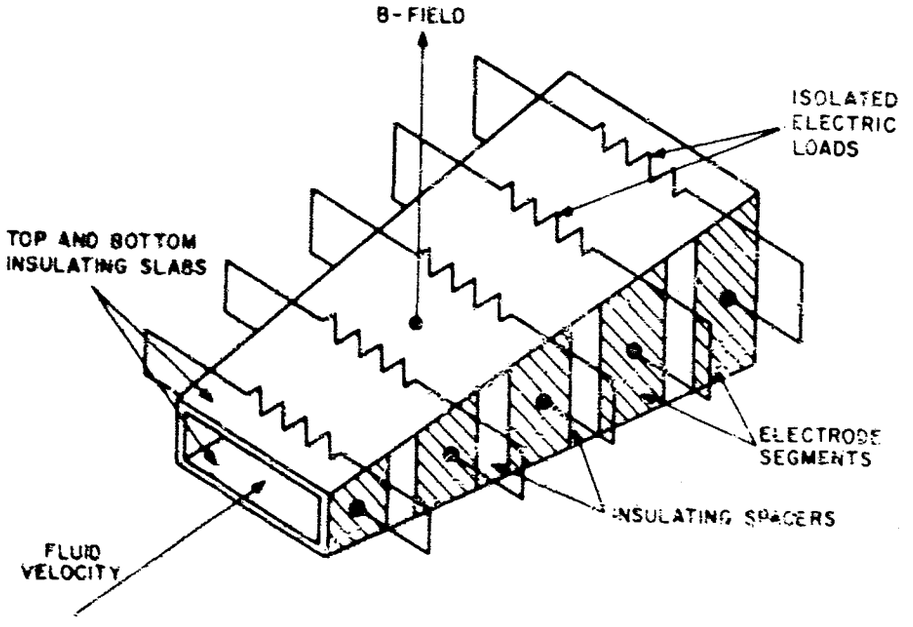

Figure 36. MHD Faraday Generator.[38]

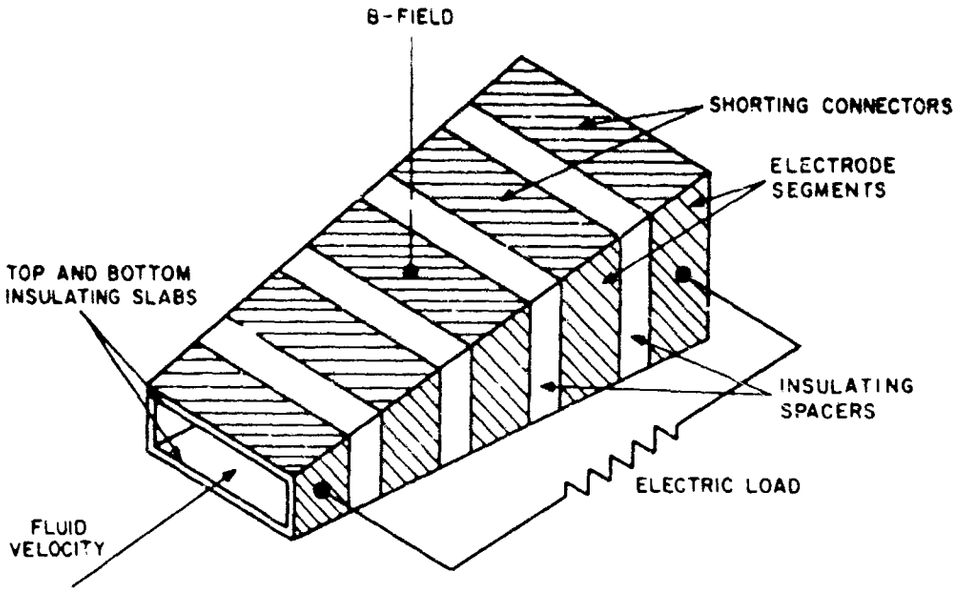

Figure 37. MHD Hall Generator.[38]

a temperature of 4500° to 5000° F. The combustion gases are "seeded" with a small quantity (<1 percent) of potassium or cesium salts. The alkali metals ionize readily at generator operating temperatures, thus providing the free electrons necessary to render the combustion gases electrically conductive. The gas then expands through a supersonic nozzle, acquiring a velocity of 2000 to 6000 ft/sec, and enters the MHD duct. In the MHD duct, where electricity is produced, the gas pressure approaches ambient and the temperature drops to 3000° to 4000° F. The gas then flows through a diffuser and is discharged into the atmosphere.

The open-cycle MHD generators can operate with almost any fuel (alcohol, JP-4, powdered coal), and the oxidant may be pure oxygen, oxygen-enriched air, or air. In the case of air, the air must be pressurized and then preheated prior to combustion in order to develop the high temperatures in the combustion gases needed for adequate electrical conductivity. The air is preheated most efficiently in a regenerator by the hot generator discharge gases, although separately fired preheaters can also be used. The maximum air preheat temperature is currently limited by materials cousiderations to about 2200° F. Generally, the gas conductivity decreases with increasing hydrogen content of the fuel, but operation with hydrocarbon fuels is permissible.[44, 45]

For electrical outputs in the range of 1 Mw to 30 Mw, thermal efficiency is on the order of 5 to 10 percent. Efficiencies can be increased to 20 percent or more by the use of higher preheat temperatures and more energetic fuels such as cyanogen or boron compounds. However, the practicality of such fuels may be limited. (For example, cyanogen can form toxic hydrogen cyanide when burned in moist air.) In terms of specific fuel consumption, current open-cycle systems using liquid oxygen consume fuel + oxidant at the rate of 7 to 9 lb/kw-hr. Advanced liquid oxygen systems may have a reactant consumption rate of 3 lb/kw-hr. The specific fuel consumption of MHD systems using energetic fuels and preheated air could be as low as 0.7 lb/kw-hr.[39]

A 1000-kw system currently under development for the Air Force is designed for a specific weight of 1 lb/kw. About 80 percent of the weight is taken up by the superconducting magnet. This unit burns JP-4 and LOX, with a specific fuel consumption of almost 8 lb/kw-hr. The specific weight of another 1000-kw design is less than 0.4 lb/kw, with a specific fuel consumption of 7 lb/kw-hr.* The use of improved energetic fuels plus increased magnetic field strengths is expected to lead to specific weights as low as 0.2 lb/kw at the 5000-kw level.[39]

If the systems just described were to burn preheated compressed air instead of LOX, specific fuel consumption, as pointed out above, might be reducible to 0.7 lb/kw-hr. However, the weight of the compressor and regenerator would then have to be added to the previous specific weights.

Startup and shutdown should occur quite rapidly in an open-cycle MHD system, most probably in a few seconds. Power level can be controlled by varying the gas or seed flow rates. Vibration and noise are quite significant.

Most current experience with open-cycle MHD systems is limited to operating periods of seconds or minutes. Some long-term tests at low power, but representative environmental conditions, have been conducted which demonstrate system lifetimes of at least 200 hours. Some performance characteristics of actual open-cycle installations are listed in Table XXV.

Gaseous Closed-Cycle MHD Systems[40, 44, 46]

An MHD generator can operate on the closed Brayton cycle with an inert gas working fluid. Conceptually, the system is similar to the open cycle, with the addition of separate heat exchangers for heat addition to and heat removal from the working fluid. Helium, neon, and argon may be considered as working fluids. These gases, seeded with potassium or cesium, are electrically more conductive than combustion gases. Therefore, peak cycle temperatures for comparable performance may be 1000° F lower than for the open cycle. Through a technique known as magnetically induced nonequilibrium ionization, peak temperatures might be lowered another 1000° F. However, the practicality of the latter technique has not yet been demonstrated.

*Personal communication with, S. Petty, Avco Everett Research Laboratory, Everett, Mass.

TABLE XXV. CHARACTERISTICS OF OPEN-CYCLE MHD GENERATING SYSTEMS[40]

	Mark II	Mark V	LORHO Pilot
Gross Output - kw	1500	40,000	20,000
Thermal Input - kw	20,000	400,000	300,000
MHD Duct Length - ft	5.0	9.8	13.1
Fuel	Kerosene	Alcohol	Toluene
Oxidizer	O_2	O_2	$O_2/N_2 = 1$
Temperature - °F	4950	4950	3870
Gas Velocity - ft/sec	3900	5600	5600-6900
Magnetic Field - gauss	32,000	33,000	19,000

While the closed cycle permits lower peak operating temperature, it becomes necessary to transfer heat from hot combustion gases to the working fluid in a heat exchanger operating at 3500° to 4000° F. The formidable material problems which result indicate that the lower operating temperature of the MHD closed-cycle generator is of little practical advantage in comparison with the open-cycle generator, where heat is added to the working fluid by direct combustion in a combustion chamber with cooled walls.

Liquid Metal Closed-Cycle MHD Systems[40,44,47-49]

The electrical conductivity of liquid metals at ambient temperature is several orders of magnitude greater than that of seeded gaseous plasmas at 4000° to 5000° F. Consideration has been given to closed-cycle liquid metal MHD systems with peak temperatures around 2000° F. Power is generated by driving a pure liquid metal or a mixture of a liquid metal and its vapor through an MHD generator duct. The liquid metal is accelerated to about 300 ft/sec by expansion of a heated vapor, which may be the same substance as the liquid or a completely different substance. In the latter case, the vapor must be separated from the liquid before the liquid enters the MHD duct. Cesium or potassium may be used as the accelerating vapor and, in a one-component cycle, as the accelerated liquid. In a two-component cycle, lithium has been considered for the liquid to be driven through the MHD duct.

Liquid metal MHD systems are somewhat complex conceptually. Overall efficiencies are in the range of 5 to 15 percent. Experimental work to date has not involved complete generating systems.

Application to Aircraft Propulsion

The open-cycle MHD generator appears to have the most potential for aircraft propulsion and hence will be the only type considered here. Recent information on airborne MHD generator concepts will be used as the basis for the evaluation.* The MHD generators burn a boron-liquid fuel slurry in air. Prior to combustion, the air is pressurized to about 6 atmospheres by a compressor and then is preheated to 2000°F by exhaust gas from the generator. The generator is a single-terminal diagonal type with a Hall parameter of 3. A superconducting magnet provides a field of 50,000 to 60,000 gauss. The peak combustion temperature is 3100°K (5130°F).

Specific Weight

A 1-Mw (1340 hp) generator has a specific weight of 2 lb/kw = 1.49 lb/hp. A 10-Mw (13,400 hp) generator has a specific weight of 0.67 lb/kw = 0.50 lb/hp. The estimated specific weight of a 500-kw (670 hp) generator is 2.5 lb/hp. The specific fuel consumption of the 1-Mw generator is 0.70 lb/kw-hr = 0.52 lb/hp-hr. The specific fuel consumption of the 10-Mw generator is 0.55 lb/kw-hr = 0.41 lb/hp-hr. The estimated specific fuel consumption of the 500-kw generator is 0.7 lb/hp-hr.

The above specific weights could be significantly reduced with further development. For example, the 1200-lb magnet of the 1-Mw generator could ultimately be reduced to 800 lb through the use of aluminum-stabilized superconductors and fiberglass composite support structures. If an ultimate weight reduction of 25 to 30 percent for the other generator components is assumed, then a future 1-Mw generator would weigh about two-thirds as much as the current concept. Reduction factors at other power levels are estimated to be three-fourths at 500 kw and one-half at 10 Mw.

It can also be expected that future development will lead to an improvement in the efficiency with which kinetic energy is converted to electricity in the MHD converter. The reduction factors applied to the specific fuel consumption resulting from such an improvement were estimated to be 0.85 at 500 kw, 0.90 at 1 Mw, and 0.95 at 10 Mw.

In order to calculate the total fuel consumption for the mission of Table II, the efficiency-load characteristic of the MHD generator is required. Since information of this type was not available, fuel consumption was taken to be the average of two extreme cases. In the first case, the specific fuel consumption was assumed to be constant and equal to the value at full load. In the second case, the specific fuel consumption was assumed to vary inversely with the power level. This situation would exist, for example, if the power output were varied by controlling the rate at which electrically conductive seed is added to the combustion gas while holding the actual fuel consumption rate constant. The average of the fuel consumption for these cases was found to

*Private communication with R. F. Cooper and Lt. R. O. Hunter, Air Force Aeropropulsion Laboratory, Wright-Patterson Air Force Base, Ohio.

be equal to the amount of fuel consumed if the converter were to operate at full power for 2.53 hrs.

During operation, the magnet must be maintained at the cryogenic temperatures required for the windings to be superconductive. Since some heat leakage into the magnet from the warmer atmosphere is inevitable, provision must be made for removal of this heat in-leakage. This can be accomplished by allowing some of the cryogenic liquid to boil off, or by the use of a refrigerating system. The use of a refrigerating system was assumed here.

It was further assumed that the superconducting magnet required the same amount of refrigeration as a superconducting motor of the same power rating. Refrigeration data for superconducting motors are given in Appendix III. For present technology systems, the use of reciprocating refrigeration machinery was assumed, plus the addition of a 4-hr reserve supply of cryogen. For future technology systems, it was assumed that much lighter turbomachinery was available and that a reserve supply of cryogen would not be needed.

The specific weight for MHD engines as determined from the above considerations is presented in Table XXVI. The term engine here denotes the MHD converter plus its refrigeration system. Data for the 500-hp, 1500-hp, and 10,000-hp levels were obtained from a curve of specific weight versus power that was plotted from the available data at other power levels (i.e., 670 hp, 1340 hp, and 13,400 hp). The refrigerator specific weight for present technology includes the weight of both the refrigerator and the emergency cryogen supply.

TABLE XXVI. SPECIFIC WEIGHT OF MHD ENGINES

	PRESENT			FUTURE		
Electric Power - hp	500	1500	10,000	500	1500	10,000
Specific Weight - lb/hp						
MHD Converter	3.18	1.40	0.57	2.60	0.92	0.29
Refrigerator	2.00	0.77	0.15	0.11	0.042	0.008
MHD Engine	5.18	2.17	0.72	2.71	0.962	0.298

The specific weights are seen to diminish rapidly with an increase in power level. Nevertheless, even at 10,000 hp, the projected future specific weight of the MHD engine is more than twice as large as the figure of 0.125 lb/hp for a 10,000-hp advanced gas turbine (see Table II).

The total specific weight for shaft power MHD systems is shown in Figure 38. The total specific weight includes the weight of the MHD engine, the motor-transmission, and the fuel. Motor-transmission weights were taken from Figure 50 of Appendix III.

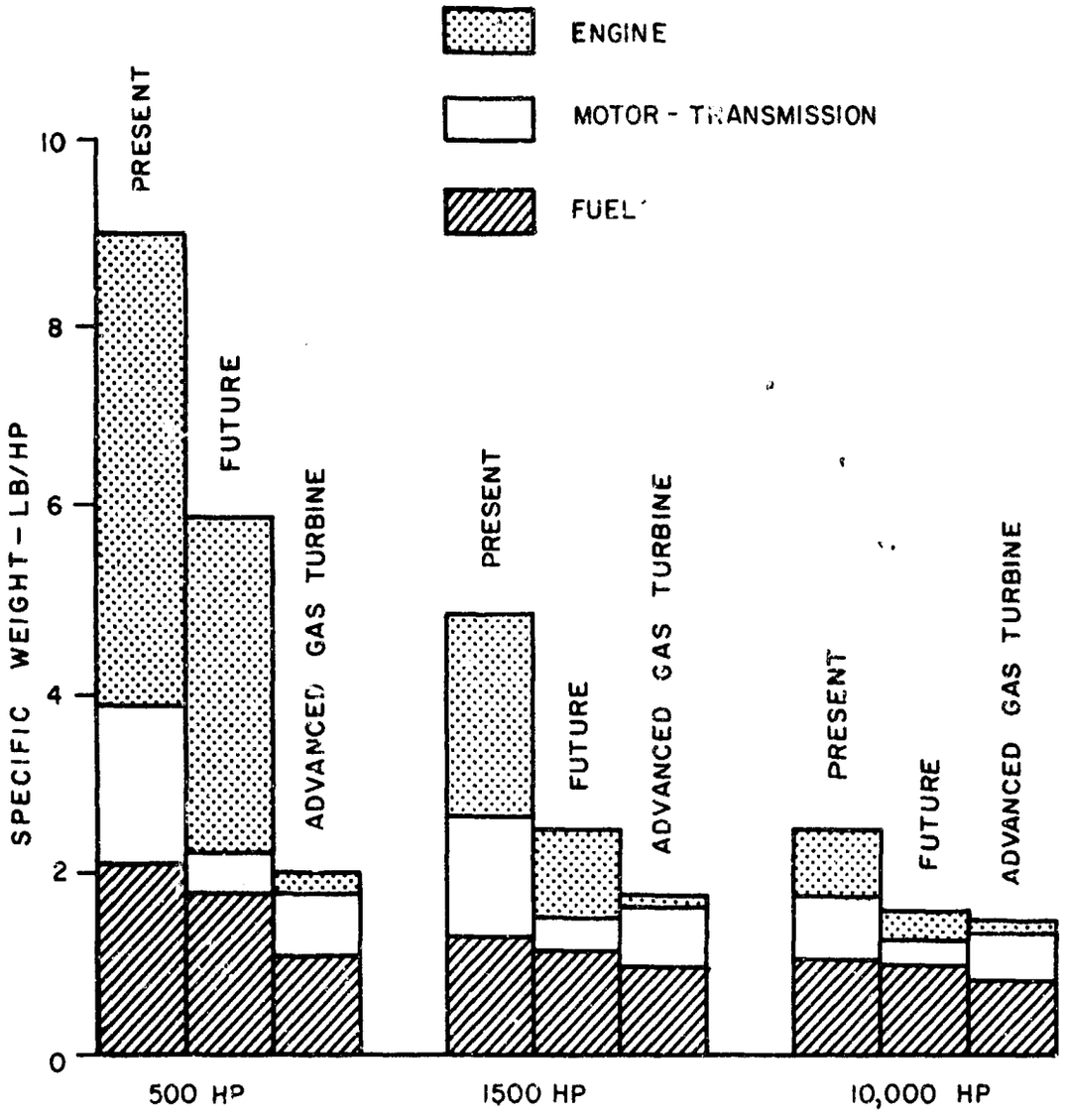

Figure 38. Specific Weight of MHD Shaft Power Systems.

It can be seen from Figure 38 that total system weight diminishes rapidly with an increase in power level. At the 10,000-hp level, the projected future total specific weight for the MHD converter is comparable to that of the advanced gas turbine. The higher MHD engine weight and fuel consumption tend to be offset by the lighter motor-transmission.

Specific Volume

The estimated specific volume for MHD engines is given in Table XXVII. The postulated reduction in the specific volume of future MHD engines is a consequence of expected future increases in power density.

TABLE XXVII. SPECIFIC VOLUME OF MHD ENGINES

Power - hp	500	1500	10,000
Specific Volume - ft^3/hp			
Present	15×10^{-3}	10×10^{-3}	5×10^{-3}
Future	8×10^{-3}	5×10^{-3}	2×10^{-3}
Advanced Gas Turbine	3.24×10^{-3}	$3.01\text{-}3.24 \times 10^{-3}$	$1.57\text{-}3.15 \times 10^{-3}$

At the 10,000-hp level, the specific volume of the MHD engine is comparable to that of the advanced gas turbine.

Cost

Because MHD generators are still in the early stages of development, little relevant cost data is available. For short-duration systems in the 100-to 1000-Mw range, capital costs of $20 to $30/kw have been estimated.[39] Costs at the power levels of interest for propulsion would probably be an order of magnitude or two greater than the above estimate. The performance of the MHD engines that have been analyzed is based on the use of a fuel consisting of a slurry of boron or aluminum in hydrocarbon liquid fuel. The cost of such a fuel slurry would be considerably greater than the cost of JP-4 alone. While an air-burning MHD converter could operate on JP-4 fuel, its weight would be at least twice that of the metal-slurry fueled generator, and fuel consumption would be appreciably greater. The cesium or potassium seed material will also contribute significantly to the operational expense of an MHD generator.

Reliability

Since the MHD converter is basically a simple device with no high-temperature moving parts, it has the potential for good reliability. On the other hand, the flow of seeded combustion gas at high temperature and high velocity can introduce problems of erosion and corrosion. In one case, the loss of material from zirconium oxide electrodes was just balanced by the deposition of zirconium oxide that had been introduced into the combustion gas.[41]

Operation of MHD generators at high power levels has generally been limited to short operating periods of a few minutes or less. Runs as long as 200 hrs have been made at representative operating temperatures and pressures, but at relatively low power. As yet, no MHD generator has operated with atmospheric air, with a supercritical magnet, or at magnetic fluxes of 50,000 to 60,000 gauss. Some of the problems associated with light-weight,

airborne MHD converters will be faced in the Project Brilliant experiment,[39] which is expected to undergo initial testing sometime during the fall of 1969.

Sensitivity to Environment

The MHD converter will exhibit sensitivity to changes in ambient temperature and pressure to about the same extent as the gas turbine. The ingestion of sand or dust could have adverse effects on converter performance, depending on the electron collision cross sections of the constituents. Also, the ingested dirt is likely to consist mostly of silicon and aluminum oxides. At temperatures above 3000°F, these materials assume a viscous, glassy form which could adhere to and/or react chemically with the electrodes. High humidity in the inlet air could also adversely affect performance because of the high electron collision cross section of water.[39] The sensitivity of the MHD engine to vibration and acceleration is probably comparable to that of the gas turbine.

Part-Load Characteristics

The output of an MHD converter can be controlled by varying the concentration of ionizing seed added to the combustion gas, thereby varying the electrical conductivity of the gas. However, this may not be the optimum method for achieving the best part-load efficiency. Little information was obtained on this aspect of operation of the MHD converter.

Transient Response

Transient response of the MHD converter should be comparable to that of a gas turbine. Startup within a few seconds is probable after the superconducting magnet has been cooled to cryogenic temperatures.

Structural Considerations

Since there are no high-temperature moving parts, since the maximum combustion pressure is about 6 atmospheres, and since the walls of the converter duct are cooled, a relatively light-weight structure can be designed. However, the superconducting magnet must be designed to withstand the substantial magnetic force associated with high magnetic flux. Electrode and electrical insulation materials that will maintain their respective properties under continuous exposure to the hot, high-velocity, seeded combustion gas must be selected.

Critical Problem Areas

Achievement of the MHD converter performance cited above will require the successful development of long-life, lightweight, efficient units. The air preheater must function at temperatures up to and preferably in excess of 2000°F; magnetic fields of 50,000 to 70,000 gauss will be required from lightweight superconducting magnets with a low rate of heat in-leakage and a lightweight refrigeration system utilizing turbomachinery. Similar considerations apply to the superconducting motor that is required for the

desired shaft output. Noise and vibration should be reduced, and a scheme for efficient part-load operation is needed. Fuel costs are high, and they must be reduced by utilizing less expensive slurry fuels or by the development of systems that can utilize conventional liquid fuels more efficiently. Many of these problems are being attacked in the course of existing MHD development programs. In particular, Project Brilliant will explore for the first time the use of high-flux, superconducting magnets for a lightweight airborne system.

Conclusions

The MHD converter combined with a superconducting motor appears to be competitive with the advanced gas turbine with respect to weight and volume at the 10,000-hp level. Fuel consumption is also comparable. However, this competitiveness is achieved by the use of expensive, slurry-type fuels.

MHD converter technology is still in a rather rudimentary state. Systems with the requisite magnetic flux levels and superconducting magnets have not yet been operated, and none of the current high-power developmental systems have operated for more than a few minutes at a time. Also, the efficiencies of these systems are low compared to values which are theoretically obtainable with energetic fuels and air preheat.

While the MHD converter may be competitive with the gas turbine with respect to weight, size, and fuel consumption, these factors alone would not justify its consideration for aircraft propulsion because of the high costs involved. However, an MHD propulsion system would have the capability for supplying large amounts of electricity as well as shaft power. This is a truly unique capability which could be utilized in situations where relatively large amounts of airborne electric power are required, as well as for situations where a highly mobile power source is needed to provide emergency power at ground installations. The availability of a few MHD-powered heavy-duty helicopters with electrical as well as shaft power capability could well be justified on tactical and logistical grounds, despite the high capital and fuel costs of such aircraft.

A preliminary study of an MHD propulsion system for helicopters may thus be warranted. Such a system might consist of a single 20,000-hp unit or two 10,000-hp units. The objective of the study would be to provide detailed information on the characteristics of an MHD shaft power system with electrical power capability and on problems of integration of the system with a helicopter.

THERMIONIC CONVERTER

A thermionic converter is a device in which thermal energy is used to drive electrons from a hot surface across a vapor-filled gap to a cooler surface. In the process, a voltage difference develops between the two surfaces. If an electrical load is connected between the surfaces, current will flow and electric power will be delivered to the load. Thermionic converters have been under development

for about 12 years. They are being considered for space and terrestrial power generation, using both nuclear and chemical thermal heat sources.

Current Status[50-54]

A schematic of a thermionic converter is shown in Figure 39. Basic components of the converter are a hot emitter plate, a cooler collector plate, and an ionized, vapor-filled gap between the plates. The vapor is a readily-ionized substance such as cesium. It serves two important purposes.

First, the vapor is absorbed on the emitter and collector surfaces, reducing the energy that electrons must acquire in order to leave the emitter surface and the energy that electrons must lose in order to penetrate the collector surface. Second, the positive vapor ions neutralize the negative charge of electrons in the gap between electrodes, which would otherwise sharply limit the flow of electrons from the emitter. Heat must be added continuously to the emitter to maintain

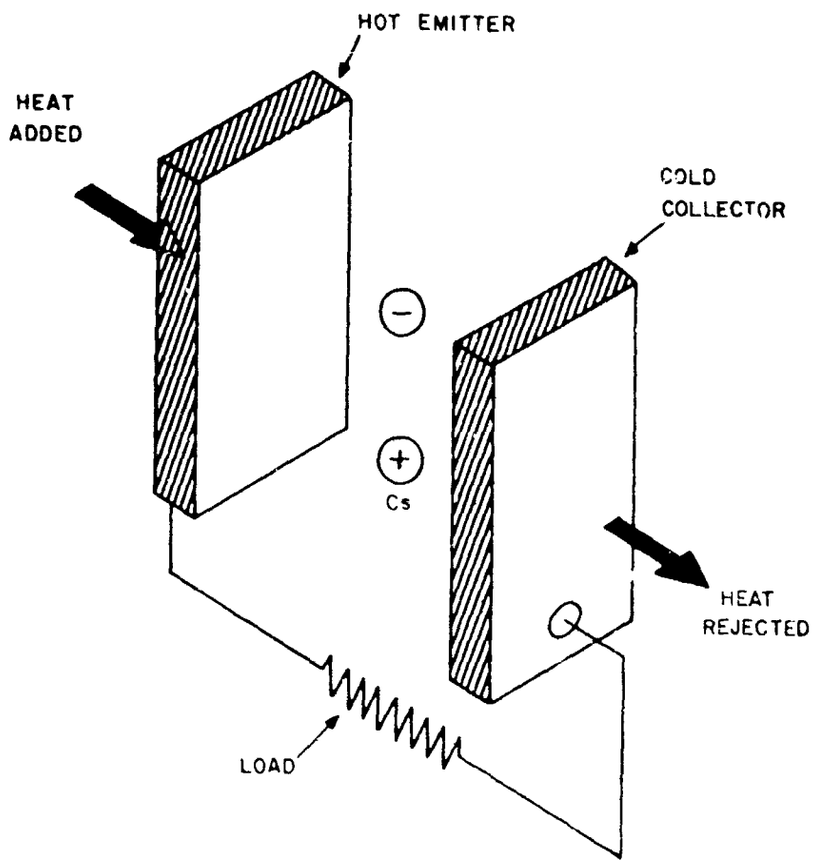

Figure 39. Thermionic Converter.[54]

its temperature. Some of this heat is converted to electrical energy, but the larger portion impinges on the collector, where it must be removed.

The converter can have a planar configuration, in which flat emitter and collector plates face each other, or a cylindrical configuration, in which a cylindrical emitter and a collector are separated by an annular gap. The gap thickness is usually in the range of 5 to 10 mils. The emitter is generally fabricated from tungsten, rhenium, or molybdenum, while the collector is usually a nickel or molybdenum structure.

When the emitter is to be heated by hot combustion gases, a protective coating of aluminum oxide or silicon carbide is necessary. The protective coating not only protects the emitter against corrosion but also prevents diffusion of combustion gas through the emitter material into the cesium vapor space. Since the ceramic protective coating is relatively brittle, care must be taken to avoid rapid temperature changes that might cause the coating to crack. Also, the maximum operating temperature will be limited by the tendency of the coating to react with or diffuse into the emitter surface with which it is in contact.

Emitter temperatures vary over the range of 1500°K (2250°F) to 2000°K (3150°F). At 1500°K, the thermal efficiency is 4 to 8 percent, the output voltage is 0.2 to 0.4, and the power density (power output/unit electrode area) is 1-2 watts/cm^2. These quantities all increase with emitter temperature. At 2000°K, typical values are: thermal efficiency, 10 to 19 percent; volts, 0.5 to 1.0; and power density, 5 to 20 watts/cm^2. Figure 40 shows the temperature variation of these quantities for converters with molybdenum emitters and nickel collectors.

Also shown in Figure 40 are the dependence on emitter temperature of the optimum gap spacing, the optimum collector temperature T_c, and the optimum cesium reservoir temperature T_r. (T_r determines the cesium vapor pressure, and hence vapor density, in the vapor gap.) The efficiency figures given refer to the diode only. Overall thermal efficiency of a complete power generation system would be significantly lower.

Attainable power densities in a thermionic converter are quite high, leading to the possibility of a light, compact power system. For example, a typical value of 5 watts/cm^2 is equivalent to almost 5000 watts/ft^2. This figure may be compared to power densities of 100 to 200 watts/ft^2, which are typical of high-efficiency fuel cells. Because of the high heat fluxes that are required at the emitter and collector surfaces, heat pipes are frequently used to "thermally transform" the high collector heat fluxes to lower values at which heat can be readily removed. Similarly, relatively low heat flux at the heat source may be transformed with a heat pipe to the high levels needed at the emitter.

Typical diode output is about 50 to 100 watts, but diodes with outputs as high as 800 watts have been considered.[51] A large number of diodes are therefore required for outputs of 100 kw or higher. The diodes may be wired in a series-parallel arrangement. A desired voltage level of 28 volts, for example, may be achieved by series-connecting 30 to 40 diodes. Alternatively, a DC-to-DC converter may be employed to yield the desired 28 volts from a series-connected module with 2 to 3 volts output. However, the converter will add considerable weight to the system.

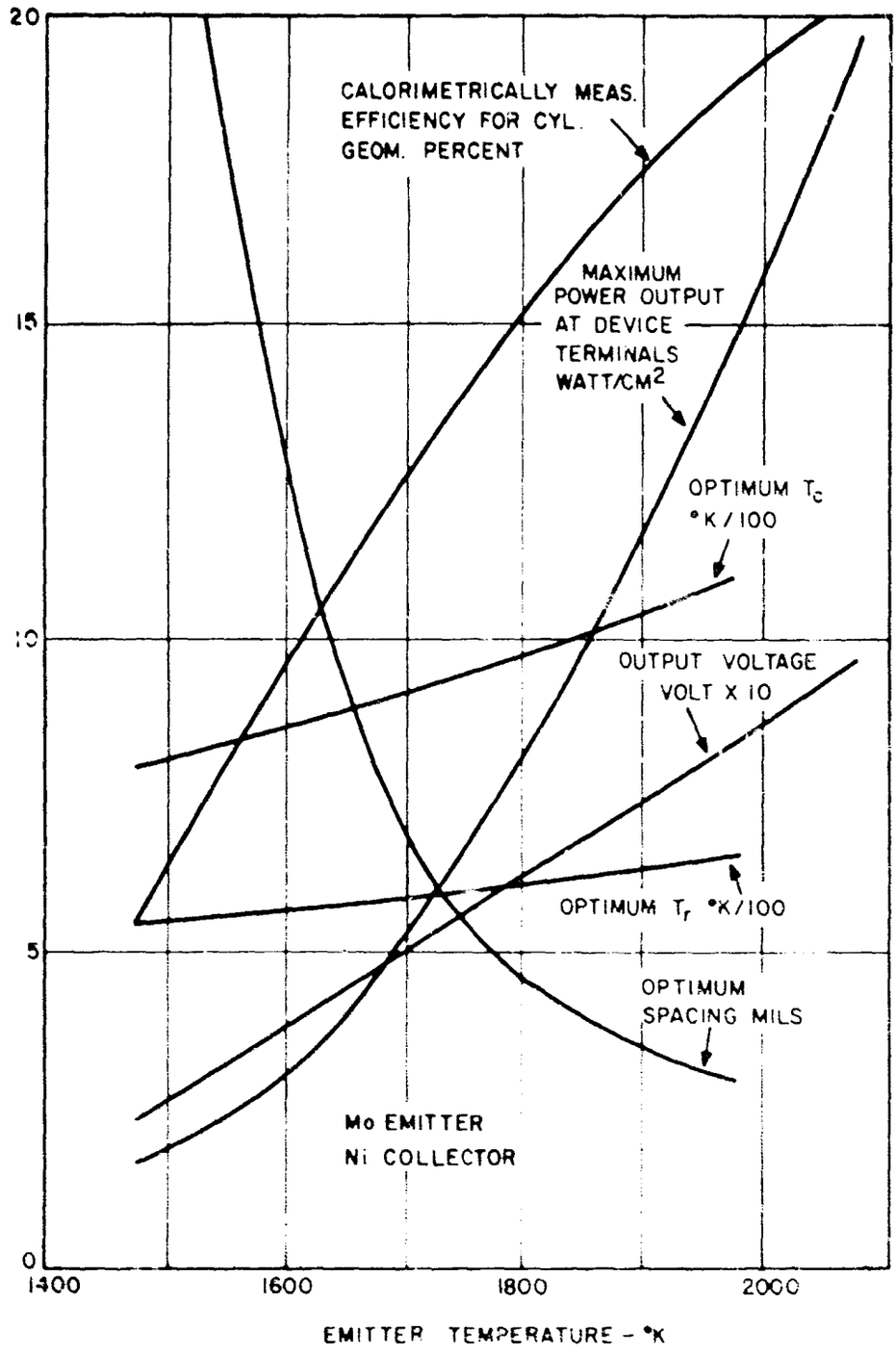

Figure 40. Thermionic Converter Characteristics.[50]

The characteristics of a fairly high performance diode are presented in Table XXVIII. The specific weight of the diode of Table XXVIII is about 2 lb/kw. By operating at 1800° to 1900°C to increase the power density to 20 watts/cm^2 and using thin emitter and collector sections, a specific diode weight of 0.3 lb/kw could be approached. It has been found that the addition of small amounts of oxygen can double or triple diode power output. Should the research now under way in this area lead to a practical device, the specific diode weight at 1800° to 1900°C emitter temperatures might conceivably be reduced to 0.1 lb/kw.

TABLE XXVIII. CHARACTERISTICS OF RD-502 CYLINDRICAL DIODE[52]

Emitter	Rhenium
Collector	Niobium, Molybdenum
Emitter temp.	1600° - 1700°C
Collector temp.	600°-700°C
Output	≈120 watts
Voltage	0.7
Power density	8.3 watts/cm^2
Efficiency	13.4%
Weight	≈1/4 lb
Dimensions	1/2 in. dia, 1-1/2 in. long
Lifetime	8200 hr
Spacing	5-10 mils

In general, thermionic diode lifetimes of thousands of hours can be expected. Lifetimes of 1000 to 2000 hours may be expected from combustion-gas-heated diodes at about 1450°C. Diode life will be limited to considerably smaller values as the emitter temperature approaches 1550°C.

Thermionic diodes have been subjected to vibration and acceleration typical of that encountered during a rocket launch. Some units survived the tests, while others failed.

Transient response should be good, with time constants on the order of 0.1 sec. If the diode is operated close to its maximum power point, then efficiency should improve until the power drops to 60 to 70 percent of the maximum value.

The current cost of a 35-watt flame-heated diode is $5800, plus $2300 for the burner, or about $165,000 kw.* Estimated future diode costs are in the range of $100 to $500/kw, based on production runs of 500 to 1000/month.**

* Personal communication with T. Spiedel, Thermo-Electron Engineering Co. Waltham, Mass.

** Personal communication with Y. Eastman, RCA, Lancaster, Pa.

The major problem area involving combustion-gas-heated diodes is the integrity of the protective coating around the emitter. Cost is also a problem, since expensive refractory materials such as rhenium and tungsten are currently required in the emitter for good diode performance.

Application to Aircraft Propulsion

The various factors involved in the evaluation of thermionic converters for aircraft propulsion are discussed below.

Specific Weight

The thermionic diode emitter temperature will be taken to be 2650°F. At this temperature the diode efficiency is about 0.10, and the specific weight is about 2 lb/kw = 1.49 lb/hp. The heat input system is the same as that shown in Figure 8. The assumed temperature distribution in the heat input and heat output systems is shown in Figure 41. In the heater, combustion gas is cooled from 5450°F to 2750°F while transferring heat to the diode emitters. In the cooler, rotor downwash air is heated from 40°F to 240°F while receiving heat from the collector. In order to maintain constant emitter and collector temperatures, the actual heat exchange would be to constant-temperature heat pipes attached to the emitter and collector surfaces, and extending the length of the heat exchangers. In order to provide the indicated peak combustion gas temperature, the preheater material temperature at the hot end will be between the heater outlet temperature of 2750°F and the combustor inlet temperature of 2450°F.

The specific weight of the heat input system was estimated to be 0.532 lb/hp. This total includes 0.190 lb/hp for the heater, 0.124 lb/hp for the combustion system, and 0.218 lb/hp for the preheater. The cooler specific weight was found to be 0.262 lb/hp at 500 hp, 0.199 lb/hp at 1500 hp, and 0.181 lb/hp at 10,000 hp.

For future systems, it was assumed that the emitter temperature would increase to 2830°F, at which the diode efficiency is about 0.12 and the power density doubles. At the same time, it was assumed that substantial reductions could be made in the emitter and collector thicknesses, reducing the weight of a given diode by a factor of 3. This factor, combined with the doubling of the power density, results in a sixfold reduction in diode specific weight, to 0.248 lb/hp. Future heat input and output system weights were obtained by assuming that they varied inversely with efficiency. The total thermionic converter engine specific weight, determined in the manner described above, is given in Table XXIX. The engine weight is the sum of the heater plus cooler weights and the converter (diode) weight.

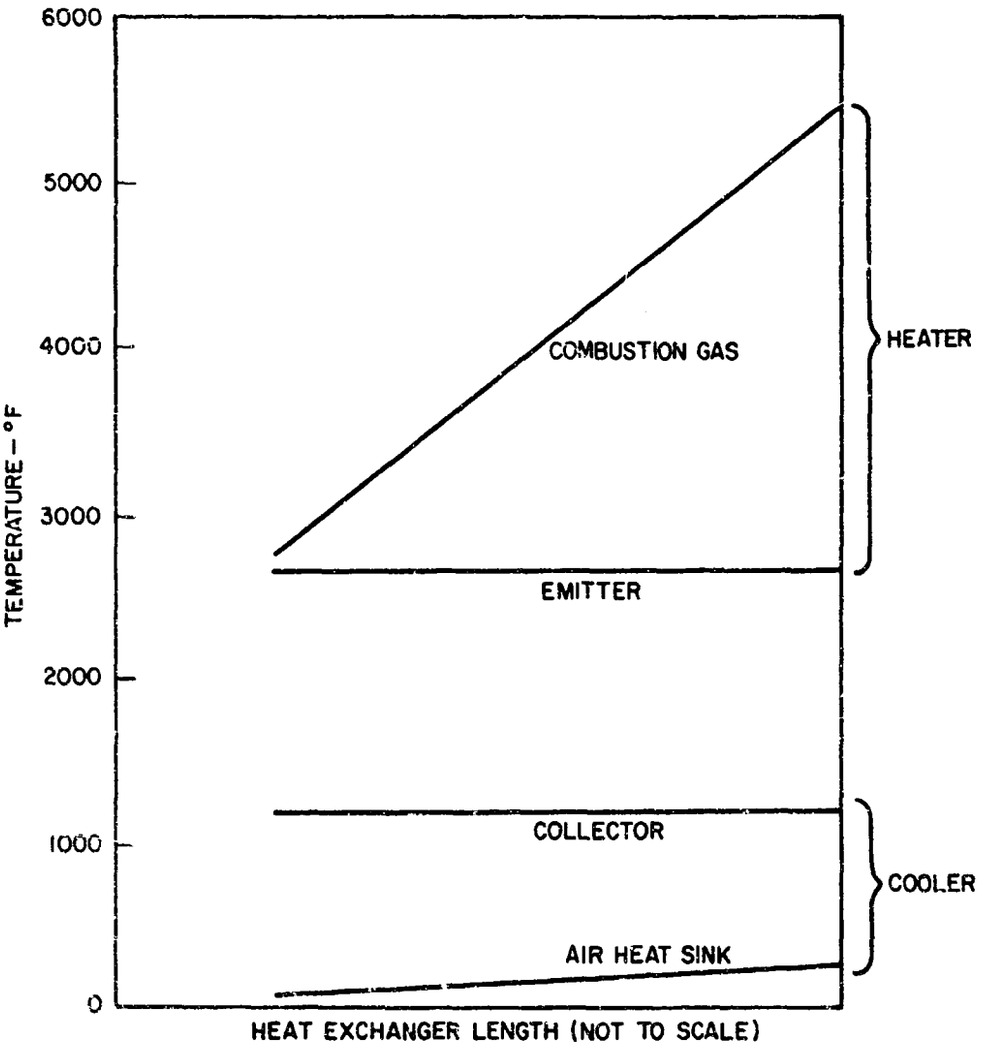

Figure 41. Temperature Distribution in Heater and Cooler of Thermionic Converter.

Fuel consumption was calculated for the mission described in Table II, with the assumption that the specific fuel consumption rate varies with load in the same manner as for the advanced gas turbines. The motor-transmission specific weights were obtained from Figure 50 of Appendix III. The total specific weight for thermionic converter shaft power systems is shown in Figure 42. Projected future system specific weights are seen to be more than twice as large as those of the advanced gas turbines.

TABLE XXIX. SPECIFIC WEIGHT OF THERMIONIC CONVERTER ENGINES

	PRESENT			FUTURE		
Power - hp	500	1500	10,000	500	1500	10,000
Specific Weight - lb/hp						
Heater + Cooler	0.794	0.731	0.713	0.673	0.621	0.606
Converter	1.490	1.490	1.490	0.248	0.248	0.248
Engine	2.284	2.221	2.203	0.921	0.869	0.854

Specific Volume

The estimated specific volume for the thermionic engine (heat input and output system plus diodes) is given in Table XXX.

It can be seen that the diodes constitute only a small fraction of the total engine volume, which is dominated by the heat input and output systems. The total engine specific volume exceeds that of the advanced gas turbines by a factor of 3 to 4.

Cost

The current specific cost of a 35-w flame-heated diode is $165,000/kw = $123,000/hp. Future costs are estimated to be in the range of $75/hp to $370/hp. This estimate is based on the production of 500 to 1000 diodes per month.

Reliability

The reliability of combustion-heated thermionic diodes can be considered to be only fair, based on experience to date with such systems. Lifetimes of 1000 to 2000 hr can be anticipated at present. The ceramic coating which encloses the emitter usually represents the life and reliability-limiting factor. The coating is sensitive to thermal shocks, and it may eventually react with the emitter substrate. Also, combustion gases may eventually diffuse through the coating and emitter material into the diode interior.

Sensitivity to Environment

The heat input system will be sensitive to variations in ambient air temperature and pressure to the same extent as the gas turbine. The driving temperature difference for heat removal in the cooler is not strongly affected by such variations. The ingestion of sand and dust particles into the heat input system could adversely affect system performance because such particles could melt at the combustion temperatures and then possibly adhere to heat transfer surfaces. The thermionic diodes proper can probably be made rugged enough to withstand aircraft vibration and acceleration loads, but the ceramic coating will be considerably more susceptible to fracture.

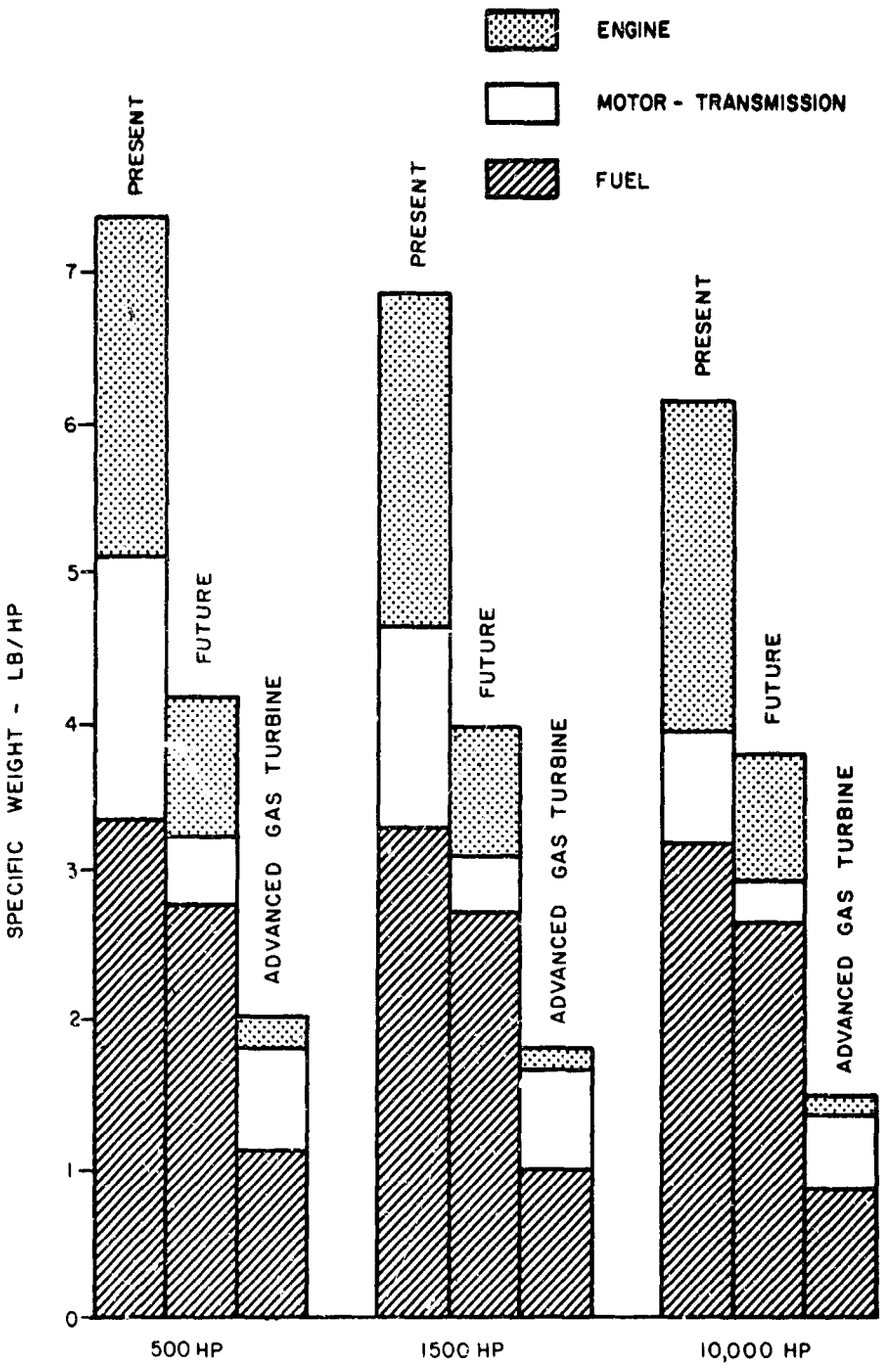

Figure 42. Specific Weight of Thermionic Converter Shaft Power Systems.

TABLE XXX. SPECIFIC VOLUME OF THERMIONIC CONVERTER ENGINES

	PRESENT			FUTURE		
Power - hp	500	1500	10,000	500	1500	10,000
Specific Volume - ft^3/hp						
Heat Input-Output System	11.2×10^{-3}	10.2×10^{-3}	9.83×10^{-3}	9.53×10^{-3}	8.65×10^{-3}	8.40×10^{-3}
Diodes	1.1×10^{-3}	1.1×10^{-3}	1.1×10^{-3}	0.21×10^{-3}	0.21×10^{-3}	0.21×10^{-3}
Engine	12.3×10^{-3}	11.3×10^{-3}	10.9×10^{-3}	9.74×10^{-3}	8.86×10^{-3}	8.61×10^{-3}
Advanced Gas Turbine				3.24×10^{-3}	$3.01\text{-}3.24 \times 10^{-3}$	$1.57\text{-}3.15 \times 10^{-3}$

Part-Load Characteristics

If a thermionic diode is operated at rated power at conditions yielding maximum diode power, then efficiency can be expected to increase at part load until the load has decreased to about 60 to 70 percent of the rated load.

Transient Response

Transient response of a thermionic diode should be fairly good, but the thermal inertia of the associated heat input and output systems should slow down the overall system response.

Structural Considerations

The protective coating around the emitter represents one of the major structural concerns, as has already been mentioned. Other areas of major concern are the combustor liner and the heater entrance, where gas temperatures of 5400° F are encountered. The hot end of the preheater also presents structural problems, since materials there will be heated to about 2600° F. The use of refractory metals covered with oxidation-resistant ceramics and/or the use of wall-cooling techniques are the only apparent approach here.

Critical Problem Areas

As has been pointed out, materials selection and their structural integrity constitute a major problem area in the development of combustion-fired thermionic converters. Cost would seem to be another important area of concern, since expensive refractories such as rhenium and tungsten are required for good diode performance and may be needed for heat transfer surfaces as well. Aside from these problems, the high engine weight and high fuel consumption are fundamental limiting factors and are likely to remain so in the foreseeable future.

Conclusions

The high engine weight and fuel consumption of the thermionic shaft power engine, along with formidable materials problems in a combustion-fired system, indicate that such an engine will not be competitive with advanced gas turbines in the foreseeable future.

THERMOELECTRIC CONVERTER

Thermoelectric converters have been considered for space and terrestrial applications requiring moderate power (<1 kw), long life, and quiet operation. The basic generator element is a thermocouple pair, one end of which is heated and the other cooled. Both nuclear and chemical heat sources have been used. Thermoelectric converter development received great impetus when semiconductor materials were introduced as thermocouple materials. Thermal efficiencies of

4 to 8 percent then became possible, representing an order of magnitude improvement over attainable efficiencies with metallic thermocouples. The semiconductor materials of most interest for power generation are lead telluride (PbTe) and silicon germanium (SiGe). Although intensive research has been carried out for the past several years, no materials have been developed which offer significant performance improvement over that attainable with PbTe and SiGe.

Current Status

As shown in Figure 43, the basic elements of a thermoelectric converter consist of two thermocouple legs, to which are attached a hot shoe and cold shoes. The thermocouple legs are both fabricated from the same basic semiconductor material (i.e., PbTe or SiGe), but one leg is an "n-type" (has an excess of electrons) and the other is a "p-type" (has a deficiency of electrons or, equivalently, an excess of positive holes). Heat is added to the hot shoe and removed from the cold shoes, maintaining a temperature differential across the thermocouple legs. As a result, a voltage of about 0.1 volt develops between the legs. If the cold shoes are connected across an electrical load, current will flow and electric power will be supplied to the load. The heat input less the power generated must be dissipated at the cold junction. The thermocouple legs are on the order of 1/2 in. in diameter and 1/2 in. in length.

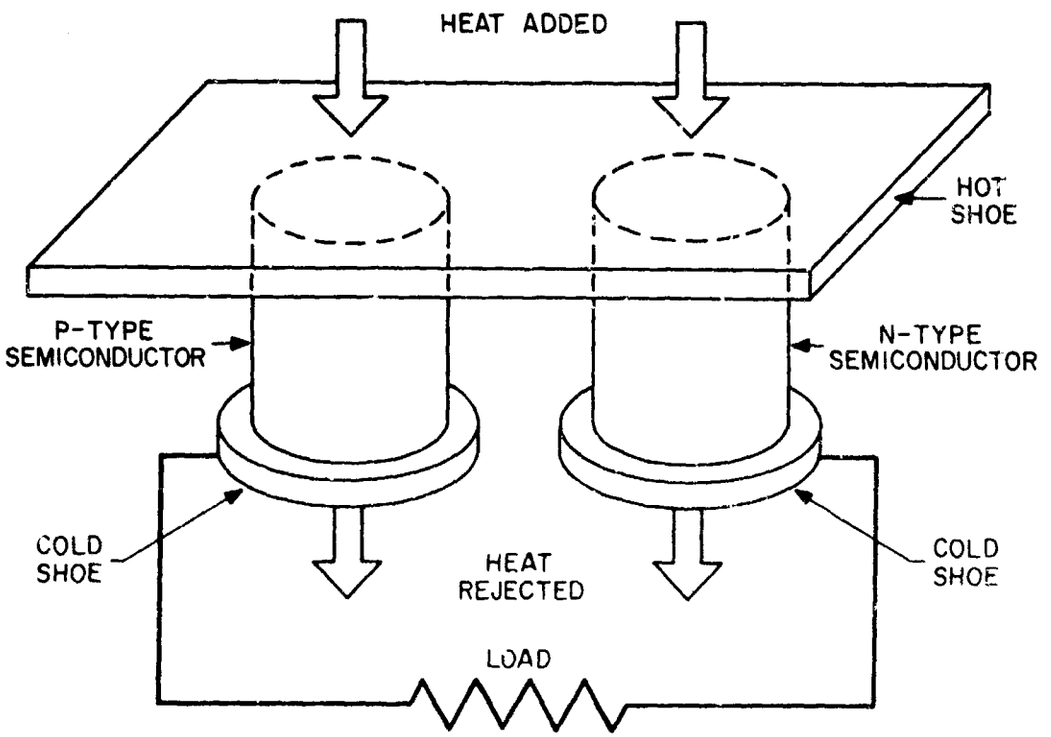

Figure 43. Thermoelectric Converter.[54]

PbTe must be canned to prevent sublimation and oxidation; it is usually limited to a maximum hot junction temperature of about 1000°F. SiGe, however, may be exposed to air, vacuum, and combustion gases at temperatures as high as 1800°F without encapsulation or special coatings.[55] Overall efficiencies of 4 to 6 percent are attainable with these materials when operating at their maximum hot junction temperatures and cold junction temperatures of 300° to 400°F.

By combining SiGe and PbTe couples in series thermally, efficiencies in excess of 10 percent may be obtained. This may be done either by cascading or by segmenting. In the cascaded arrangement, heat rejected from the cold shoes of SiGe converters is directed onto the hot shoes of adjacent PbTe converters.[56] In the segmented arrangement, PbTe legs are mechanically bonded to SiGe legs of the same type.[57]

Data on three recent thermoelectric converter modules are presented in Table XXXI. The modules include the thermocouples, insulation, hot shoes, and cold shoes. Heat source, heat sink, and structural support weights are not included.

TABLE XXXI. CHARACTERISTICS OF THERMOELECTRIC CONVERTER MODULES

Type	Output (w)	Voltage (v)	No. Couples	Hot Junction Temp (°F)	Cold Junction Temp (°F)	Efficiency (%)	Thermo-couple Wt (lb/kw)	Module Wt (lb/kw)	Ref
SiGe Segmented	150	27	480	1450	800	3.6	10.8	89	58
SiGe-PbTe Cascaded	2.3	0.3	1	1470	125	8.7	13.9		57
SiGe-PbTe	38.4	4.3	48	1840	400	10.8		26	56

It can be seen from Table XXXI that cascaded converters yield the best performance in terms of efficiency and weight. To obtain total generator weight, the weight of structure, the heat source, and the heat rejector must be added. For a radio-isotope-powered thermoelectric space generator, total system weights are in the range of 500 to 1000 lb/kw.[59-60]

Thermoelectric converters are reliable, fairly rugged devices with lifetimes of several years. They have been designed to withstand the rigors of rocket launch. The current cost of gas-fired converters is on the order of $30,000/kw. The cost of propane fuel is about 40¢/kw-hr.[61]

Application to Aircraft Propulsion

The cascaded SiGe-PbTe converter will be used as a basis for evaluation. This system exhibits an efficiency of 0.10 for a hot junction temperature of 1850° F and a cold junction temperature of 400° F.

Specific Weight

The module specific weight is 26 lb/kw = 19.4 lb/hp. As was the case for the thermoelectric converter, the heat input system of Figure 8 is employed, and rotor downwash air is used as the heat sink. The temperature distributions in the heater and cooler are shown in Figure 44. Combustion gas is cooled from 4650°F to 1950°F while transferring heat to the hot junctions at 1850°F. Rotor downwash air is heated from 40°F to 240°F in the process of receiving heat from the cold junctions at 400°F. The hot and cold junction temperatures are held constant by securing the hot and cold junctions to constant-temperature heat pipes which extend over the length of the heat exchangers. The combustor inlet temperature is 1650°F. The material temperature at the hot end of the preheater will be between the combustor gas inlet temperature of 1650°F and the heater gas outlet temperature of 1950°F. Because of the low cold junction temperature, titanium was specified as the cooler material.

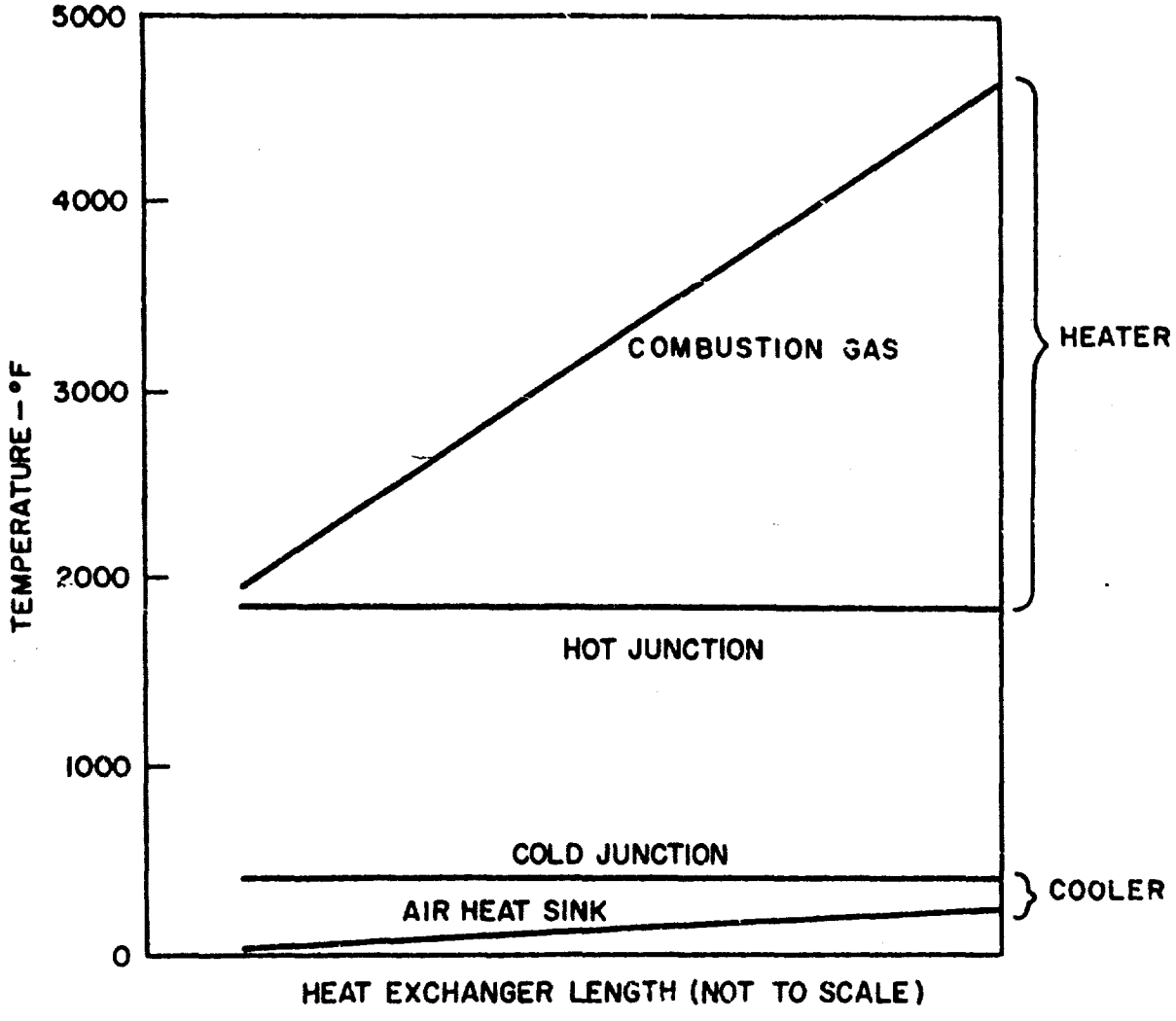

Figure 44. Temperature Distribution in Heater and Cooler of Thermoelectric Converter.

The specific weight of the heat input system was found to be 0.747 lb/hp; it is comprised of 0.493 lb/hp for the heater, 0.124 lb/hp for the combustion system, and 0.130 lb/hp for the preheater. The specific weight of the titanium cooler is 0.664 lb/hp at 500 hp, 0.505 lb/hp at 1500 hp, and 0.457 lb/hp at 10,000 hp.

For future systems it was assumed that improvements in thermoelectric properties and reduced heat losses could increase the efficiency to 0.12. A reduction factor of 2 in module weight was assumed to be attainable through the use of lighter insulation, thinner hot and cold shoes, more closely spaced couples, and less conservative design. Also, an aluminum cooler was used rather than a titanium cooler. In addition, the module weight, as well as the weight of the other components, was assumed to vary inversely as the efficiency. The total thermoelectric converter engine specific weight, calculated as described above, is given in Table XXXII. The engine is comprised of the converter modules plus the heat input and output system.

TABLE XXXII. SPECIFIC WEIGHT OF THERMOELECTRIC CONVERTER ENGINES

	PRESENT			FUTURE		
Power - hp	500	1500	10,000	500	1500	10,000
Specific Weight - lb/hp						
Heat Input-Output Systems	1.41	1.25	1.20	0.93	0.86	0.83
Converter Modules	19.40	19.40	19.40	8.10	8.10	8.10
Engine	20.81	20.65	20.60	9.03	8.96	8.93

Fuel consumption was calculated in the same manner as was fuel consumption for the thermionic converter engine. Since present and future system efficiencies are the same for both the thermionic and thermoelectric converters, fuel consumption is likewise the same in both cases. Motor-transmission weights, as obtained from Figure 50 of Appendix III, are also taken to be the same for the two engine types. The total specific weight for thermoelectric converter shaft power systems (engine, motor-transmission, and fuel) is shown in Figure 45. It can be seen that the specific weight is 6 or more times greater than that of the advanced gas turbines for the future systems, and it is more than 12 times greater for current systems.

Specific Volume

The specific volume of the cascaded SiGe-PbTe thermocouple modules is about 0.202 ft^3/hp. It is estimated that this figure could be halved in future systems.

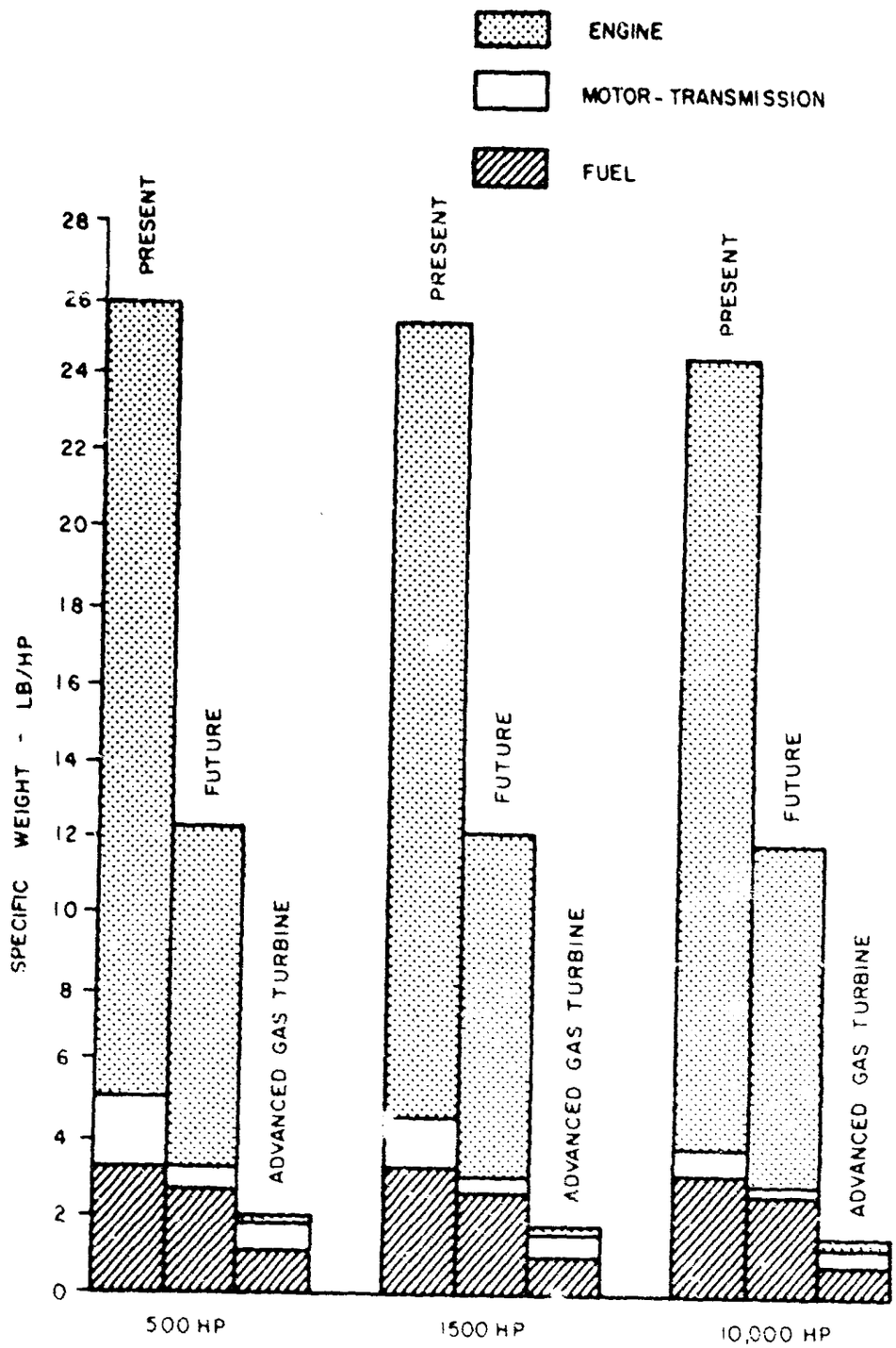

Figure 45. Specific Weight of Thermoelectric Converter Shaft Power Systems.

The specific volume of the heat input and output heat exchangers was estimated from heat transfer data on the assumption of an area-volume ratio of 200 ft^2/ft^3. The specific volume for thermoelectric engines (modules plus heat input and output systems) is given in Table XXXIII.

The engine specific volumes for future systems are seen to be more than 30 times greater than the specific volumes of the advanced gas turbines.

Cost

The current cost of thermoelectric converters is about $30,000/kw in sizes of 100 w or less. The price could conceivably come down by an order of magnitude if the converters were turned out in large numbers on a mass production basis.

Reliability

Thermoelectric converters are fairly rugged devices and have been designed to withstand the rigors of a rocket launch. Lifetimes of several years may be expected.

Sensitivity to Environment

The thermoelectric engine will be fairly sensitive to variations in ambient temperature and pressure because of its low cold junction temperature of 400°F. System operation will also be influenced by changes in density of air entering the heat input system which result from changes in ambient conditions. Sensitivity to sand and dust ingestion is about the same as for a gas turbine, although the high combustion gas temperatures could conceivably cause dust particles to melt and then adhere to heat transfer surfaces. Operation should be quite insensitive to vibration and acceleration.

Part-Load Characteristics

No information was obtained on part-load characteristics.

Transient Response

Transient response should be quite sluggish because of the large thermal inertia of the thermocouples.

Structural Considerations

Thermoelectric converters require careful design to assure that the expansion, thermal, and electrical characteristics of the thermocouples and the hot and cold junctions are mutually compatible. However, such problems have been successfully attacked, and the thermoelectric converter may be regarded as a basically rugged device.

TABLE XXXIII. SPECIFIC VOLUME OF THERMOELECTRIC CONVERTER ENGINES

	PRESENT			FUTURE		
Power - hp	500	1500	10,000	500	1500	10,000
Specific Volume - ft^3/hp						
Heat Input-Output Systems	$30x10^{-3}$	$225x10^{-3}$	$23x10^{-3}$	$24x10^{-3}$	$20x10^{-3}$	$19x10^{-3}$
Thermoelectric Modules	$202x10^{-3}$	$202x10^{-3}$	$202x10^{-3}$	$101x10^{-3}$	$101x10^{-3}$	$101x10^{-3}$
Engine	$232x10^{-3}$	$227x10^{-3}$	$206x10^{-3}$	$125x10^{-3}$	$121x10^{-3}$	$120x10^{-3}$
Advanced Gas Turbine				$3.24x10^{-3}$	$3.01\text{-}3.24x10^{-3}$	$1.57\text{-}3.15x10^{-3}$

Critical Problem Areas

High specific weight and low efficiency constitute the most critical problem areas of a thermoelectric converter. Although research and development in thermoelectric materials and devices has been under way for a number of years, no materials more suited for power generation than SiGe and PbTe have been discovered. Hence, on the basis of experience to date, there is little likelihood of significant improvements in either specific weight or efficiency.

Conclusions

Thermoelectric converters are not suitable for consideration in aircraft propulsion systems because of high fuel consumption and excessive weight and volume.

NUCLEAR SYSTEMS

The energy released in the form of energetic nuclear radiation by the decay of unstable atomic nuclei or by the fission of uranium or plutonium isotopes is rapidly converted to heat as the nuclear radiation is absorbed in surrounding matter. Radioisotopes (unstable nuclei) and nuclear reactors (structures designed to maintain and control the fission reaction) constitute thermal energy sources that can be integrated into a thermodynamic cycle in a manner entirely analogous to that of a heat source which derives its thermal energy from chemical combustion. The most significant feature of nuclear heat sources is their extremely low rate of fuel consumption in comparison to that of chemical heat sources. However, fundamental considerations limit the universal application of nuclear heat sources, as will now be delineated.

RADIOISOTOPE HEAT SOURCES[50, 62]

Radioisotopes are a normal byproduct of fission reactions in nuclear reactors. In addition, they can be produced by exposing stable materials to the neutrons in a reactor.

Current Status

In terms of thermal power capability, radioisotopes are among the rarest and most expensive heat sources. Hence, their use is generally limited to applications where less than a kilowatt of electrical or shaft power is required, where a relatively small number of devices are involved, and where, as in space, there may not be any other feasible method for meeting long-term, unattended power needs.

The radioisotopes of major interest as thermal heat sources are: cobalt-60 (Co^{60}), strontium-90 (Sr^{90}), cerium-144 (Ce^{144}), and plutonium-238 (Pu^{238}). Their characteristics are listed in Table XXXIV.

Application to Aircraft Propulsion

Radioisotope heat sources can be utilized with any of the thermodynamic energy conversion systems that have been considered in previous sections of this report, with the exception of open-cycle MHD converters. Peak cycle temperatures in the MHD converter are above the limit of currently available materials. Only the heat source and shield weights and volumes are considered, since these components are the main contributors to system weight. All of the radioisotopes require shielding to reduce the intensity of emitted nuclear radiation to a tolerable level.

TABLE XXXIV. CHARACTERISTICS OF RADIOISOTOPE HEAT SOURCES[60]

	Co^{60}	Sr^{90}	Ce^{144}	Pu^{238}
Radiation	Gamma, beta	Beta	Gamma, beta	Alpha, neutron
Half-Life - yr	5.3	28	30	86
Chemical Form	Metal	$SrTiO_3$	CeO_2	PuO_2
Specific Wt* - lb/hp	3.87	28.6	1.73	16.8
Specific Vol* - ft^3/hp	6.77×10^{-3}	105×10^{-3}	4.29×10^{-3}	54.0×10^{-3}
Availability - hp/yr	>200	163 (1980)	200**	200 (total by 1980)
Specific Cost* - $/hp	98,800	57,000**	2990**	2,680,000

* Based on 25 percent cycle efficiency.

** Based on production from the proposed Hanford Isotopes Plant.

Specific Weight

The weight of shielding required to reduce the radiation dose to the acceptable level of 2 mr/hr (milliroentgens/hr) at 100 cm (3.28 ft) from the center of a spherical heat source has been calculated for 500 hp, 1500 hp, and 10,000 hp engines. Shielding data from Reference 63 were used in the calculations. Depleted uranium (uranium for which most of the fissionable U-235 isotope has been used up) was used as the shield for gamma rays and for the X-rays that are associated with the emission of beta rays, and water was used as the shield for neutrons. The calculated shield weights are minimum values, because the shield enclosed only the volume occupied by the radioisotope compounds; no additional volume was allowed for structural material or heat transfer passages.

The specific weight of the radioisotope heat sources and their associated shields is given in Table XXXV.

TABLE XXXV. SPECIFIC WEIGHT OF RADIOISOTOPE HEAT SOURCES AND SHIELDS

		Shaft Power (hp)		
		500	1500	10,000
Isotope	Component	Specific Weight (lb/hp)		
Co^{60}	Heat Source	3.87	3.87	3.87
	Shield	23.7	14.80	6.60
	Total	27.57	18.67	10.47

TABLE XXXV - Continued

		Shaft Power (hp)		
		500	1500	10,000
Isotope	Component	Specific Weight (lb/hp)		
Sr^{90}	Heat Source	28.6	28.6	28.6
	Shield	93.6	65.5	36.1
	Total	122.2	94.1	64.7
Ce^{144}	Heat Source	1.73	1.73	1.73
	Shield	32.0	18.15	8.04
	Total	33.73	19.88	9.77
Pu^{238}	Heat Source	16.8	16.8	16.8
	Shield	48.0	31.4	15.01
	Total	64.8	48.2	31.81

The lightest radioisotope heat source/shield combination occurs for Ce^{144} at 10,000 hp. The specific weight of 9.77 lb/hp is 78 times larger than that of the 10,000-hp advanced gas turbine, and more than 6 times the specific weight of the total propulsion system (engine, transmission, and fuel).

Specific Volume

The specific volume of the radioisotope heat sources and their associated shields is given in Table XXXVI.

TABLE XXXVI. SPECIFIC VOLUME OF RADIOISOTOPE HEAT SOURCES AND SHIELDS

		Shaft Power (hp)		
		500	1500	10,000
Isotope	Component	Specific Volume ($ft^3/hp \times 10^3$)		
Co^{60}	Heat Source	6.77	6.77	6.77
	Shield	20.2	12.6	5.6
	Total	26.97	19.37	12.37
Sr^{90}	Heat Source	105.0	105.0	105.0
	Shield	79.0	55.9	30.8
	Total	184.0	160.9	135.8

TABLE XXXVI - Continued				
		Shaft Power (hp)		
		500	1500	10,000
Isotope	Component	Specific Volume (ft^3/hp x 10^3)		
Ce^{144}	Heat Source	4.29	4.29	4.29
	Shield	27.2	15.5	6.80
	Total	31.49	19.79	11.09
Pu^{238}	Heat Source	5.40	5.40	5.40
	Shield	626.0	387.0	170.0
	Total	631.4	392.4	175.4

The most compact heat source/shield combination occurs at 10,000 hp for Ce^{144}. The specific volume of 11.09 ft^3/hp is 3.5 to 7 times greater than that of the 10,000-hp advanced gas turbine.

Cost

Initial radioisotope heat source costs are included in Table XXXIV. A more meaningful cost figure is the specific cost per year if the heat source is used for one half-life and the remaining isotope (one-half of the original amount) is salvaged at full value. This cost is given in Table XXXVII.

TABLE XXXVII. SPECIFIC COST/YR OF RADIOISOTOPE HEAT SOURCES USED FOR ONE HALF-LIFE

Radioisotope	Specific Cost ($/hp-yr)
Co^{60}	9,330
Sr^{90}	1,120
Ce^{144}	1,920
Pu^{238}	15,600

The yearly specific cost for the various radioisotopes is still much greater than the maximum specific cost of $76/hp for the advanced gas turbines (see Table II).

Reliability

While radioisotope heat sources are basically rugged and reliable components, the use of large quantities such as are contemplated here would pose a

tremendous maintenance problem. Since the radioisotopes continuously decay and generate heat, means would have to be provided for dissipation of this heat when the energy converter, which is coupled to the heat source, is not in operation. Failure of the heat dissipation system would lead to rapid meltdown and release of radioactivity.

Availability

From Table XXXIV, the maximum anticipated radioisotope production rate would be sufficient for only about one engine per year at a rating of a few hundred hp.

Sensitivity to Environment

The environmental sensitivity of a radioisotope heat source would be very low.

Part-Load Characteristics

Since a radioisotope produces heat continuously, means must be provided for dissipating the excess heat not utilized by the energy converter at part load. Also, the heat source must be overloaded initially to compensate for the reduced heat generation rate as the radioisotope continues to decay.

Transient Response

Transient response should be quite sluggish because of the high thermal inertia associated with the large radioisotopic specific power.

Structural Considerations

Radioisotopes must be securely encapsulated in nonreactive materials to prevent the loss of radioactivity to the environment. The capsules must withstand the maximum anticipated impact loads. Since Pu^{238} emits alpha particles, which are helium nuclei, the design of a Pu^{238} capsule must also allow for the internal buildup of helium gas.

Critical Problem Areas

Many considerations limit the use of radioisotope heat sources to specialized, low-power applications. These limiting factors include: low availability, high isotope and shielding weight, high cost, and the continuous generation of heat. There is no apparent way to alleviate any of these problems.

Conclusions

The availability of radioisotope heat sources is insufficient to power even a single 500-hp energy converter per year. This fact alone confirms the inapplicability of radioisotope heat sources to aircraft propulsion. Additional confirming factors are the high specific weight, the high cost, and the continuous heat generation characteristic.

NUCLEAR REACTOR HEAT SOURCES [64, 65]

In contrast to the limited availability of radioisotope heat sources, nuclear reactor heat sources are capable of power levels of a million thermal kw or more, and reactor fuel is available in sufficient quantity to fuel many such megawatt heat sources. Nuclear propulsion systems have become predominant in submarines and, to a lesser extent, in surface ships. Nuclear propulsion of aircraft has not yet been achieved.

Current Status

Efforts to develop a nuclear aircraft propulsion system were initiated in 1951, and were abandoned in 1961 after 10 years of intensive development. Interest in nuclear aircraft has been revived within the last couple of years, and studies of a revised nuclear aircraft propulsion system are being conducted by NASA and the Air Force.

Two principal factors have limited the application of nuclear power to aircraft propulsion: shield weight and safety. A radiation shield is necessary to attenuate the intense neutron and gamma radiation that is emitted by any nuclear reactor operating at thermal power levels in excess of a few watts. The shield is several feet thick and weighs thousands of pounds. The second factor – safety – is concerned with the problem of preventing widespread contamination of the atmosphere with radioactivity in the event of a crash that damages the reactor.

Although a reactor shield is heavy, its weight increases at a relatively slow rate with an increase in reactor power level. At a sufficiently high power level, the reactor shield weight will be less than that of the fuel load of a chemical propulsion system. The longer the aircraft range, the heavier will be its chemical fuel load, and consequently the lower the power level at which the nuclear propulsion system starts to become competitive from a weight viewpoint.

Studies have shown that nuclear propulsion systems have competitive advantages in long-range aircraft with gross weights of one million lb or more. The expected availability of aircraft such as the Lockheed C-5A and the Boeing 747, whose gross weights are on the order of 750,000 lb, has been a primary factor in sparking renewed interest in nuclear aircraft propulsion.

A subsonic 1,000,000-lb nuclear aircraft will require a reactor thermal power level of about 250,000 kw, which should produce about 60,000 lb of thrust or about 60,000 shaft hp. The reactor shield weight will be on the order of 200,000 lb.

In order to insure that reactor fission products do not contaminate the atmosphere in the event of a crash, it is contemplated that the reactor would be surrounded with a structure which can absorb the energy of crash impact without rupture of the reactor containment vessel. At a reactor power level of 250,000 kw, the estimated weight of impact absorber needed is in the range of 40,000 to 100,000 lb.

Application to Aircraft Propulsion

Nuclear reactors can be considered for any of the thermal energy conversion schemes that have been surveyed in this report, with the exception of the open-cycle MHD converter. Again, the high gas temperatures in the MHD converter exceed limiting temperatures of currently available reactor materials.

Specific Weight

As was the case for radioisotope heat sources, only the weight of the reactor and its radiation shield will be considered, since they will be dominant weight components of any nuclear energy conversion system.

The estimated specific weight for the reactor and the shield is given in Table XXXVIII. The reactor weights are derived from data appearing in Reference 66. The shield weights were extrapolated from the 200,000-lb weight of a 60,000-hp engine by applying appropriate reduction factors. These reduction factors were assumed to be the same factors used in estimating the effect of power level on shield volume. A system efficiency of 25 percent was used.

TABLE XXXVIII. SPECIFIC WEIGHT OF REACTOR HEAT SOURCES AND SHIELDS

	Shaft Power (hp)		
	500	3000	20,000
Component	Specific Weight (lb/hp)		
Reactor	2.60	1.33	0.60
Shield	165.3	40.4	8.45
Total	167.9	41.73	9.05

The specific weight is given for shaft powers of 3000 hp and 20,000 hp instead of 1500 hp and 10,000 hp because it was assumed that, at other than the lowest power level, a single reactor would service two engines. At the 20,000-hp level, the specific weight of the reactor plus shield is 9.05 lb/hp. This figure is almost seven times greater than the total system specific weight (engine, transmission, and fuel) for the 10,000-hp advanced gas turbine.

Specific Volume

Reactor core volumes were estimated from data in Reference 66. The reactor shield volume at 20,000 hp was obtained by assuming a shield thickness of 200 cm (6.56 ft). The variation of shield thickness with power level was estimated from data in Reference 63 for the attenuation of fast neutrons in

water. (Most of the shield volume is occupied by the neutron-attenuating component of the shield.) Then the volume corresponding to the change in shield thickness was calculated. A system efficiency of 25 percent was assumed.

The resulting specific volume for the reactor and the shield is given in Table XXXIX.

TABLE XXXIX. SPECIFIC VOLUME OF REACTOR HEAT SOURCES AND SHIELDS

	Shaft Power (hp)		
	500	3000	20,000
Component	Specific Volume (ft^3/hp x 10^3)		
Reactor	2.1	1.2	0.5
Shield	1882.0	460.0	96.0
Total	1884.1	461.2	96.5

The lowest specific volume for the reactor/shield combination occurs at 20,000 hp; it is 96.5 x 10^{-3} ft^3/hp. This figure is 30 to 60 times larger than the specific volume of the 10,000-hp advanced gas turbine.

Cost

The capital cost of large nuclear generating stations which are rated at several hundred thousand kw is in the range of $150 to $200/kw. The specific cost increases substantially as the power level is reduced. For power ranges of interest, specific costs of the reactor portion of the power plant are estimated to be $3000/hp at 500 hp, $1000/hp at 3000 hp, and $500/hp at 20,000 hp. These figures are well in excess of advanced gas turbine specific costs, which range from about $70/hp at 500 hp to $20/hp at 10,000 hp.

Reliability

Nuclear reactors have good potential reliability. A 10,000-hr lifetime has been established as a goal in current nuclear aircraft studies.

Sensitivity to Environment

Environment sensitivity should be the same as that of the energy conversion system to which the reactor is coupled.

Part-Load Characteristics

Again, part-load system characteristics will be determined primarily by the energy conversion system.

Transient Response

Transient response of a nuclear energy conversion system should be reasonably fast. The great bulk of the system weight resides in the radiation shield, which is not thermally coupled to the power generation components. Neutron kinetics will play a significant role in determining the rapidity with which the system can respond to load changes. The rate at which the reactor power level changes is ultimately determined by the half-lives of the small fraction of delayed neutrons which are produced during the fission process.

Structural Considerations

Nuclear reactors can be designed as rugged, structurally sound devices. However, at high operating temperatures, the accumulation of fission product gases within fuel elements can result in swelling and distortion after a sufficiently long period of operation. The fuel elements must be designed to accommodate the buildup of fission product gases over the desired reactor lifetime.

Critical Problem Areas

High shield weight, high cost, and the necessity for protection of the reactor against the release of radioactivity in the event of a crash constitute the principal critical problem areas of nuclear aircraft propulsion systems. The only apparent way to overcome these problems is by restricting consideration of nuclear propulsion to very large, long-range aircraft. The total system weight and cost can then be competitive with a chemically fueled, gas-turbine propulsion system.

Conclusions

Nuclear reactor aircraft propulsion systems are not competitive with chemically fueled advanced gas turbines at aircraft power levels in the range of 500 to 20,000 hp for the short mission time (≈3 hr) considered in this survey.

CONCLUSIONS

None of the energy conversion systems that have been considered in this survey are competitive with advanced gas-turbine aircraft propulsion systems at engine shaft power levels of 500 hp and 1500 hp. The same conclusion holds for auxiliary power applications in the 25-hp to 100-hp range. The principal factor limiting competitiveness is the high specific weight of the systems that have been surveyed in comparison to the specific weight of the advanced gas turbines. This situation is expected to prevail in the foreseeable future.

At the 10,000 shaft hp level, two systems appear to be potentially competitive with advanced gas turbines after extensive development: the open-cycle MHD converter and the intercool-reheat cycle.

The open-cycle MHD converter propulsion system consists of an air compressor, a preheater, a combuster which burns a boron-slurry fuel, an MHD duct with a superconducting magnet, a superconducting motor which converts the electrical output to shaft power, and a mechanical transmission which couples the motor to a helicopter rotor. The predicted competitive performance of the MHD converter engine is based on a design concept. The maximum continuous operating time of an MHD converter to date has been a few hundred hours. The duration of power runs at significant power levels usually covers a much shorter time span. This situation is considered to be a reflection of the current rudimentary state of the art rather than a result of any inherent limitation on operating time.

One area in which the MHD converter engine does not compete is fuel cost. The boron-slurry fuel that is necessary to achieve competitive weight and fuel consumption is expensive. For this reason, an MHD propulsion system might best be utilized in special dual-purpose helicopters with electrical as well as shaft power capability. Such aircraft would offer a truly unique capability that could not be achieved with any but the MHD-type propulsion system.

An MHD-powered helicopter could not only be used for equipment and personnel transport but could also supply large quantities of airborne electrical power for special communications, lighting, or other requirements. In addition, the MHD-powered helicopter would be available for use as a highly mobile source of emergency electrical power for ground installations. Contrary to other types of emergency power systems, the airborne MHD system would have a high utilization factor when not actually supplying emergency ground power. The dual-purpose capability of an MHD-powered helicopter could well justify its higher fuel cost. A development period of 10 to 20 years would probably be required.

The intercool-reheat cycle engine employs many of the same basic elements as the conventional gas turbine. Competitiveness with advanced gas turbines is achieved through high cycle pressure ratios and intercoolers and reheaters that are integral with compressors and turbines. High turbine inlet temperatures with attendant blade-cooling schemes and high-temperature materials problems are not necessary in the intercool-reheat cycle. Implementation of the intercool-reheat cycle would require the development of polytropic compressors with integral interstage

intercoolers utilizing rotor downwash air as the heat sink, very high pressure adiabatic compressors, and very high pressure isothermal turbines with integral interstage reheaters.

RECOMMENDATIONS

It is recommended that additional studies be carried out to investigate the applicability of the MHD converter and the intercool-reheat cycle to Army aircraft propulsion requirements. The object of such studies should be:

1. To establish the design, performance, and economic characteristics of such systems.

2. To define the aircraft integrational and the logistical problems associated with their use.

3. To outline the steps involved in system development.

The development plan should include estimates of time and cost required to carry out the various developmental phases.

The studies should be carried out for a shaft power output of 10,000 hp. Two engines would be used to power a single helicopter rotor. Results should include determinations of: system size and weight, including the transmission; fuel consumption for a typical mission; and optimum shaft speed.

For each system component, determinations should be made of efficiency, operating temperature and pressure, materials, size, weight, and rotational speed (where applicable). The characteristics of the overall system should also be established, including configuration, size, weight, and fuel consumption for a typical mission.

For the MHD converter, particular attention should be paid to: superconducting magnets for the MHD duct and the superconducting motor, the effect of stray magnetic fields on magnetic shielding requirements, cooling of MHD duct walls, output voltages and currents, switching facilities for dividing the electrical output between the superconducting motor and another electrical load, cryogenic refrigeration requirements, integration of the propulsion system into a helicopter, auxiliary facilities for startup and maintenance, system transient response, part-load efficiency, the compressor and preheater design, the system for injecting electrically conductive ions into the combustion gas, and the effect of fuel selection on system performance.

For the intercool-reheat cycle, particular attention should be paid to: design of the polytropic compressor and integral intercooler, use of heat pipes in the intercooler, design of the isothermal turbine with integral reheaters, backleakage of high-pressure air, seal and bearing design, high-pressure fuel injection, startup requirements, part-load efficiency, overall system configuration, and integration of the propulsion system into a helicopter.

The results of such studies should provide a firm basis for assessing the potential of the MHD converter and the intercool-reheat cycle for use in future Army aircraft propulsion systems and will indicate the scope of the effort which would be required for their development.

LITERATURE CITED

1. Robinson, S.F., THE CLOSED CYCLE GAS TURBINE POWER PLANT, Paper No. 52-A-137. Presented at Annual ASME Meeting, New York, N.Y., November 30-December 5, 1952.

2. Keller, C., and Frutschi, H., CLOSED CYCLE PLANTS-DESIGN, APPLICATION OPERATION, Gas Turbine Engineering Handbook, Gas Turbine Publications, Inc., Stamford, Connecticut, 1966, pp. 419-432.

3. Berman, P.A., GAS TURBINES FOR NUCLEAR APPLICATIONS, Gas Turbine Engineering Handbook, Gas Turbine Publications, Inc., Stamford, Connecticut, 1966, pp. 358-362.

4. Klann, J.L., 2 TO 10 KW SOLAR OR RADIOISOTOPE BRAYTON POWER SYSTEM, Intersociety Energy Conversion Engineering Conference-1968 Record, IEEE, New York, N.Y., 1968, pp. 407-415.

5. Klann, J.L., ANALYSIS AND SELECTION OF DESIGN CONDITIONS FOR A RADIOISOTOPE BRAYTON-CYCLE SPACE POWERPLANT, NASA TN D-4600, NASA, Washington, D.C., June 1968.

6. FINAL TEST REPORT-AIRESEARCH BRAYTON CYCLE DEMONSTRATOR, APS-5270-R, AiResearch Manufacturing Company, Phoenix, Arizona, November 1967.

7. McCormick, J.E., and Redding, T.E., 3-KW RECUPERATED CLOSED BRAYTON CYCLE ELECTRICAL POWER SYSTEM, Advances in Energy Conversion Engineering, New York, N.Y., 1967, pp. 1-7.

8. Stewart, W.L., et al, BRAYTON CYCLE SYSTEMS, Selected Technology for the Electric Power Industry, NASA SP-5057, NASA, Washington, D.C., 1968, pp. 91-137.

9. Stewart, W.L., et al, BRAYTON CYCLE TECHNOLOGY, Space Power Systems Advanced Technology Conference, NASA SP-131, NASA, Washington, D.C., 1966, pp. 95-145.

10. Kays, W., and London, A.L., COMPACT HEAT EXCHANGERS, New York, McGraw-Hill, 1964.

LITERATURE CITED (Continued)

11. Silverstein, C. C., PRELIMINARY EVALUATION OF GAS TURBINE REGENERATORS EMPLOYING HEAT PIPES, USAAVLABS Technical Report 68-10, U.S. Army Aviation Materiel Laboratories, Fort Eustis, Virginia, April 1968, AD 671028.

12. Manson, S. V., A REVIEW OF THE ALKALI METAL RANKINE TECHNOLOGY PROGRAM, Journal of Spacecraft and Rockets, Vol. 5, No. 11, November 1968, pp. 1249-1259.

13. Zipkin, M. A., COMPONENTS AND SYSTEMS DESIGN FOR A 400 KW RANKINE CYCLE SPACE POWER SYSTEM, Advances in Energy Conversion Engineering, ASME, New York, N. Y., 1967, pp. 1063-1090.

14. Thur, G. M., SNAP-8 POWER CONVERSION SYSTEM ASSESSMENT, Intersociety Energy Conversion Conference - 1968 Record, IEEE, New York, N. Y., 1968, pp. 329-337.

15. Hodgson, J. N., and Macosko, R. P., A SNAP-8 BREADBOARD SYSTEM - OPERATING EXPERIENCE, Intersociety Energy Conversion Conference - 1968 Record, IEEE, New York, 1968, pp. 338-351.

16. SNAP-8 PERFORMANCE POTENTIAL STUDY - FINAL REPORT, NASA-CR-72254, April 1967.

17. Gordon, R., and Lessley, R., GROWTH POTENTIAL OF THE SNAP-8 ELECTRICAL GENERATING SYSTEM, AGC-3109, Aerojet-General Corporation, Azuza, California, May 1968.

18. Slone, H. O., SNAP-8 DEVELOPMENT STATUS, Space Power Systems Advanced Technology Conference, NASA SP-131, NASA, Washington, D. C., August 1966, pp. 147-168.

19. Leighton, G. S., THE ORGANIC RANKINE CYCLE, Intersociety Energy Conversion Conference - 1968 Record, IEEE, New York, N. Y., 1968, pp. 389-397.

20. Macauley, B. T., and Marick, J. J., ORACLE-TECHNICAL ASSESSMENT OF AN ORGANIC RANKINE POWER CONVERSION SYSTEM OPERATED AS A BREADBOARD ENGINE, Report No. 3512, Aerojet-General Corporation, Azuza, California, June 1968.

21. ORACLE-A BROAD SPECTRUM POWER SYSTEM, Report 3486, Aerojet-General Corporation, Azuza, California, December 1967.

22. Niggeman, R.E., SYSTEM ANALYSIS AND CONCEPTUAL DESIGN OF A 150 KWE ORGANIC RANKINE CYCLE POWER CONVEPSION MODULE, Report No. AER 532, Sundstrand Aviation, Rockford, Illinois, June 1968.

23. Austin, L.G., FUEL CELLS-A REVIEW OF GOVERNMENT-SPONSORED RESEARCH, 1950-1964, NASA SP-120, NASA, Washington, D.C., 1967.

24. Bartas, J.G., HEAT AND MASS TRANSFER CHARACTERISTICS IN ION EXCHANGE MEMBRANE FUEL CELLS, Engineering Developments in Energy Conversion, ASME, New York, N.Y., 1965, pp. 309-327.

25. Stedman, J.K., HIGH POWER DENSITY FUEL CELL, Technical Report AFAPL-TR-68-24, Air Force Aero Propulsion Laboratory, Wright-Patterson AFB, Ohio, March 1968.

26. Platner, J.L., ALLIS-CHALMERS CAPILLARY MATRIX FUEL CELL SYSTEMS-AN ADVANCED AEROSPACE POWER SOURCE, Intersociety Energy Conversion Engineering Conference - 1968 Record, IEEE, New York, N.Y., pp. 52-64.

27. Kirkland, T.C., and Looft, D.J., FUEL CELLS-PRESENT STATUS AND DEVELOPMENT PROBLEMS, Paper 660230, SAE, Earthmoving Industry Conference, Peoria, Illinois, April 1966.

28. Engle, M.L., and Klotz, E.E., 5 KVA HYDROCARBON-AIR FUEL CELL SYSTEM, AC SDS 066627, Vol. I, Research Division, Allis-Chalmers, Milwaukee, Wisconsin, June 1966, (Contract No. DA-44-009-AMC-240CT), U.S. Army Engineer Research and Development Laboratories, Fort Belvoir, Virginia.

29. Johnson, C.K., and Peak, W.R., COMPACT HYDROGEN-AIR MULTI-CELL FUEL CELL STACK, PWA-2721, Pratt and Whitney Aircraft, E. Hartford, Connecticut, Contract No. DA-44-009-AMC-1076(T), U.S. Army Engineer Research and Development Laboratories, Fort Belvoir, Virginia, February, 1966.

30. Connors, J.W., Thompson, R.A., and Sanderson, R.A., SYSTEM SELECTION FOR A LOW TEMPERATURE FUEL CELL POWERPLANT, Presented at 58th Annual Meeting of AIChE, Philadelphia, Pennsylvania, December 1965, Pratt and Whitney Aircraft, E. Hartford, Connecticut.

31. Chesner, R., DESIGN OF HYDROGEN-OXYGEN CAPILLARY TYPE FUEL CELL, AFAPL-TR-66-99, Air Force Aero Propulsion Laboratory, Wright-Patterson, AFB, Ohio, Allis-Chalmers, Research Division, Milwaukee, Wisconsin, Oct. 1966.

32. Schwartz, H.J., et al, SPACE POWER SYSTEMS TECHNOLOGY CONFERENCE, NASA SP-131, NASA, Washington, D.C., August 1966, pp. 9-52.

33. Kirkland, T.G., and Hopkins, R.E., U.S. ARMY RESEARCH IN ELECTRICAL PROPULSION, Paper 670454, SAE, Mid-Year Meeting, Chicago, Illinois, May 1967.

34. Ciprios, G., Batzold, J.S., and Lieberman, M., RECENT DEVELOPMENTS IN METHANOL-AIR FUEL CELLS, Advances in Energy Conversion Engineering, ASME, New York, N.Y., 1967, pp. 357-364.

35. Frysinger, G.R., HIGH EFFICIENCY HYDROCARBON-AIR ACID ELECTROLYTE FUEL CELL SYSTEM, Advances in Energy Conversion Engineering, ASME, New York, N.Y., 1967, pp. 801-808.

36. Tarmy, B.L., and Ciprios, G., THE METHANOL FUEL CELL BATTERY, Engineering Developments in Energy Conversion, ASME, New York, N.Y., 1965, pp. 272-283.

37. Hoffman, K.C., METAL HYDRIDE ENERGY STORAGE SYSTEMS, Intersociety Energy Conversion Conference - 1968 Record, IEEE, New York, N.Y., 1968, pp. 981-985.

38. Harris, L.P., and Cobine, J.D., THE SIGNIFICANCE OF THE HALL EFFECT FOR THREE MHD GENERATOR CONFIGURATIONS, ASME Transactions, Journal of Engineering for Power, October 1961, pp. 392-396.

39. Barthelemy, R.R., MAGNETOHYDRODYNAMIC POWER GENERATION STATE-OF-THE-ART (JUNE 1968), AFAPL-TR-68-78, Air Force Aero Propulsion Laboratory, Wright-Patterson AFB, Ohio, June 1968.

40. STATUS REPORT ON MHD ELECTRICAL POWER GENERATION, IAEA/ENEA International Liaison Group on MHD Electrical Power Generation, International Atomic Energy Agency, Vienna, 1967.

41. Hals, F.A., MAGNETOHYDRODYNAMIC POWER GENERATION, Paper 67-PWR-12, ASME, New York, N.Y., September 1967.

42. Schulze, K.H., and Bhada, R. K., DIRECT ENERGY CONVERSION STATUS FOR LARGE-SCALE POWER GENERATION, Intersociety Energy Conversion Engineering Conference - 1968 Record, IEEE, New York, N.Y., 1968, pp. 874-882.

43. Rosa, R.J., PLASMA MHD POWER GENERATION, Intersociety Energy Conversion Engineering Conference - 1968 Record, IEEE, New York, N.Y., 1968, pp. 1017-1023.

44. STATE OF THE ART-OPEN CYCLE, CLOSED CYCLE, AND LIQUID METAL MHD - IN THE UNITED STATES, 4th Meeting, International MHD Liaison Group, April 8-10, 1968, Washington, D.C., pp. 6-10.

45. Steinberg, M., et al, A POLLUTION-FREE HYBRID FOSSIL-NUCLEAR FUELED MHD POWER CYCLE, Intersociety Energy Conversion Engineering Conference - 1968 Record, IEEE, New York, N.Y., 1968, pp. 861-873.

46. Lindley, B.C., THE PROSPECTS FOR CLOSED-CYCLE MPD POWER GENERATION, Engineering Developments in Energy Conversion, ASME, New York, N.Y., 1965, pp. 125-140.

47. Jackson, W.D., LIQUID METAL MHD POWER GENERATION, Intersociety Energy Conversion Engineering Conference - 1968 Record, IEEE, New York, N.Y., 1968, pp. 1024-1032.

48. Powell, J.R., et al, STUDIES OF A REPETITIVE LIQUID METAL SLUG MHD GENERATOR, Engineering Developments in Energy Conversion, ASME, New York, N.Y., 1965, pp. 15-32.

49. Bjerklie, J.W., and Powell, J.R., A LIQUID METAL MHD POWER GENERATION SCHEME USING INTERMITTENT VAPORIZATION, Paper SM 107/212, International Symposium on MHD, Warsaw, Poland, IAEA, July 1968.

LITERATURE CITED (Continued)

50. Houston, J.M., SURVEY OF THEORY AND LABORATORY PERFORMANCE OF CESIUM THERMIONIC CONVERTERS, Engineering Developments in Energy Conversion, ASME, New York, N.Y., 1965, pp. 216-237.

51. Engdahl, R.E., et al, THERMIONIC ENERGY CONVERSION FOR CENTRAL POWER STATIONS, Intersociety Energy Conversion Conference - 1968 Record, IEEE, New York, N.Y., 1968, pp. 883-888.

52. Speidel, T., PERFORMANCE COMPARISON OF NINE RD-502 CYLINDRICAL DIODES WITH ETCHED PHENIUM EMITTERS, Thermo Electron Corporation. Waltham, Massachusetts.

53. Fry, J.F., EVALUATION OF A SET VIII THERMIONIC GENERATOR, Advances in Energy Conversion Engineering, ASME, New York, N.Y., 1967, pp. 151-161.

54. Schwartz, H.J., and Ward, J., DIRECT ENERGY CONVERSION, Selected Technology for the Electric Power Industry, NASA SP-5057, NASA, Washington, D.C., 1968, pp. 281-303. Also, Stewart, W.L. et al, BRAYTON CYCLE SYSTEMS, pp. 91-137.

55. Klein, R.L., and Dingwall, A.G.F., SILICON-GERMANIUM THERMOELECTRIC POWER GENERATING DEVICES, Engineering Developments in Energy Conversion, ASME, New York, N.Y., 1967, pp. 141-155.

56. Rocklin, S.R., DESIGN AND DEVELOPMENT OF A HIGH EFFICIENCY CASCADED AND SEGMENTED THERMOELECTRIC MODULE, Advances in Energy Conversion Engineering, ASME, New York, N.Y., 1967, pp. 207-219.

57. Bates, H.E., and Weinstein, M., ON THE EFFICIENCY OF SEGMENTED SiGe-PbTe THERMOCOUPLES, Intersociety Energy Conversion Engineering Conference - 1968 Record, IEEE, New York, N.Y., 1968, pp. 229-233.

58. Raag, V., Berlin, E.P., and Bifano, W.J., FLAT-PLATE THERMOELECTRIC GENERATORS FOR SOLAR PROBE MISSIONS, Intersociety Energy Conversion Engineering Conference - 1968 Record, IEEE, New York, N.Y., 1968, pp. 241-248.

59. Brunings, J.E., SiGe DIRECT RADIATING CONVERTER RADIOISOTOPE THERMOELECTRIC GENERATOR, Advances in Energy Conversion Engineering, ASME, New York, N.Y., 1967, pp. 1003-1016.

60. Hittman, F., and Silverstein, C.C., RADIOISOTOPE-FUELED THERMOELECTRIC GENERATORS, Engineering Developments in Energy Conversion, ASME, New York, N.Y., 1967, pp. 156-173.

61. Rubinstein, M.A., COMMERCIAL THERMOELECTRIC GENERATOR APPLICATIONS AND ECONOMIC CONSIDERATIONS, General Instrument Corporation, Newark, N.J. Presented at Intersociety Energy Conversion Engineering Conference, Boulder, Colorado, August 1968.

62. Schulman, F., ISOTOPES AND ISOTOPE THERMOELECTRIC GENERATORS, Space Power Systems Advanced Technology Conference, NASA SP-131, NASA, Washington, D.C., 1966, pp. 73-93.

63. Arnold, E.D., HANDBOOK OF SHIELDING REQUIREMENTS AND RADIATION CHARACTERISTICS OF ISOTOPIC POWER SOURCES FOR TERRESTRIAL, MARINE, AND SPACE APPLICATIONS, ORNL 3576, Oak Ridge National Laboratory, Oak Ridge, Tennessee, April 1964.

64. Rom, F.E., and Finnegan, P.M., WILL THE NUCLEAR-POWERED AIRCRAFT BE SAFE?, Astronautics and Aeronautics, March 1968, pp. 32-40.

65. Wild, J.M., NUCLEAR PROPULSION FOR AIRCRAFT, Astronautics and Aeronautics, March 1968, pp. 24-30.

66. King, A.E., DESIGN STUDY-ELECTRICAL COMPONENT TECHNOLOGY FOR 0.25 TO 10.0 MEGAWATT SPACE POWER SYSTEMS, SAN-679-8, Aerospace Electrical Division, Westinghouse Electric Corporation, Lima, Ohio, February 1968.

67. King, A.E., Fanger, J.B., and Leighton, G.S., ELECTRICAL COMPONENT TECHNOLOGY FOR 0.25 TO 10 MEGAWATT SPACE POWER, Intersociety Energy Conversion Engineering Conference - 1968 Record, IEEE, New York, N.Y., 1968, pp. 277-289.

68. Conboy, J.D., STATE OF THE ART REVIEW ON HELICOPTER TRANSMISSIONS, TURBOPROP GEARBOXES, AND LUBRICATION THEREOF, NAEC-AEL-1849, U.S. Naval Air Engineering Center, Philadelphia, Pennsylvania, February 1967.

69. Robinson, H.A., Blutt, J.R., and Mooncai, H.W., SUPERCONDUCTING ELECTRICAL MACHINERY AS A MEANS OF POWER TRANSMISSION IN AIRCRAFT, USAAVLABS Technical Report 66-11, U.S. Army Aviation Materiel Laboratories, Fort Eustis, Virginia, January 1966, AD 629635.

70. LaFrance, J.C., and Lucas, E.L., EXPERIMENTAL INVESTIGATION OF SUPERCONDUCTING SYNCHRONOUS MACHINES, Contract DA-44-177-AMC-410(T), USAAVLABS Technical Report 69-70, U.S. Army Aviation Materiel Laboratories, Fort Eustis, Virginia.

71. Stekly, E.J.J., et al, STUDY OF POTENTIAL SIZE AND WEIGHT REDUCTIONS IN MARINE ELECTRIC PROPULSION MACHINE BY UTILIZING SUPERCONDUCTORS, Avco Everett Research Laboratory; Contract No. Nobs-94528, Department of the Navy, Naval Ship Systems Command, Washington, D.C., February 1968, AD827104-L.

APPENDIX I
INTERCOOL-REHEAT CYCLE ANALYSIS

IDEAL CYCLE

The ideal intercool-reheat cycle consists of the following processes—isothermal compression, isentropic compression, isothermal expansion, isentropic expansion—as shown by the solid lines of Figure 24.

Now let

$$P_1 = \frac{p_2}{p_1}\ ,\ P_2 = \frac{p_3}{p_2}\ ,\ P_3 = \frac{p_3}{p_1}\ ,\ P_4 = \frac{p_4}{p_1} \tag{1}$$

and

$$\alpha = \frac{k-1}{k} \tag{2}$$

where p_i = pressure at state point i, i = 1, 2, 3, 4
$k = c_p/c_v$
c_p = specific heat at constant pressure
c_v = specific heat at constant volume

It may be shown that

$$P_1 = P_3\ ,\ P_2 = P_4 \tag{3}$$

The ideal cycle efficiency is the same as that of the Carnot cycle, or

$$\eta_i = \frac{T_3 - T_1}{T_3} = 1 - \frac{T_1}{T_3} = 1 - \frac{T_2}{T_3}$$

$$= 1 - \frac{1}{P_2{}^{\alpha}} = 1 - \left(\frac{P_1}{P}\right)^{\alpha} \tag{4}$$

where η_i = ideal cycle efficiency
T_i = absolute temperature at state point i, i = 1, 2, 3, 4
$P = p_3/p_1 = P_1 P_2$ = overall pressure ratio

It may be shown that the net ideal cycle work is

$$W_j = \alpha c_p T_1 \ln P_1 \left[\left(\frac{P}{P_1} \right)^{\alpha} - 1 \right] \tag{5}$$

The optimum pressure ratio P_{10} for which cycle work is a maximum may be found by differentiating Equation (5) with respect to P_1 and then setting the result equal to zero. When this operation is performed, the following equation for P_{10} results:

$$1 - \alpha \ln P_{10} = \left(\frac{P_{10}}{P} \right) \tag{6}$$

The ideal cycle efficiency η_{io} corresponding to maximum cycle work is, from Equations (4) and (6),

$$\eta_{io} = 1 - \left(\frac{P_{10}}{P} \right)^{\alpha} = \alpha \ln P_{10} \tag{7}$$

The maximum value of P_{10m} occurs when $P \rightarrow \infty$. From Equation (6),

$$P_{10m} = e^{1/\alpha} \tag{8}$$

The value of P_{10m} for air, for which $\alpha = 0.286$, is 33.0. From Equation (7), the ideal cycle efficiency η_{io} when $P_{10} = P_{10m}$ is 1.0.

REAL CYCLE

In the real intercool-reheat cycle, as indicated by the dashed lines of Figure 24, the isentropic processes are replaced by adiabatic processes and the isothermal processes are replaced by polytropic processes. In the polytropic compression process,

$$\frac{T_2'}{T_1} = P_1^{\beta_c} \tag{9}$$

where

$$\beta_c = \frac{n_c - 1}{n_c} \tag{10}$$

and n_c = polytropic compression coefficient

When $n_c = k$, the polytropic process is the same as an isentropic process. When $n_c = 1$, the polytropic process is the same as an isothermal process.

Similarly, in the polytropic expansion process,

$$\frac{T_3'}{T_4'} = P_3^{\beta_t} = P_1^{\beta_t} \tag{11}$$

where

$$\beta_t = \frac{n_t - 1}{n_t} \tag{12}$$

and n_t = polytropic expansion coefficient

It should be realized that T_2' and T_4' are independent variables which are determined by the extent of heat removal in the intercooler and by the extent of heat addition in the reheater. The polytropic coefficients are then dependent variables which are determined from T_2' and T_3'. From Equations (9), (10), (11), and (12),

$$\beta_c = \frac{n_c - 1}{n_c} = \frac{\ln T_2'/T_1}{\ln P_1} \tag{13}$$

$$\beta_t = \frac{n_t - 1}{n_t} = \frac{\ln T_3'/T_4'}{\ln P_1} \tag{14}$$

In general, β_c will not be equal to β_t.

The various cycle temperatures can be found using Equations (9), (11), and Equations (15) and (16) that follow.

$$\frac{T_3'}{T_2'} = 1 + \frac{P_2^{\alpha} - 1}{\eta_{c2}} \tag{15}$$

$$\frac{T_5'}{T_4'} = 1 - \eta_{t2} (1 - P_2^{-\alpha}) \tag{16}$$

where η_{c2} = adiabatic compressor efficiency
η_{t2} = adiabatic turbine efficiency

The polytropic compression work W_{c1} can be expressed as

$$W_{c1} = \frac{\alpha}{\beta_c \eta_{c1}} c_p (T_2' - T_1) \tag{17}$$

where η_{c1} = polytropic compressor efficiency

The heat removed during intercooling Q_i is equal to the polytropic compression work minus the enthalpy change between state points 1 and 2'. Q_i can be expressed as

$$Q_i = \left(\frac{\alpha}{\beta_c \eta_{c1}} - 1 \right) c_p (T_2' - T_1) \tag{18}$$

The adiabatic compression work W_{c2} is given by

$$W_{c2} = \frac{c_p}{\eta_{c2}} T_2' \left(P_2^{\alpha} - 1 \right) \tag{19}$$

The polytropic expansion work W_{t1} can be expressed as

$$W_{t1} = \frac{\alpha \eta_{t1}}{\beta_t} cp (T_3' - T_4') \tag{20}$$

where η_{t1} = polytropic expansion efficiency

The heat added to the cycle during reheat Q_r is equal to the work done by the polytropic expansion minus the enthalpy change between state points 3' and 4'. Q_r can be expressed as

$$Q_r = \left(\frac{\alpha \eta_{t1}}{\beta_t} - 1 \right) cp \, (T_3' - T_4') \tag{21}$$

The adiabatic work of expansion W_{t2} is given by

$$W_{t2} = \eta_{t2} \, c_p \, T_4' \left(1 - P_2^{-\alpha} \right) \tag{22}$$

The cycle efficiency η is equal to the net work output W divided by the heat added during reheat, or

$$\eta = \frac{W}{Q_r} = \frac{W_{t1} + W_{t2} - (W_{c1} + W_{c2})}{Q_r} \tag{23}$$

HEAT TRANSFER IN INTERCOOLER

The general shape of the temperature distribution in the intercooler is shown in Figure 46. Heat is transferred from the cycle working fluid to ambient cooling air, while the temperature of both fluids increases. The dashed line represents the change in temperature of the working fluid during continuous intercooling, which has been assumed in the analysis. Actually, the temperature of the working fluid should be raised a few degrees by adiabatic compression prior to the initiation of intercooling, in order to have a finite temperature difference at the intercooler entrance. The working fluid temperature at the intercooler entrance is then T_1' rather than the ambient temperature T_1. Although the heat removed along path $T_1' - T_2'$ is not the same as that removed along path $T_1 - T_2'$, the difference is small when $(T_1' - T_1)/T_1 << 1$. The heat removed is assumed to be the same for both cases in the analysis performed here.

The heat transferred in the intercooler is then, with the aid of Eq. (18),

$$w_c \, Q_i = w_c \left(\frac{\alpha}{\beta_c \, \eta_{c1}} - 1 \right) c_p \, (T_2' - T_1) = w_a \, c_p \, (T_{2a} - T_1)$$

$$\approx w_c \left(\frac{\alpha}{\beta_c \, \eta_{c1}} - 1 \right) c_p \, (T_2' - T_1') \tag{24}$$

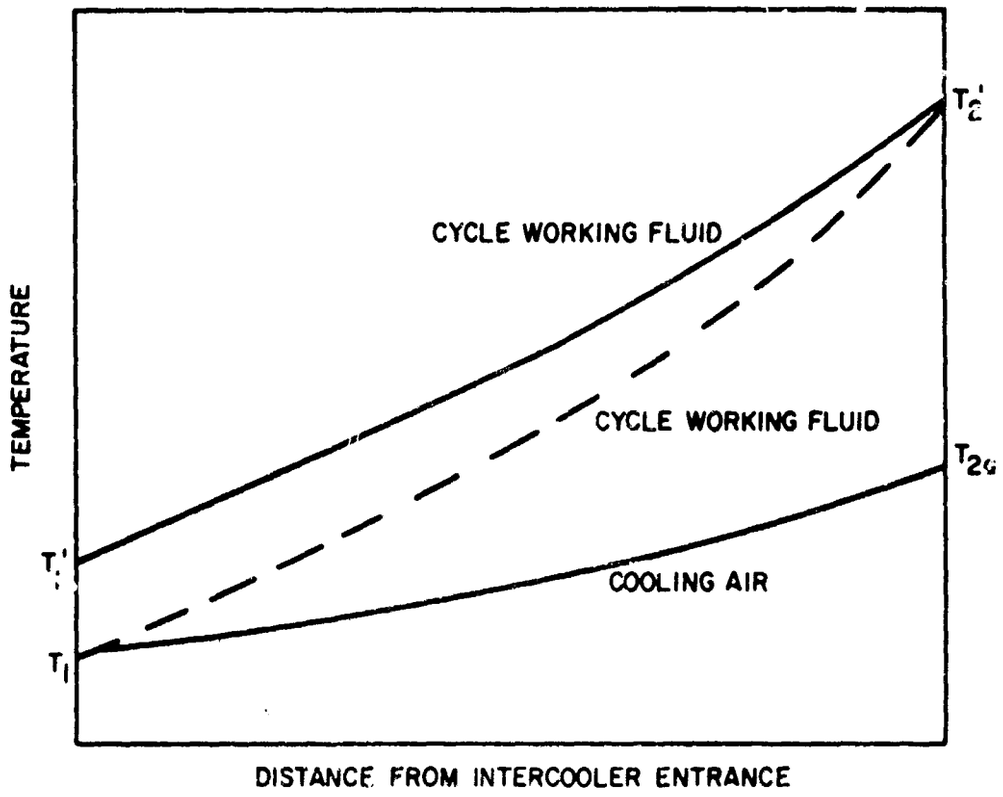

Figure 46. Temperature Distribution in Intercooler of Intercool-Reheat Cycle.

where w_c = cycle air mass flow rate
w_a = cooling air mass flow rate

For convenience, let

$$\left.\begin{aligned} C_h &= w_c\left(\frac{\alpha}{\beta_c \eta_{c1}} - 1\right) c_p = \frac{w_c Q_i}{T_{2'} - T_1'} \\ C_c &= w_a c_p = \frac{w_c Q_i}{T_{2a} - T_1} \end{aligned}\right\} \quad (25)$$

In differential terms, Equation (24) can be written

$$dq = C_c dT_c = C_h dT_h = U (T_h - T_c)\, dA \quad (26)$$

where T_c = temperature of cooling air at some point
T_h = temperature of working fluid at same point
U = overall heat transfer coefficient
dA = differential heat transfer area
dq = differential heat transfer rate

From Equation (26), one can write

$$d (T_h - T_c) = dT_h - dT_c = \left(1 - \frac{C_h}{C_c}\right)\frac{dq}{C_h} = \left(1 - \frac{C_h}{C_c}\right)\frac{U (T_h - T_c)\, dA}{C_h} \quad (27)$$

or

$$\frac{d (T_h - T_c)}{T_h - T_c} = \left(1 - \frac{C_h}{C_c}\right)\frac{U\, dA}{C_h} \quad (28)$$

When Equation (28) is integrated,

$$\ln\left(\frac{T_2' - T_{2a}}{T_1' - T_1}\right) = \left(1 - \frac{C_h}{C_c}\right)\frac{UA}{C_h} \quad (29)$$

Now, from Reference 10,

$$NTU = \frac{UA}{C_{min}} \tag{30}$$

where C_{min} = the smaller of C_h or C_c
NTU = number of heat transfer units
A = heat transfer area

Since $T_2' - T_1'$ is generally larger than $T_{2a} - T_1$, it follows from Equation (25) that $C_h = C_{min}$. Therefore, Equation (29) can be rewritten, with the aid of Equation (25),

$$\frac{NTU}{T_2' - T_1'} = \frac{\ln (T_2' - T_{2a}) - \ln (T_1' - T_1)}{(T_2' - T_{2a}) - (T_1' - T_1)} \tag{31}$$

From Equations (30) and (25), and recalling that $C_h = C_{min}$,

$$A = \frac{w_c Q_i}{U} \left(\frac{NTU}{T_2' - T_1'} \right) \tag{32}$$

Now

$$P = W w_c \tag{33}$$

where W = net cycle work/unit mass working fluid
P = output power

If Equation (33) is substituted into Equation (32),

$$A = \frac{Q_i}{UW} \left(\frac{NTU}{T_2' - T_1'} \right) \tag{34}$$

For the intercooler, U may be considered approximately equal to the product of the cooling air-side heat transfer coefficient and the air-side fin effectiveness, and A/P is then the air-side heat transfer surface area in the intercooler per unit output power. A/P is readily calculated from Equations (18), (23), and (31).

APPENDIX II
HEAT INPUT AND HEAT REJECTION SYSTEMS

In a closed thermodynamic cycle, heat generated external to the cycle must be added to the cycle, and the fraction of the heat which is not converted to work must be rejected from the cycle. The closed Brayton cycle, Rankine cycle, thermionic converter, and thermoelectric converter require heat input and rejection systems. Since little information was obtained on combustion-fired heat input systems and air heat sink heat rejection systems during the survey, these components were investigated on a limited basis in order to provide data necessary in the evaluation of the four energy conversion systems cited above. The same conceptual approach was used for each system.

HEAT INPUT SYSTEM

The heat input system that was adopted is shown in Figure 8. Atmospheric air is compressed, heated in a preheater, and then further heated by combustion in the combuster. The hot combustion gas passes through the heater or heat exchanger, where most of the thermal energy released by combustion is transferred to the energy converter. The gas then flows through the preheater, transferring its heat to the compressor discharge air. From the preheater, the combustion gas enters the turbine, where just enough power is produced to drive the compressor, and is finally discharged to the atmosphere.

An additional heat exchanger could be located between the compressor discharge air and the preheater in order to recover waste heat from the energy converter. Studies of the heat rejection system indicated that the additional waste heat exchanger was not desirable.

In order to minimize the weight of the heat input system, the mass flow rate through the system should be minimized. Not only does minimum mass flow rate reduce the size of the compressor and turbine, but the resulting large temperature rise in the combuster provides for a large ΔT in the heater, reducing the heater size. The minimum air flow rate is that corresponding to stoichiometric combustion, when the air supply is just sufficient to fully consume the fuel. This occurs for an air-fuel mass ratio of about 14.8, for which the associated temperature rise in the combuster is about 3500°F. However, at stoichiometric conditions, there is no excess air available for cooling the combustor liner. Therefore, in the studies performed here, a temperature rise of 3000°F was assumed, which corresponds to about 18 percent excess air.

The preheater is necessary to achieve reasonable combustion efficiency (defined here as the fraction of heat released in the compressor which is transferred to the energy conversion system in the heater). For example, if the hot end of the energy converter is at 1500°F, the combustion gas cannot be cooled below 1500°F in the heater. Without a preheater, the combustor gas would enter the heater at 3000°F, and only half its sensible heat added in the combustor could be transferred to the energy converter (i.e., the combustion efficiency would be 0.5). With a preheater, air could be heated to 1500°F before entering the combustor, and the combustion gas could then be heated to 4500°F. All the sensible heat added in the combustor could then be transferred to the energy converter, and the combustion efficiency would approach unity.

The combustion efficiency must always be less than 1, however. Otherwise, the preheater air outlet temperature (combustor inlet temperature) would be equal to the preheater combustion gas inlet temperature (combustion gas heater outlet temperature), and the preheater would then have to be infinitely large. In the studies conducted here, the temperature drop of the combustion gas in the heater was taken to be 2700°F. The combustion efficiency is then 0.9, and a 300°F temperature drop is available between the cooled gas and heated air in the preheater.

Heater

The heater effectiveness ϵ is defined as

$$\epsilon = \frac{T_i - T_o}{T_i - t_i} \tag{35}$$

where T_i = combustion gas inlet temperature
T_o = combustion gas outlet temperature
t_i = inlet temperature of energy converter medium

Now let

$$\gamma = \frac{t_o - t_i}{T_i - T_o} \tag{36}$$

where t_o = outlet temperature of energy converter medium

Equation (35) is applicable only when $\gamma < 1$. This condition prevails in the situations considered here. The number of heat transfer units NTU is defined as

$$NTU = \frac{AU}{Q} \quad (T_i - T_o) \tag{37}$$

where Q = heat transfer rate = heat input rate to energy converter
A = heat transfer surface area on one side of heat exchanger
U = overall heat transfer coefficient corresponding to A

Now

$$\eta = \frac{P_r}{Q} \tag{38}$$

where η = energy converter efficiency
P_r = output power

From Equations (37) and (38),

$$\frac{A}{P_r} = \frac{NTU}{\eta\, U\, (T_i - T_o)} \tag{39}$$

Equation (39) gives the heat transfer area of the heater per unit of output power (for the side of the heat exchanger corresponding to U).

For counterflow of the combustion gas and the energy converter medium, NTU can be found from the relation[10]

$$\epsilon = \frac{1 - e^{-(1-\gamma)\,NTU}}{1 - \gamma\, e^{-(1-\gamma)\,NTU}} \tag{40}$$

It is now assumed that

$$h_g A_g << h_e A_e \tag{41}$$

where h = heat transfer coefficient
g = subscript denoting gas-side
e = subscript denoting energy converter side

Equation (41) is reasonably valid for all the energy converters under consideration. Then U in Equation (39) may be replaced by h_g, and the area A is the gas-side heat transfer area A_g. For the cases under consideration, A_g is usually larger than A_e by a significant factor, and will be so considered here. For equal thicknesses of the gas- and converter-side heat transfer surfaces, most of the heater weight will then be accounted for by the gas-side heat transfer surface. On the assumption that the heater will be of the plate-fin type, the weight of the gas-side heat transfer surface W_{hg} is

$$W_{hg} = \rho \frac{A_g \delta}{2} \tag{42}$$

where ρ = density of fin material
δ = fin thickness

The contribution of the converter-side heat transfer surface, the structure, and the flow headers to the total heater weight W_h was estimated by applying a factor of 2 to W_{hg}. Thus,

$$W_h = \rho A_g \delta \tag{43}$$

The specific heater weight W_h/P_r (weight per unit output power) is then found by substituting Equation (39) into Equation (43), recalling that $A \equiv Ag$ and $U \equiv h_g$. Thus,

$$\frac{W_h}{P_r} = \frac{\rho \delta NTU}{\eta h_g (T_i - T_o)} \tag{44}$$

For calculational purposes, a value of 50 Btu/hr-ft^2 - °F was used for h_g. This figure is characteristic of the heat transfer coefficient for air at 3 atmospheres, 3000°F, and a velocity of 100 ft/sec that flows across interrupted surfaces with a hydraulic diamter of 1/4 in. The fin thickness δ was taken to be 3.6 mils. Unless stated otherwise, the density ρ was taken to be that of stainless steel. The heater specific volume (volume per unit power output) was obtained from Equation (39) for specific area by assuming an area-volume ratio of 200 ft^2/ft^3.

Combustion System

The combustion system consists of the compressor, turbine, and combustor of the heat input system. A compression ratio of 3 was used, and a 20-percent pressure drop was assumed between the compressor discharge and the turbine inlet. The compressor efficiency was 0.83, and the turbine efficiency was 0.87. The ambient temperature was assumed to be 40°F. The compressor discharge air temperature is then 263°F (a temperature of 240°F was actually used for preheater calculations). For these conditions, the turbine output power will be just equal to the compressor input power when the turbine inlet temperature is 540°F.

The weight of the combustion system was assumed to be the same as that of a standard gas turbine with the same pressure ratio of 3 and the same mass flow rate w_a. On the assumption that two-thirds of the turbine power is used to drive the compressor, the power output of gas turbine P_a may be expressed as

$$P_a = \frac{1}{2} w_a \Delta h_c \tag{45}$$

where Δh_c = compressor work per unit mass

For a pressure ratio of 3, $\Delta h_c \approx 53$ Btu/lb. The heat input rate Q to the energy converter can be expressed as

$$Q = w_a c_p (T_i - T_o) \tag{46}$$

From Equations (46) and (38), the power output P_r of the energy converter is

$$P_r = \eta\ w_a c_p (T_i - T_o) \tag{47}$$

The ratio P_a/P_r is then, from Equations (47) and (44),

$$\frac{P_a}{P_r} = \frac{\Delta h_c}{2 \eta c_p (T_i - T_o)} \tag{48}$$

The specific weight of the combustion system W_{cs}/P_r is obtained by multiplying P_a/P_r from Equation (48) by the specific weight W_{cs}/P_a of the comparable gas turbine. In this study, it was assumed that $W_{cs}/P_a = 0.5$ lb/hp.

Preheater

The preheater effectiveness ϵ_p is defined as

$$\epsilon_p = \frac{T_o - T_t}{T_o - T_c} \tag{49}$$

where T_t = inlet temperature of combustion system turbine
T_c = outlet temperature of combustion system compressor

Since both the air and the gas flow rates are the same, the air temperature rise is equal to the gas temperature drop. Then γ, defined as the ratio of these temperature changes, is equal to 1. For this case, NTU for counterflow reduces to[10]

$$NTU = \frac{\epsilon_p}{1 - \epsilon_p} \tag{50}$$

It can be shown that the specific area A/P_r for the preheater is identical in form to Equation (39), with NTU given by Equation (50) and U the overall heat transfer coefficient for the preheater. In the preheater, $h_g A_g \approx h_a A_a$, and $h_g \approx h_a$. Then it may be shown that $U_g = h_g/2$. Also, the air- and gas-side heat transfer areas will be equal, and the total heat transfer surface weight will be twice the weight of the gas-side heat transfer surface. If the heater weight is assumed to be a small fraction of the preheater weight, then the above data plus Equations (42) and (39) may be used to show that the preheater specific weight W_p/P_r is

$$\frac{W_p}{P_r} = \frac{2 \rho \delta \ NTU}{\eta \ h_g (T_i - T_o)} \tag{51}$$

where NTU is given by Equation (50). When calculating W_p/P_r, δ was taken to be 3.6 mils, a value of 100 Btu/hr-ft^2-°F was used for h_g, and the density of stainless steel was used for ρ.

HEAT REMOVAL SYSTEM

Three possible heat sinks were considered for removal of waste heat from the energy converters: fuel, combustion system air, and rotor downwash air.

Fuel Heat Sink

With a fuel heat sink, fuel would flow through a heat exchanger, absorbing waste heat from the energy converter, and then enter the combustor. The fuels considered in the analysis included JP-4, methane, and hydrogen. The hydrogen was stored in one of three forms: pressurized gas, cryogenic liquid, and the compound $Mg H_2$. The JP-4 was heated from its freezing point of -85°F to its boiling point of 350°F and vaporized. The methane was heated from its freezing point of -259°F, vaporized, and superheated to 1000°F. The liquid hydrogen was heated from its boiling point of -428°F, vaporized, and superheated to 572°F. The gaseous hydrogen was heated from 50°F to 1100°F. The $Mg H_2$ was heated from room temperature to its dissociation temperature of 550°F at 1 atmosphere and dissociated to yield free hydrogen gas.

The total waste heat load per hp was calculated to be 15,300 Btu/hp, on the assumption of a system efficiency of 0.25 and a total operating time of 2 hours. Results of the analysis are given in Table XXXX.

TABLE XXXX. CHARACTERISTICS OF FUELS AS HEAT SINKS

Fuel	Heating Value (Btu/lb)	Heat Absorbed (Btu/lb)	Fuel for Propulsion (lb/hp)		Fuel for Heat Absorption (lb/hp)	
			Fuel	Fuel & Storage	Fuel	Fuel & Storage
JP-4	18,400	324	1.11	1.11	47.2	47.2
Liquid Methane	21,200	1,100	0.96	0.96	13.9	13.9
Liquid H_2	51,600	3,700	0.40	3.10	4.14	32.5
6,000 psi H_2 gas	51,600	3,700	0.40	4.74	4.14	49.7
H_2 in Mg H_2	51,600	16,000	0.49	6.07	0.96	14.7

In all cases, the weight of fuel plus fuel storage required for absorption of cycle waste heat substantially exceeds that required for propulsion. Therefore, the use of chemical fuel as a heat sink for waste heat discharged by the energy converter is not feasible.

Combustion System Air as Heat Sink

In this scheme, energy converter waste heat is transferred in a heat exchanger to the compressor discharge air of the combustion system. The scheme was examined briefly for the closed Brayton cycle with nitrogen as the working fluid. The nitrogen must be cooled from about 1200°R to 800°R in the waste heat exchanger or precooler. The compressor discharge air will be heated from its discharge temperature of about 700°R to some value T_d' less than 1200°R. Since nitrogen and air have about the same value of the specific heat c_p, the ratio w_a/w_c of air and nitrogen flow rates is $(1200-800)/(T_d' - 700)$.

The value of w_a/w_c will generally be greater than 1. Its minimum value, which occurs as T_d' approaches 1200°R, is 0.8. Thus, the use of compressor discharge air as a heat sink requires that the flow rate in the combustion system (and hence the entire heat input system) be comparable to or greater than the flow rate of nitrogen working fluid.

The w_a/w_c ratio for minimum heat input system weight and a combustion efficiency of 0.9 is about 0.25. An increase in the w_a/w_c ratio to 1 would result in a reduction in combustion efficiency and an increase in the specific weight of the heat input system by roughly a factor of 4. The waste heat exchanger would represent an additional, although relatively small, weight increment.

Because of the strong adverse effect on the heat input system weight, the use of combustion system compressor discharge air as a heat sink for energy converter waste heat was not considered to be feasible.

Rotor Downwash Air as Heat Sink

In this scheme, downwash air from the helicopter rotor is directed through the energy converter waste heat exchanger. Air flow rates and velocities can be obtained by equating the thrust produced by the rotor to the air momentum flow rate. For a hovering vehicle, the rotor thrust is equal to the helicopter weight. Flow and heat transfer characteristics that were calculated on this basis are given in Table XXXXI. The heat transfer coefficients apply for flow over tubes or interrupted surface fins with a hydraulic diameter of 1/4 in.

TABLE XXXXI. FLOW AND HEAT TRANSFER CHARACTERISTICS OF ROTOR DOWNWASH AIR

Shaft Power (hp)	Helicopter Weight* (lb)	Rotor Diameter* (ft)	Area (ft^2)	Velocity (ft/sec)	Specific Mass Flux (lb/hp-hr-ft^2)	Heat Transfer Coefficient (Btu/hr-ft^2-°F)
500	3,000	37.2	1,090	34.8	17.92	24.8
3,000	18,000	57.5	2,600	55.1	4.80	32.6
20,000	130,000	132.0	13,700	64.5	0.85	35.9

*Personal communication with D. Cale, U.S. Army Aviation Material Laboratories, Fort Eustis, Va.

The specific weight of the heat removal heat exchanger, or cooler, is determined as follows: The number of heat transfer units NTU is

$$NTU = \frac{AU}{(1-\eta)Q} \Delta T_{max} \tag{52}$$

where ΔT_{max} = larger of the air temperature rise ΔT_a or the energy converter temperature drop ΔT_e

If Equation (38) is substituted into Equation (52),

$$\frac{A}{P_r} = \frac{1-\eta}{\eta} \frac{NTU}{U \Delta T_{max}} \tag{53}$$

The cooler effectiveness ϵ is defined as

$$\left.\begin{aligned} \epsilon &= \frac{T_{ei} - T_{eo}}{T_{ei} - T_{ai}} \quad \text{when } T_{ei} - T_{eo} = \Delta T_{max} \\ &= \frac{T_{ao} - T_{ai}}{T_{ei} - T_{ai}} \quad \text{when } T_{ao} - T_{ai} = \Delta T_{max} \end{aligned}\right\} \tag{54}$$

where T_{ei} = energy converter inlet temperature
T_{eo} = energy converter outlet temperature
T_{ai} = air inlet temperature
T_{ao} = air outlet temperature

Now γ is defined as

$$\gamma = \frac{\Delta T_{min}}{\Delta T_{max}} \tag{55}$$

where ΔT_{min} = the smaller of ΔT_a or ΔT_e

NTU can then be found from Equation (40).

The inequality of Equation (41) is also valid for the cooler, with the understanding that the subscript a for air is used instead of g. Then h_a can be substituted for U and A_a for A in Equation (53). As was the case for the heater, most of the heater weight will be accounted for by the air-side heat transfer surface. If the same assumptions regarding the heat transfer surface were made for the cooler as were made for the heater, the equivalent of Equation (43) results.

$$W_c = \rho A_a \delta \tag{56}$$

where W_c = cooler weight

The fin thickness δ was taken to be 3.6 mils. The fin density was that of the construction material. Stainless steel, titanium, or aluminum was used, depending on the peak cooler temperature.

If Equation (53) is substituted into Equation (56), the desired equation for the specific cooler weight W_e/P_r results.

$$\frac{W_c}{P_r} = \left(\frac{1-\eta}{\eta}\right) \frac{\rho \delta \, NTU}{h_a \, \Delta T_{max}} \tag{57}$$

The area A_a under the rotor through which the cooler air supply flows is also of interest. A large air temperature rise through the cooler will require a smaller air flow rate w_a and hence a smaller A_a. However, cooler size and weight are reduced by a small air temperature rise through the cooler and hence a large air rate and a large A_a.

The heat removal rate Q_c by airflow through the cooler is

$$Q_c = w_a \, c_p \, (T_{ao} - T_{ai}) = \left(\frac{1-\eta}{\eta}\right) P_r \tag{58}$$

Therefore, the specific airflow rate w_a/P_r is

$$\frac{w_a}{P_r} = \left(\frac{1-\eta}{\eta}\right) \frac{1}{c_p \, (T_{ao} - T_{ai})} \tag{59}$$

The specific air flow rate w_a/P_r will have the units of lb/hp-hr when c_p is in Btu/lb-°F and T is in °F, if the right side of Equation (59) is multiplied by the conversion factor 2545 Btu/hp-hr.

The cooling air flow area A_a in ft^2 is then obtained by dividing the specific air flow rate in lb/hr-hr by the specific mass flux in lb/hp-hr-ft^2, as given in Table XXXXI.

Table XXXXII lists the cooling air flow area for the energy conversion systems that require a cooler. At the air outlet temperature indicated in Table XXXXII, the dual objectives of low cooler weight and small cooling air flow area are in reasonable balance. The air inlet temperature was 40°F in all cases. The converter efficiencies are estimates based on future technology.

TABLE XXXXII. FLOW AREA OF COOLING AIR FROM ROTOR DOWNWASH

Power (hp)	Energy Conversion System	Converter Efficiency	Air Outlet Temperature (°F)	Flow Area (ft^2)
500	Closed Brayton Cycle	0.296	240	6.77
	K Rankine Cycle	0.266	240	7.85
	Hg Rankine Cycle	0.193	240	13.60
	Organic Rankine Cycle	0.290	140	13.96
	Thermionic Converter	0.120	240	21.0
	Thermoelectric Converter	0.120	240	21.0
3000	Closed Brayton Cycle	0.309	240	23.8
	K Rankine Cycle	0.278	240	27.6
	Hg Rankine Cycle	0.199	240	42.7
	Organic Rankine Cycle	0.297	140	50.3
	Thermionic Converter	0.120	240	78.3
	Thermoelectric Converter	0.120	240	78.3
20,000	Closed Brayton Cycle	0.326	240	124
	K Rankine Cycle	0.300	240	140
	Hg Rankine Cycle	0.212	240	222
	Organic Rankine Cycle	0.308	140	270
	Thermionic Converter	0.120	240	443
	Thermoelectric Converter	0.120	240	443

APPENDIX III
ELECTRIC MOTORS

An electric motor is needed to convert the DC electrical output of the direct-electricity generators to shaft power. Conventional and superconducting motors were considered.

CONVENTIONAL MOTORS

DC motors are generally not suitable for high-power-density, high-speed operation because brush life varies inversely with rotational speed and the square of the current.* However, brushless DC motors capable of high-speed operation are being developed.[33] The role of the commutator in such cases is taken by a silicon-controlled rectifier. The weight of a brushless DC motor is probably not too different from that of a conventional DC motor that operates at the same speed.

Brushless AC motors are generally 20 percent to 50 percent lighter than DC motors of comparable speed and rating. Since an inverter is needed to convert the DC generator output to AC, the inverter weight must be added to that of the AC motor to assess the total weight penalty associated with AC motor use. Inverters are heavy, with specific weights on the order of 20 lb/kw = 15 lb/hp.*

Data on AC generator weights are presented in Table XXXXIII. These generators operate at 500°F and at a power factor of 0.85. They are of the radial-gap, homopolar inductor type. The frequency, speed, and voltage have been optimized for minimum weight.

TABLE XXXXIII. MINIMUM-WEIGHT AC GENERATORS[66, 67]

Rating (KVA)	Frequency (Hz)	Speed (rpm)	Voltage (v)	Specific Wt (lb/kw)	Efficiency (%)
400	2,000	40,000	500	0.85	91
1,200	1,600	24,000	500	0.95	92
6,000	1,200	12,000	500	1.00	92
12,000	1,200	12,000	500	1.00	92

Estimated specific weights for AC and DC brushless motors are given in Table XXXXIV. The specific weights of the AC motors were assumed to be the same as the AC generator specific weight of Table XXXXIII. The specific weights of the DC motors were assumed to be 1.7 to 2.7 times greater than the AC motor specific weights.

---

*Personal communication with D. Rife, Westinghouse Electric Corp., Lima, Ohio.

TABLE XXXXIV. SPECIFIC WEIGHT OF AC AND DC MOTORS			
Shaft Power - hp	500	1500	10,000
Speed - rpm	30,000	20,000	15,000
Voltage - v	500	500	500
Efficiency	0.91	0.92	0.92
Component	Specific Weight (lb/hp)		
AC Motor	0.64	0.71	0.74
AC Motor and Inverter	15.6	15.7	15.7
DC Motor	1.06-1.70	1.19-1.90	1.25-2.00

From Table XXXXIV, it is seen that the brushless DC motor is much lighter than the AC motor/inverter combination.

SUPERCONDUCTING MOTORS[69-71]

If the motor windings are fabricated from superconducting wire and the temperature is maintained below the critical value at which the wires become superconducting, substantial reductions in motor weight become possible. These reductions arise because at superconducting temperatures there is no resistance to the flow of electric current; maximum current is then limited only to the critical value above which the superconducting state is lost.

The high current densities possible in the superconducting state result in magnetic flux densities far in excess of those obtainable in field windings of conventional motors with iron cores. The heavy iron core can therefore be dispensed with. However, ferromagnetic material may still be useful for field shaping and shielding against stray magnetic fields. Also, refrigeration equipment needed to maintain the temperature of the windings at a superconducting level is fairly heavy.

Superconducting motor technology is presently in the early stages of development. Experimental and analytical studies indicate marked reduction in weight of superconducting electrical machinery in comparison with conventional machinery. The major problem area seems to be the relatively high weight of refrigerators that are capable of maintaining superconductive temperatures. This problem is expected to yield to engineering development as ways are found to further reduce the refrigeration heat load, to increase the upper temperature limit of the superconducting state, and to build lighter, more efficient refrigeration machinery.

The use of superconducting windings is reasonably well established for DC field windings, but seems to be less certain for AC windings because of hysteresis losses which increase the refrigeration heat load.

Table XXXXV gives weight data for a 3000-hp, 400-cps synchronous superconducting AC motor. This motor has a rotating superconducting field inside a helium-cooled rotating Dewar. The armature is outside the rotating field. It does not rotate and is not superconducting. The refrigerator weight given is based on a heat load of about 2 watts, a refrigeration temperature of 4.2°K, and a refrigerator which employs turbomachinery rather than reciprocating machinery. Turbomachinery refrigerators are not available now, but should be developed within the next few years. If a current flight-weight type refrigerator were used, the refrigerator weight would be about 250 lb.

TABLE XXXXV. WEIGHT OF 3000-HP SUPERCONDUCTING AC MOTORS[70]

Pole Pairs	Speed (rpm)	Motor Weight (lb)	Refrig Wt (lb)	Total Wt (lb)	Total Specific Wt (lb/hp)
1	24,000	326	75	401	0.134
2	12,000	415	75	490	0.163
3	8,000	524	75	599	0.200
4	6,000	650	75	725	0.241

Data for a 30,000-hp superconducting DC homopolar, air core motor are given in Table XXXXVI. The heat load for this machine is about 2.75 w. The efficiency is most probably 0.98 or better.

The weight of the 30,000-hp, 4000-rpm DC motor is 65 percent of the weight of a comparable single-pole synchronous unshielded AC superconducting motor.[71] This factor was used to estimate the weight of 3000 hp DC homopolar superconducting motors from the data of Table XXXXV.*

* If magnetic shielding is required, the weight of the DC motor increases to 9,600 lb, compared to about 3,700 lb for the shielded AC motor.

TABLE XXXXVI. CHARACTERISTICS OF 30,000-HP SUPERCONDUCTING DC HOMOPOLAR, AIR CORE MOTOR[71]

Speed - rpm	4000	1300	200
Weight - lb	1910	4100	13,680
Volume - ft^3	5.78	12.42	41.5
Diameter - ft	2.28	2.97	4.4
Length - ft	1.42	-	2.7

Added Weight and Volume

Component	Weight (lb)	Volume (ft^3)
Field	516	3.09
Transmission Line	360/ft length	2.18/ft length
24 hr Stored Cryogens	3750	46.8
Reciprocating Refrigerator*	1100	14.
Turbo Refrigerator*	100	≈1.4

* Either the reciprocating refrigerator or the turbo refrigerator can be used.

In Table XXXXVII, the specific weights of 3000-hp and 30,000-hp DC homopolar motors are given, along with the specific volume of the 30,000-hp motor at 4000 rpm. The specific weights of refrigerators and cryogens at 3000 hp were estimated by multiplying the weights at 30,000 hp by the factor (2/2.75)10. The quantity in parentheses is the ratio of estimated heat loads at 3000 hp and 30,000 hp. Motor weights at 3000 hp were obtained by multiplying the AC motor weights of Table XXXXV by 0.65, as was explained above. The motor, field exciter, and 5 ft of transmission line are all included in the term "motor". In addition, a reciprocating refrigerator and a 4-hr stored cryogen supply are included with the present motors, and a refrigerator with turbomachinery is included with future motors.

The data of Table XXXXVII, while fragmentary, can be used to generate curves of specific weight versus power for speeds covering the range of 100 rpm to 30,000 rpm. Such curves for present and future technology are shown in Figures 47 and 48. The dashed curves represent the locus of specific weights if the motor were coupled directly to the helicopter rotor.

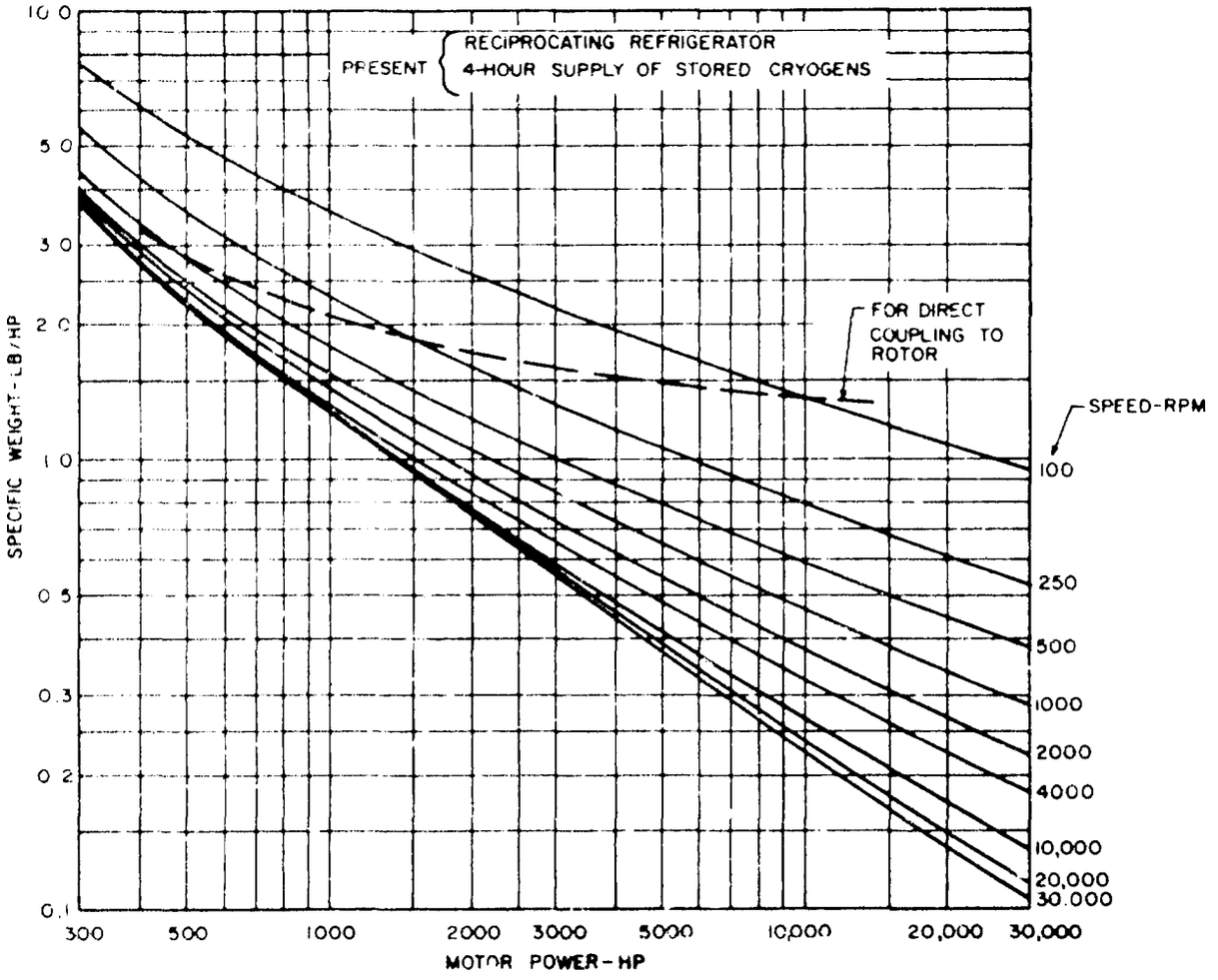

Figure 47. Specific Weight of Present Superconducting DC Homopolar Motors.

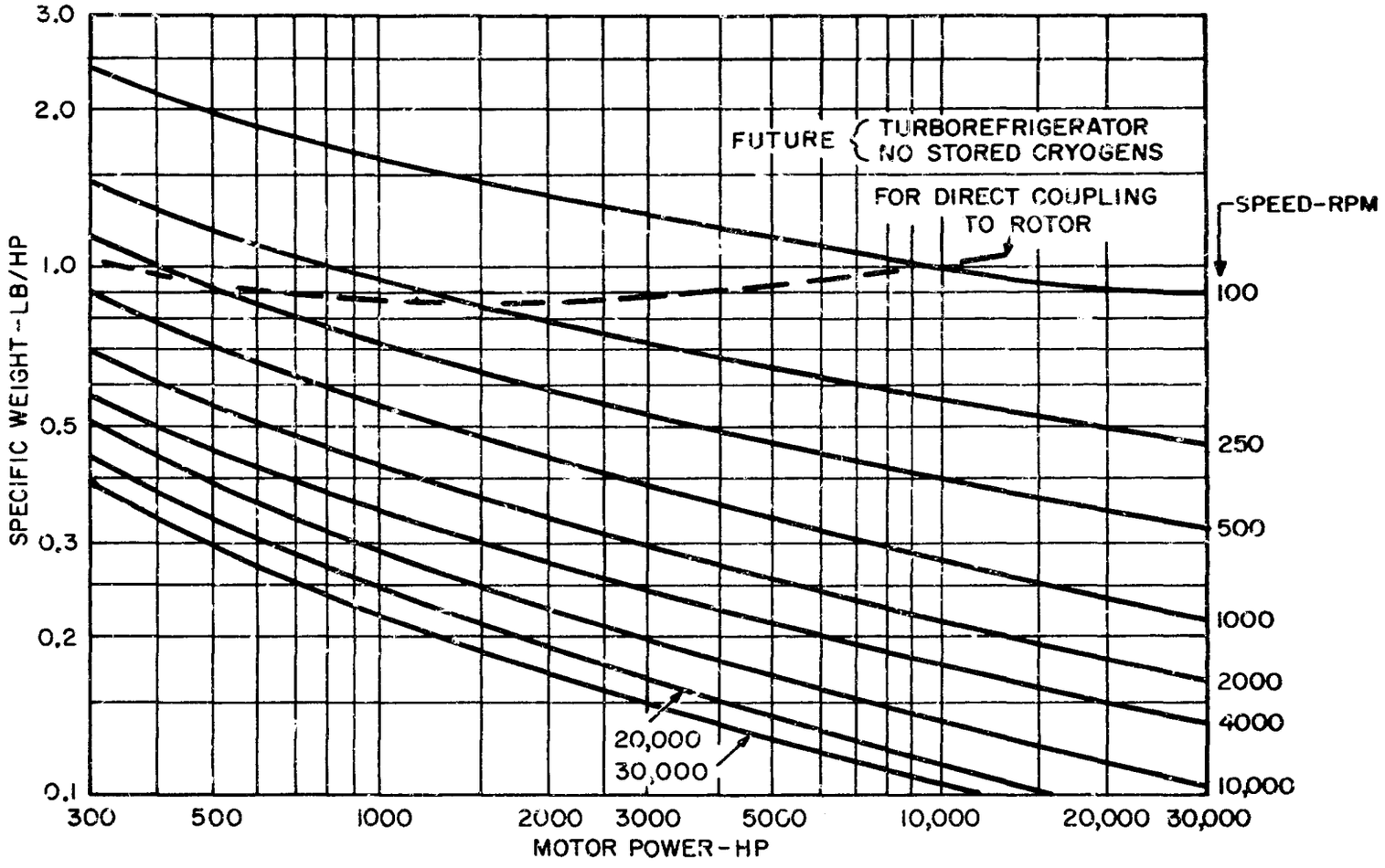

Figure 48. Specific Weight of Future Superconducting DC Homopolar Motors.

TABLE XXXXVII. SPECIFIC WEIGHT AND VOLUME OF DC SUPERCONDUCTING MOTORS

Power - hp	30,000	30,000	30,000	
Speed - rpm	200	1300	4000	
Present Specific Wt - lb/hp	0.582	0.263	0.190	
Future Specific Wt - lb/hp	0.528	0.209	0.135	
Present Specific Vol - ft^3/hp			1.39×10^{-3}	
Future Specific Vol - ft^3/hp			0.70×10^{-3}	
Power - hp	3000	3000	3000	3000
Speed - rpm	6000	8000	12,000	24,000
Present Specific Wt - lb/hr	0.628	0.601	0.578	0.558
Future Specific Wt - lb/hp	0.232	0.205	0.182	0.162

MOTOR-TRANSMISSION COMBINATIONS

The specific weight of main helicopter transmissions, based on actual data,[68] is shown as the solid part of the curve in Figure 49, which is marked "horizontal mounting". If this curve is extrapolated to a speed reduction ratio of 1, the specific weight is 0.36 lb/hp. This fact indicates that the weight of a section of the transmission is fixed and that this fixed-weight section is present even when there is no speed reduction. The fixed-weight section most probably consists of the bevel gears and shafting that are needed to transmit power from the horizontal shaft of a gas turbine to the vertical helicopter rotor shaft.

With an electric motor transmitting shaft power to the transmission, it may be possible to eliminate most of the fixed-weight section by mounting the motor and transmission in the vertical direction. The curve of Figure 49 marked "vertical mounting" was constructed on the assumption that the transmission specific weight could be reduced by 0.30 if the transmission were mounted vertically.

Since the transmission weight falls off as the transmission inlet (motor) speed decreases, while motor weight increases as the speed decreases, it is evident that there is an optimum speed for minimum combined weight of the motor and transmission. The specific weight for four motor-transmission combinations was plotted against speed to determine the optimum speed and the corresponding minimum combined motor-transmission specific weight. The resulting minimum specific weights and optimum speeds are shown in Figure 50. The curve for a reciprocating refrigerator with cryogenic storage and a horizontal transmission was considered to be representative of present technology. The curve for a turbo refrigerator with no cryogenic storage and a vertical transmission was considered to be representative of future technology.

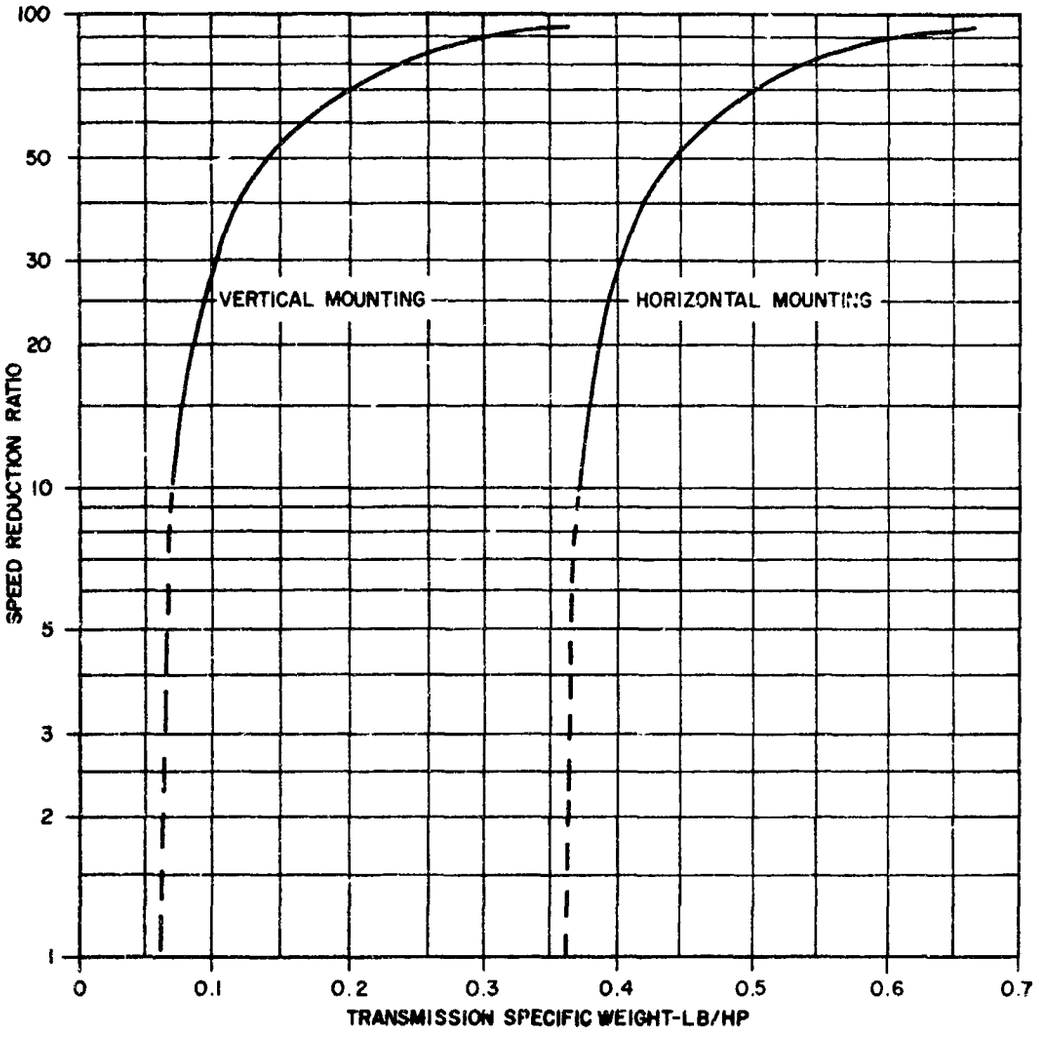

Figure 49. Specific Weight of Main Helicopter Transmissions.[65]

At 500 hp, the minimum specific weight of the superconducting DC motor/transmission combination for present technology (2.6 lb/hp) is larger than the specific weight of a conventional DC motor and horizontal transmission (1.76 to 2.40 lb/hp). Therefore, the combined specific weight at 500 hp for present technology was taken to be 2.40 lb/hp, implying the use of a conventional rather than a superconducting motor.

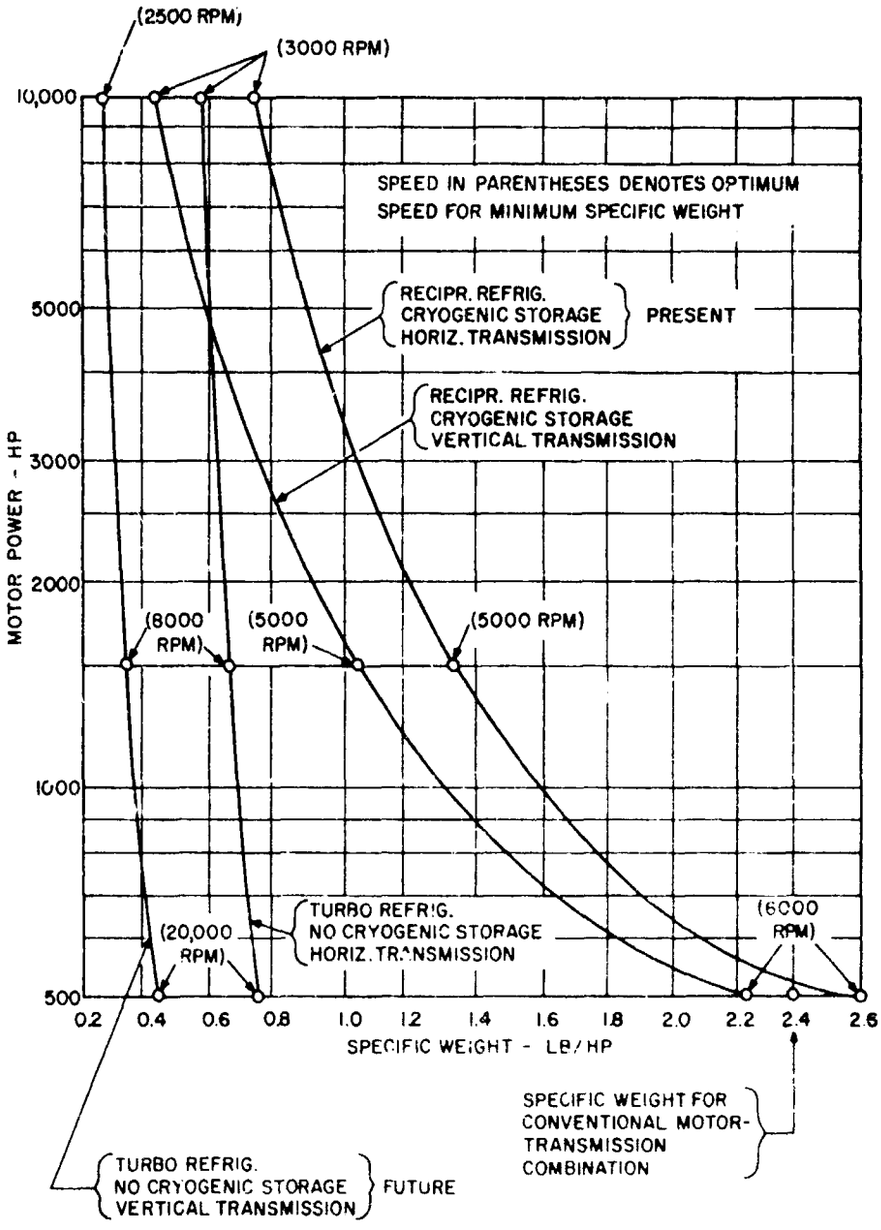

Figure 50. Minimum Specific Weight of Superconducting DC Motor-Transmission Combinations.

UNCLASSIFIED
Security Classification

DOCUMENT CONTROL DATA - R & D

(Security classification of title, body of abstract and indexing annotation must be entered when the overall report is classified)

1. ORIGINATING ACTIVITY (Corporate author) Calvin C. Silverstein, Engineering Consultant 2525 Farringdon Road Baltimore, Maryland 21209	2a. REPORT SECURITY CLASSIFICATION Unclassified 2b. GROUP

3. REPORT TITLE

A Survey of Advanced Energy Conversion Systems and Their Applicability to Army Aircraft Propulsion Requirements

4. DESCRIPTIVE NOTES (Type of report and inclusive dates)

Final Report

5. AUTHOR(S) (First name, middle initial, last name)

Calvin C. Silverstein

6. REPORT DATE	7a. TOTAL NO. OF PAGES	7b. NO. OF REFS
October 1969	177	71

8a. CONTRACT OR GRANT NO.	9a. ORIGINATOR'S REPORT NUMBER(S)
DAAJ02-69-C-0001	USAAVLABS Technical Report 69-81
b. PROJECT NO. 1G162204A01409	
c.	9b. OTHER REPORT NO(S) (Any other numbers that may be assigned this report) SIL-103
d.	

10. DISTRIBUTION STATEMENT

This document is subject to special export controls, and each transmittal to foreign governments or foreign nationals may be made only with prior approval of US Army Aviation Materiel Laboratories, Fort Eustis, Virginia 23604.

11. SUPPLEMENTARY NOTES	12. SPONSORING MILITARY ACTIVITY
	U.S. Army Aviation Materiel Laboratories Fort Eustis, Virginia

13. ABSTRACT

A survey of advanced energy conversion methods and an evaluation of their applicability to Army aircraft propulsion requirements were carried out. Systems surveyed included: closed Brayton cycle, Rankine cycle, intercool-reheat cycle, fuel cells, MHD converters, thermionic converters, thermoelectric converters, radioisotope heat sources, and nuclear reactor heat sources. Information was also obtained on conventional and superconducting motors, which are required to convert the output of direct electrical generators to shaft power. None of the energy conversion systems were competitive with advanced gas turbines at power levels of 500 and 1500 hp. At 10,000 hp, both the MHD converter and the intercool-reheat cycle appear to be competitive with gas turbines on the basis of weight and other considerations. It was recommended that these systems be studied in more detail.

DD FORM 1 NOV 68 1473 REPLACES DD FORM 1473, 1 JAN 64, WHICH IS OBSOLETE FOR ARMY USE.

UNCLASSIFIED
Security Classification

14. KEY WORDS	LINK A		LINK B		LINK C	
	ROLE	WT	ROLE	WT	ROLE	WT
Energy Conversion						
Closed Brayton Cycle						
Rankine Cycle						
Intercool-Reheat Cycle						
Fuel Cells						
MHD Converter						
Thermionic Converter						
Thermoelectric Converter						
Radioisotope						
Nuclear Reactor						
Helicopter						
Gas Turbine						
Propulsion						
Motor						
Superconducting Motor						
Transmission						